

Graduate School for Cellular and Biomedical Sciences

University of Bern

# **A database framework to incorporate statistical variability in biomechanical simulations**

PhD Thesis submitted by

**Michael Kistler**

from **Reichenburg SZ**

for the degree of

PhD in Biomedical Engineering

Supervisor

Prof. Dr. Philippe Büchler

Institute for Surgical Technology and Biomechanics

Faculty of Medicine of the University of Bern

Co-advisor

Prof. Dr. Philippe Cattin

Medical Image Analysis Center, Department of Biomedical

Engineering

Medical Faculty of the University of Basel

“There’s never enough time to do all the nothing you want.” Bill Watterson



Accepted by the Faculty of Medicine, and the Faculty of Science of the University of Bern at the request of the Graduate School for Cellular and Biomedical Sciences.

Bern,

Dean of the Faculty of Medicine

Bern,

Dean of the Faculty of Science

Bern,

Dean of the Vetsuisse Faculty Bern

**Copyright © 2014 Michael KISTLER**

"The copyright of this thesis rests with the author. No quotations from it should be published without the author's prior written consent and information derived from it should be acknowledged".

## Acknowledgements

First of all I would like to thank Prof. Dr. Lutz P. Nolte, the director of the Institute for Surgical Technology and Biomechanics. His passion for Biomedical Engineering and leadership navigates the institute safely through past, present and upcoming times.

Secondly, I would like to thank my advisor PD Dr. Philippe Büchler for his support throughout the years, my co-advisor Prof. Philippe Cattin and my mentor PD Dr. med. Richard Nyffeler.

I would also like to thank our development partner, Marcel Pfahrer, Roman Niklaus, Rajib Mitra, Nicolas Biedermann, Viktor Tomas, and Frederique Giulinao at the University of Applied Science in Biel for their coding and support of the VirtualSkeleton Database. A special thanks goes to Adrian Gschwend for the lesson about the semantic Web and his efforts to integrate the FMA ontology into the database. I thank Lars Ebert at the Forensic Institutes of Bern and Zurich for his efforts to provide us high quality CT datasets, and Stefan Bauer for the excellent collaboration on the BRATS segmentation challenge. Marcel Lüthi who assembled many of us together and brought Statismo to life. And Alex Panos for treating my English Patient.

I thank the ISTB Backoffice Barbara, Annelies, Karin, Denise, Julia, Alexandra, Ulla, and Urs's Machine Shop team for their support on daily tasks. I would like to thank all colleagues of the institute, especially the computational biomechanics group, Christoph and Lexu for having great launch conversations.

I am deeply grateful for the support and love of my family and friends over the last years. Peps, Mom, Bro, Jela, Müllers, thanks for being there.

... love to Melanie and Roja - my wonderful family.

Funding for this PhD was gratefully received from NCCR-COME.



## Abstract

The statistical shape model (SSM) enjoys a remarkable popularity within the medical image analysis community to model the variability of human anatomy in specific populations [Blanz et al.; Cootes and Taylor, 2001; Lamecker et al.; Rajamani et al., 2007]. They are routinely implemented for automatic image segmentation or object identification in medical images. In these fields, however, the acquisition of the large training datasets required to develop these models is usually a time-consuming process.

As a tool to evaluate the mechanical performance of the bone from a computed tomography (CT), finite element (FE) models are commonly used. With the help of FE, load transfer from implant to bone, bone-cement interface mechanics and fracture risks can be evaluated [Querol; Bonaretti et al., 2008; Bryan et al., 2009]. Recent work started to consider variability [Taddei et al., 2006a; Laz et al., 2007; Viceconti et al., 2006]. Khalaji et al. [Khalaji et al., 2009] proposed to combine FE calculations with SSM to accelerate tissue deformation estimation. And Bryan et al. used SSM to analyse population fracture risk [Bryan et al., 2010, 2012].

The aim of this work is the development of a database framework which provides tools for the fast application of the methodological developments achieved in statistical shape modeling. The database should be able to handle data essential for SSM generation of anatomical structures, but using a concept which allows to be extended with highly heterogeneous data formats like SSM, 3D geometries, and simulation results. In a second part, this work proposes a method that uses statistical tools to predict biomechanical response of an anatomical structure to a given loading condition. This method should help to overcome time consuming aspects of finite element analysis (FEA).

The developed database framework (Virtual Skeleton Database) provides an online repository system tailored to the needs of the medical research community. The processing of the most common image file types, a SSM framework, and an ontology-based search provide the generic tools to store, exchange, and retrieve digital medical datasets. The hosted data are accessible to the community, and collaborative research catalyzes their productivity.

To solve this time constrain of FE, we propose to combine a statistical description of bone shape and mechanical properties with pre-calculated FE calculations in order to obtain *patient-specific* mechanical information without additional time-consuming simulations. First a femur model for normal walking based published work by Haller et al. and Speirs et al. [Heller et al., 2005; Speirs

et al., 2007] was developed. The proposed method was then evaluated against 25 synthetic bone models and on five patient datasets.

To illustrate the need for an online repository for medical research, three exemplary projects of the VirtualSkeleton database (VSD) are presented: (1) an international collaboration to achieve improvement in cochlear surgery and implant optimization, (2) a population-based analysis of femoral fracture risk between genders, and (3) an online application developed for the evaluation and comparison of the segmentation of brain tumors.

Results showed that the proposed prediction method is able to instantaneously provide the distribution of bone stresses with a prediction error below 0.1MPa and of nodal displacements with an accuracy of less than 70  $\mu\text{m}$  for the in-silico data. The prediction accuracy dropped to an average mean absolute error (MAE) of 2.04 MPa for the Von Mises stress and 1.21 mm for the displacement magnitude.

The Virtual Skeleton Database is a novel system for scientific collaboration for the medical image community with a data-centric concept and semantically driven search option for anatomical structures. The repository has been proven to be a useful tool for collaborative model building, as a resource for biomechanical population studies, or to enhance segmentation algorithms.

This work outlines a method to predict *patient-specific* FE results to bring FE closer to clinical application. However, to ensure accurate results a statistical mechanical model (SMM) which includes bone shape, material properties, and boundary conditions is required. The presented method does not reduce the amount of work to obtain mechanical results, but shifts the calculation time to a pre-processing step.

To conclude, this work provided valuable tools to the biomedical community. The developed database framework is available online, and a generic method to accelerate FE simulations using a statistical prediction approach has been proposed.

# Contents

<b>1</b>	<b>Introduction</b>	<b>1</b>
1.1	Aim of the thesis . . . . .	2
<b>2</b>	<b>Background</b>	<b>5</b>
2.1	Internet research repository . . . . .	5
2.1.1	Web technology . . . . .	6
2.1.2	Database . . . . .	12
2.1.3	Semantic Web . . . . .	14
2.1.4	Biomedical repository software . . . . .	17
2.2	Patient specific FE models in orthopedics . . . . .	21
2.3	Population FE models in orthopedics . . . . .	27
<b>3</b>	<b>The Virtual Skeleton Database</b>	<b>33</b>
3.1	VSD - Open access repository . . . . .	33
3.1.1	Abstract . . . . .	33
3.1.2	Introduction . . . . .	34
3.1.3	Methods . . . . .	36
3.1.4	Results . . . . .	41
3.1.5	Discussion . . . . .	45
3.2	Technical aspects . . . . .	49
3.2.1	Ontology . . . . .	49
3.2.2	Data acquisition . . . . .	50
3.2.3	The VSDUploader . . . . .	56
<b>4</b>	<b>Femur prediction model</b>	<b>67</b>
4.1	Finite element model of the femur . . . . .	67
4.1.1	Introduction . . . . .	67
4.1.2	Method . . . . .	69

4.1.3	Results . . . . .	71
4.1.4	Discussion . . . . .	74
4.2	Accelerate FE in Biomechanics: Preliminary Study . . . . .	75
4.2.1	Summary . . . . .	75
4.2.2	Introduction . . . . .	75
4.2.3	Methods . . . . .	76
4.2.4	Results and Discussion . . . . .	78
4.2.5	Conclusion . . . . .	78
4.3	Accelerate FE using database of pre-calculated simulations . . . . .	81
4.3.1	Abstract . . . . .	81
4.3.2	Introduction . . . . .	81
4.3.3	Methods . . . . .	82
4.3.4	Results . . . . .	83
4.3.5	Discussion . . . . .	87
4.4	Methods to accelerate finite element calculation in biomechanics using a statistical database of pre-calculated simulations . . . . .	88
4.4.1	Abstract . . . . .	88
4.4.2	Introduction . . . . .	88
4.4.3	Methods . . . . .	90
4.4.4	Results . . . . .	95
4.4.5	Discussion . . . . .	98
4.5	Patient-specific fe predictions . . . . .	101
4.5.1	Methods . . . . .	101
4.5.2	Results . . . . .	101
4.5.3	Discussion . . . . .	104
<b>5</b>	<b>Discussion, Conclusion and Outlook</b>	<b>105</b>
5.1	Discussion . . . . .	105
5.2	Conclusion . . . . .	109
5.3	Outlook . . . . .	110
<b>6</b>	<b>Appendix A - VSD</b>	<b>113</b>
6.1	User interface of the VSD . . . . .	113
6.2	FMA conversion . . . . .	121



6.3	REST API . . . . .	122
6.3.1	Example use case . . . . .	146
<b>7</b>	<b>Appendix B - Prediction model</b>	<b>153</b>
7.1	Patient specific results . . . . .	153
7.1.1	VSD subject 2 . . . . .	153
7.1.2	VSD subject 3 . . . . .	155
7.1.3	VSD subject 8 . . . . .	157
7.1.4	VSD subject 14 . . . . .	159
7.1.5	Standard Femur Model . . . . .	161



## List of Figures

2.1	Cadaver WebDAV client . . . . .	11
2.2	CrossFTP WebDAV client . . . . .	11
2.3	Semantic Web stack . . . . .	15
2.4	Conceptual differences of available biomedical Web repositories . . . . .	18
2.5	FE modeling workflow . . . . .	22
2.6	Material property conversion . . . . .	25
3.1	VSD architecture . . . . .	37
3.2	Registration process . . . . .	38
3.3	Conceptual overview . . . . .	39
3.4	VSD Web interface . . . . .	40
3.5	Hear-EU project . . . . .	43
3.6	Geometrical measurements . . . . .	44
3.7	BRATS segmentation . . . . .	46
3.8	Ontology search . . . . .	51
3.9	Search results for <i>Leg</i> . . . . .	52
3.10	Masked VSD head dataset . . . . .	56
3.11	Upload scheme . . . . .	59
3.12	Reference object version: multifile objects . . . . .	61
3.13	Multi file versioning . . . . .	62
3.14	Reference objection version: combined objects . . . . .	63
3.15	Versioning scheme for combined objects . . . . .	64
3.16	Single file decision tree . . . . .	65
4.1	Simplification of the hip muscles . . . . .	68
4.2	Load and boundary model . . . . .	69
4.3	Standardized femur model . . . . .	70
4.4	Adapted load and boundary model . . . . .	72

4.5	Qualitative model comparison . . . . .	73
4.6	Principal strain comparison . . . . .	73
4.7	Femur landmark locations . . . . .	77
4.8	FE model for normal walking . . . . .	77
4.9	Path along the medial femur shaft . . . . .	78
4.10	Mises stress along the path . . . . .	79
4.11	Relative error along the normalized path . . . . .	79
4.12	Predictive model workflow . . . . .	84
4.13	Prediction error . . . . .	85
4.14	Absolute prediction error of two patients . . . . .	86
4.15	FE femur model . . . . .	93
4.16	Prediction model schematics . . . . .	94
4.17	Compactness of the statistical stress tensor model . . . . .	95
4.18	Prediction error of the stress tensor . . . . .	96
4.19	Von Mises stress comparison . . . . .	97
4.20	MAE of the stress tensor . . . . .	97
4.21	Mises and displacement prediction error of the SFM . . . . .	103
4.22	Mises and displacement prediction error of the VSD subject 2 . . . . .	103
6.1	VSD landing page . . . . .	113
6.2	Object list view . . . . .	114
6.3	Expanded list view . . . . .	115
6.4	Object details . . . . .	116
6.5	Object details cont. . . . .	117
6.6	Forum . . . . .	118
6.7	Object thread . . . . .	119
6.8	BRATS challenge . . . . .	120
7.1	VSD subject 2: displacement prediction error . . . . .	153
7.2	VSD subject 2: stress prediction error . . . . .	154
7.3	VSD subject 3: displacement prediction error . . . . .	155
7.4	VSD subject 3: stress prediction error . . . . .	156
7.5	VSD subject 8: displacement prediction error . . . . .	157
7.6	VSD subject 8: stress prediction error . . . . .	158

7.7	VSD subject 14: displacement prediction error . . . . .	159
7.8	VSD subject 14: stress prediction error . . . . .	160
7.9	VSD subject SFM: displacement prediction error . . . . .	161
7.10	VSD subject SFM: stress prediction error . . . . .	162



## List of Tables

2.1	REST data elements . . . . .	9
2.2	WebDAV Clients . . . . .	11
2.3	Data Management Systems . . . . .	12
2.4	Database popularity . . . . .	14
2.5	Biomedical image repositories . . . . .	20
3.1	Geometrical measures . . . . .	44
3.2	Anatomical regions containing the <i>Leg</i> . . . . .	53
3.3	Demographics of the full body datasets . . . . .	54
3.4	Technical image data (BE) . . . . .	55
3.5	Technical image data (ZH) . . . . .	55
4.1	Forces used in the femur model . . . . .	71
4.2	Demographics of the statistical model . . . . .	90
4.3	Demographics VSD subjects . . . . .	101
4.4	Patient specific stress prediction accuracy . . . . .	102
4.5	Patient specific displacement prediction accuracy . . . . .	102
4.6	Patient specific prediction accuracy: SFM . . . . .	102
4.7	Patient specific prediction accuracy: VSD subject 2 . . . . .	103
7.1	Patient specific prediction accuracy: VSD subject 2 . . . . .	153
7.2	Patient specific prediction accuracy: VSD subject 3 . . . . .	155
7.3	Patient specific prediction accuracy: VSD subject 8 . . . . .	157
7.4	Patient specific prediction accuracy: VSD subject 14 . . . . .	159
7.5	Patient specific prediction accuracy: SFM . . . . .	161





# Abbreviations

**.NET** .NET framework. 6, 13, 106

**AJAX** asynchronous JavaScript and XML. 6

**ANN** artificial neural network. 31, 80, 98, 108

**API** application programming interface. 9, 10, 12, 105

**ASA** anatomical structural abstraction. 17

**AT** anatomy taxonomy. 17

**ATA** anatomical transformation abstraction. 17

**BC** boundary condition. 72, 74, 77, 93, 99

**BMD** bone mineral density. 24

**BMI** body mass index. 42, 83, 92, 101

**BRATS** multimodal brain tumor segmentation. 45, 107

**CAD** computer aided design. 69

**CBCT** cone beam computed tomography. 55

**CC** Creative Commons. 39

**CERN** European organization for nuclear research. 5

**CIA** cancer imaging archive. 106

**CSS** cascading style sheets. 7

**CSS3** cascading style sheets 3. 6, 8

**CSV** comma separated values. 45

**CT** computed tomography. vii, 2, 17, 21, 24, 29, 30, 42, 50, 53–56, 58, 67, 76, 77, 81, 82, 87, 90, 92, 101, 107, 108, 111

**DASL** DAV searching and locating. 10

**DAV** Distributed Authoring and Versioning. 10

**DICOM** digital imaging and communications in medicine. 18, 35, 36, 38, 45, 58, 60

**DOF** degrees of freedom. 69, 72

**DOM** document object model. 6

**EOT** embedded OpenType. 7

**ESP** European spine phantom. 54

**FCS** femur coordinate system. 72

**FE** finite element. vii, viii, 2, 3, 21–24, 26, 30, 31, 42, 67, 69, 76–79, 81–83, 87–93, 95–99, 101, 102, 104, 107, 108, 110–112

**FEA** finite element analysis. vii, 2, 27, 29, 30, 76, 82

**FEM** finite element method. 2, 5, 21, 81

**FMA** foundational model of anatomy. 16, 17, 39, 49–51, 105, 121

**FoV** cantonal regulation on research studies on humans. 50

**FTP** file tranfer protocol. 10

**GCS** global coordinate system. 72, 93

**GO** generic object. 60

**HDF5** hierarchical data format. 41, 58

**HTML** hypertext markup language. 6–9, 105

**HTML5** hypertext markup language 5th revision. 6

**HTTP** hypertext transfer protocol. 9, 10

**HU** Hounsfield unit. 24

**IE** Internet Explorer. 7, 8

**IIS** Microsoft internet information service. 36

**IRI** internationalized resource identifier. 15

**ISO** international organization for standardization. 6

**ISTB** institute for surgical technology and biomechanics. 55

**ITK** Insight toolkit. 36, 38

**JPEG** joint photographic expert group. 9

**JS** JavaScript. 6, 7, 9

**JSON** JavaScript object notation. 9

**KEK** cantonal ethics committee. 50, 53

**LCS** lcoal coordinate system. 72, 77, 93

**MAE** mean absolute error. viii, 95, 97, 102–104

**MICCAI** medical image computing and computer assisted intervention. 45

**Mk** metaknowledge. 17

**MR** magnetic resonance. 17, 23, 31, 45, 55, 56

**NIPALS** nonlinear iterative partial least squares. 81, 83, 92

**NoSQL** no structured query language. 6, 12, 14, 106, 111

**NSR** normalized shape ratio. 108

**OBO** open biological and biomedical ontologies. 49

**OT** OpenType. 8

**OV** object version. 60, 61, 63

**OWL** Web ontology language. 15, 49

**PACS** picture archiving and communication system. 1, 2, 17, 18, 35, 36

**PC** principal component. 31

**PCA** principal component analysis. 27–31, 77, 82, 90, 92, 98, 99, 108, 110

**PHP** PHP hypertext preprocessor. 6, 18

**PLS** partial least square. 83, 95, 108

**RBF** radial basis function. 77, 90

**RDBMS** relational database management system. 12–14

**RDF** resource description framework. 15, 49, 50

**RDFS** resource description framework schema. 15

**REST** representational state transfer interface. 8–10, 36, 48, 105, 111

**RIF** Rule Interchange Format. 15

**RMSE** root mean square error. 21, 23

**SAM** statistical appearance model. 67, 81, 82, 87, 90–92, 101, 104, 108, 109, 111

**SD** standard deviation. 92, 96, 104

**SFEM** statistical finite element model. 78–80

**SFM** standard femur model. 69, 72, 101–104, 107, 111, 161, 162

**SGML** Standard Generalized Markup Language. 6

**SHA-1** secure hash algorithm. 58, 63

**SIM** statistical intensity model. 27, 29, 82, 91

**SM** statistical model. 27, 29–31, 77, 82, 89, 90, 99, 104, 106–108, 110, 146, 148

**SMM** statistical mechanical model. viii, 82, 92, 99, 107

**SPARQL** SPARQL protocol and RDF Query Language. 15, 40, 49, 50, 53

**SQL** structured query language. 6, 12, 13, 36, 50, 57, 106, 111

**SSA** statistical shape analysis. 1

**SSM** statistical shape model. vii, 1, 2, 27, 29–31, 33, 34, 36, 46, 47, 67, 76, 77, 82, 83, 89–91, 99, 101, 106, 109–111, 146

**SVD** singular value decomposition. 29, 83

**SVG** scalabel vector graphics. 8

**TCIA** the cancer imaging archive. 1

**THA** total hip arthroplasty. 67

**TT** TrueType. 8

**URI** uniform resource identifier. 8, 9, 15, 53

**URL** uniform resource location. 9

**URN** uniform resource names. 9

**VSD** VirtualSkeleton database. viii, 2, 3, 18, 19, 33, 35, 36, 38–42, 45–49, 52–54, 56–60, 62, 63, 101, 102, 104–107, 109–111, 146

**VTk** visual toolkit. 36

**W3C** World Wide Web Consortium. 14

**WebDAV** Web-based distributed authoring and versioning. 10, 11, 36, 38, 41, 105, 106

**WOFF** Web open font format. 8

**WWW** World Wide Web. 5, 10, 14, 16, 17, 106

**XHTML** extensible hypertext markup language. 6, 7

**XML** extensible markup language. 6, 7, 10, 12, 15, 16

**XNAT** extensible neuroimaging archive toolkit. 18, 35



# Nomenclature

*E* The modulus of elasticity (Young’s Modulus). 24, 78, 83

$\rho_{APP}$  The hydrated bone mass divide by the total specimen volume. 24

$\rho_{ASH}$  The bone ash mass divided by the total specimen volume. 24

$\rho_{QCT}$  The mineral content of the bone represented by the Hounsfield unit (HU). 24

**representation** The ability of the model to map an object into the PCA space. 108

**Owner** The user with ownership rights on a dataset. 57, 60

**RESTful** A Web API implemented using HTTP and REST principles. 9, 10

**Unvalidated Data Folder** The folder containing uploaded objects which are only visible to the user. 57

**VSD ID** The unique identfier of a VSD dataset. 58

**compactness** The ability of the model to describe the training data using the smallest number of eigenmodes. 108

**generalization** The ability of the model in recreating objects outside the training population. 108

**patient-specific** A model derived form patient data. vii, viii, 5, 21, 23, 27, 67, 76, 77, 80–82, 88, 89, 98, 99, 101, 104, 107, 109–111

**tags** The general term to describe an object of HTML syntax. 7





# Chapter 1

## Introduction

One great thing about human beings is their unique appearance. Human variability can be described according to different parameters, the most common being genetic variations (i.e. sex, race, eye color etc.), body shape, size, and weight. Beyond the obvious variabilities in appearance, the human skeleton has, even among similar looking people, a large variability in bone shapes, internal structures and bone density. As a consequence, the anatomical variability results in different biomechanical behaviours, due to the fact that shape and mechanical properties are the two most significant parameters responsible for mechanical stiffness of skeletal structures. Recently, statistical shape analysis (SSA) has been developed to model shape variability. This method enjoys a remarkable popularity within the community of medical image analysis to model the variability of human anatomy in specific populations. Since its invention, various groups worldwide started to investigate the capabilities of these techniques in order to study human anatomy [Banz et al., 2004; Cootes and Taylor, 2001; Lamecker et al., 2002; Rajamani et al., 2007]. Nonetheless, a recurrent problem, that is faced when applying SSM to a specific clinical indication, is the large amount of data required to build a valid model. Therefore, having a data repository is vital for a fast development of new applications or to build new image processing algorithms based on this technology. For handling medical image data, existing picture archiving and communication system (PACS) are widely spread. They are used to manage and provide network storage for the retrieval, distribution and presentation of medical images. But a traditional PACS is designed for clinical use and does not serve as a repository for processed data and SSM. In past years, a few attempts have been made to provide an image repository for academic researchers. The resulting archives and repositories were designed for a limited number of subjects [Spitzer and Whitlock, 1998] or faced problems in information structuring and database querying [Brinkley and Rosse, 2002] with an increasing number of datasets. An exception is the cancer imaging archive (TCIA) [TCI, 2009], which contains more than 1'000 examinations. This archive provides access to image resources in order to improve the use of imaging in cancer research. But this archive is still specific

for either an organ or pathology and a mix of thereof. More recent medical image databases focus on specific diseases or medical research areas [DDS, 2009; Marcus et al., 2006, 2007; Staal et al., 2004; UTH, 2009]. A general database where unprocessed medical image datasets are stored and can be later be processed in a customized framework focused around SSM is not yet available.

The main function of the human skeleton is to provide a strong mechanical framework that supports the body and therefore mechanical bone variability needs to be include for biomechanical calculations. FE models are commonly used as a tool to evaluate the mechanical performance of the bone from a CT. With the help of FE, load transfer from implant to bone, bone-cement interface mechanics, and fracture risks can be evaluated [Querol; Bonaretti et al., 2008; Bryan et al., 2009]. FE models are build out of CT scan data by first label the desired bony structure, followed by creating a 3D representation of the anatomical structure. The model is then further processed to generate a mesh which serves as the digital representation of bone for FE calculation. However, most analyses do not take the wide variation in material properties and geometry that may occur in natural tissues or manufacturing imperfections in synthetic materials into account, because the the underlaying information came from only one anatomical structure. Recent work started to consider this variability, for example, Taddei et al. [Taddei et al., 2006c] proposed a method that includes geometric and material uncertainties in FEsimulations based on a Monte Carlo simulation. The technique was improved by Laz et al. [Laz et al., 2007] who proposed a probabilistic platform to include uncertainties in the mechanical properties of fracture risk predictions. Viceconti et al. [Viceconti et al., 2006] used a similar approach to evaluate the primary stability of a cementless hip prosthesis. Khalaji et al. [Khalaji et al., 2009] proposed to combine FE calculation with SSM, but this work was limited to simplified analytical shapes. To extend this techniques, and to further improve the result of finite element method (FEM), a large collection of high quality images is required. Ideally, this collection accessible and extensible by the community.

## 1.1 Aim of the thesis

An important part of the presented PhD project is the development of a database framework tool for fast application of methodological developments in statistical shape modelling. This database should provide tools to handle data essential for SSM generation of anatomical structures. The objective of the VSD is not to re-develop existing PACS systems, but rather to extend this capabilities with a focus on SSM for research, with a concept expandable with highly heterogeneous data formats like SSM, 3D geometries, and simulation results.

In a second part, the aim of this work is to generate a model which contains the statistical

variability of bone biomechanics of a population. This model is then used to propose a method that overcomes time consuming aspects of FEA. The proposed method uses statistical tools to predict biomechanical response of an anatomical structure to a given loading condition. To illustrate this method, a femur model for a walking situation is presented and evaluated on in-silico and patient data.

Both parts of this thesis, the VSD and the FE prediction method, should provide sustainable research which can further be applied to other applications or fields, can catalyze research needed to push FE forward and finally into clinics.



## Chapter 2

### Background

In this chapter, essential technologies and standards of this thesis are described. Important aspects of web services and recent developments to understand online repositories are described and possibilities of web based applications are outlined. In a second part, the usage of FEM in orthopedics for *patient-specific* and population based models are introduced.

#### 2.1 Internet research repository

The initial development of the World Wide Web (WWW) was driven by researchers at the European organization for nuclear research (CERN) to build a global computer network information system based on a hypertext model. The vision was for it to be information forming, platform independent and scalable ([Hoogland and Weber, 1993]). Website locations were shared as bookmarks or collected in lists, and viewed through Web browsers of limited capability.

With the introduction of the graphical browser Netscape Communicator, the popularity of the WWW increased and was ready for commercialization. For several years Netscape represented the static behavior of the Web by focusing on creating software with occasional updates. The concept Encyclopedia Britannica Online is an example of the static content during the time of Web 1.0 where articles were authored by a small group of experts and finally added to the table of content.

This changed with the presence of new and dynamic companies like Google, who focussed on providing a service based on data, such as links between websites and offered web search through the *PageRank* [Page et al., 1998] algorithm. Wikipedia is the role model of dynamic, user-generated content, which updates, corrects, and produces new articles constantly.

As the number of people with access to fast Internet connection increased, more and more functionalities found their way to the cloud, meaning data is hosted on a webserver, and access is offered through a web service. With the massive amount of data stored in the cloud from numerous devices and through different interfaces, the current difficulties lie in data protection, data security,

cross-device compatibility, and scalability.

The core aspects to building such a web service are describe in the following sections. Not only the development in Web related programming languages has increased, but also the client side (i.e. web browsers) are receiving constant updates to improve speed, stability, and diversity to build Web 2.0. The applied languages on the server side have not drastically changed compared to the Web 1.0, but the way developers interact with data has changed significantly.

### 2.1.1 Web technology

Available core technologies to build dynamic web services are hypertext markup language 5th revision (HTML5), the successor of hypertext markup language (HTML) and extensible hypertext markup language (XHTML), for building, and cascading style sheets 3 (CSS3) to style and layout a page. JavaScript (JS), extensible markup language (XML), and combinations like asynchronous JavaScript and XML (AJAX) are used to build a smooth user experience. To build rich Web applications, many client-sided frameworks (interpreted by the Web browser) are both strong and popular. These JS, AJAX, and document object model (DOM) based frameworks smooth over inconsistencies between Web browsers and extend the functionality available to developers. They even provide the developer with pre-made plugins which fulfil common task like tabbed documents, showing a progress bar, and in-page dialogs. The benefit for the user of these libraries like YUI Library, Dojo Toolkit, MooTools, and jQuery is that they can communicate (upload and download) with the server without the need of a full page reload. Additionally, the data request from and to the server is sent asynchronously. This separated communication allows the user to continuously interact with the page and therefore allows for Web services to be designed with functions like desktop applications. Hereby, the dynamic web content is served either by a structured query language (SQL) database or a no structured query language (NoSQL) database in combination with the open sourcePHP hypertext preprocessor (PHP) or the proprietary .NET framework (.NET) by Microsoft.

## Web design

### HyperText Markup Language

HTML is a computer language used for website creation and is an application of the international organization for standardization (ISO) Standard 8879:1986 about *Information Processing Text and Office Systems; Standard Generalized Markup Language (SGML)*. HyperText describes the method to move around the Web using hyper-link connections which are not linear. The

markup consists of *tags* to define HTML elements which are used to create the structure. These tags tell the browser how to display text or graphics in a document. In modern Web design, styling of the HTML structure is then done through cascading style sheets (CSS).

### **Cascading Style Sheets**

CSS is used to design a Web document which is most commonly HTML or XHTML formatted. But it can be applied to any kind of XML based document. CSS enables the separation between content and presentation attributes like fonts, colors and typesetting. This improves the accessibility, flexibility and controllability even among different rendering methods. The CSS can be styled to work according to the rendering method: on-screen, printing and voice. Technically, CSS specifies a priority scheme to determine which style rules apply if more than one rule matches against a particular element. Today, existing frameworks like Bootstrap, Gumby or Foundation are providing powerful tools to generate responsive designs which work across device of changing screen resolution.

### **Web fonts**

Until recently, the font usage on the Web was very limited. Most websites could only display system fonts already installed on client computers. To introduce some typographic flair, designers needed to create raster images which are not scalable or indexable by Google's search engine. Other workarounds included the usage of technologies like Flash or JS to render their font of choice.

Today, web fonts allow web designers to use fonts that are not installed on the viewer's computer. This was missing in the toolbox of web designers for proper typography. Nowadays, the CSS declaration (@font-face) is used by Web developers to specify a font. The font file will either be saved in a directory on a host server (like images), or it could be hosted by a specialized third party service provider like Google (<https://www.google.com/fonts>). The most common web font formats are listed below [Wikipedia, 2013]:

**TrueDoc** TrueDoc was the first standard for embedded fonts. Developed by Bitstream and discontinued due to the overly powerful competition of Microsoft's format embedded OpenType (EOT).

**EOT** Supported by Microsoft's Internet Explorer (IE), EOT includes a digital rights management system to protect fonts rights.

**TrueType (TT)/OpenType (OT)** TT is the industry standard font and OT is its open source counterpart. Both are fully supported by all major browsers including IE9+ which restricts the usage to fonts with embedded permission sets.

**Web open font format (WOFF)** This is a compressed file format that contains the font data (TT or OT) and instructions for the browser on how to display the font. This effectively neutralizes compatibility issues, and is therefore supported by all modern Web browser; Google's Chrome, Mozilla's Firefox, Opera's Presto, Apple's Safari and Microsoft's IE.

**scalabel vector graphics (SVG)** All SVG specifications can define a font module which allows to create a font within a SVG document. Through the font-face rule, CSS3 can be applied to a SVG document in a similar manner as to HTML.

### Representational state transfer interface

A representational state transfer interface (REST) is an architectural style which describes its elements within a distributed hypermedia system. It is in the nature of such a system that information has to be moved from the storage location to its usage location. The distributed hypermedia architecture has three options to perform their task to transmit data:

1. It can send a fixed-format data from the local storage to the recipient.
2. Both the rendering engine and the rendered data are sent together to the target.
3. Meta-data about the data type can be send together with the actual data. The recipient then can chose the rendering engine.

Each option has its advantages and disadvantage. Cleverly, REST represents a combination of all three [Fielding and Taylor, 2002]. It shares the understanding of data types with metadata, and limits the scope of what is revealed to a standardize interface. A dynamically selected representation of resources of a standard data type is the way REST components are communicating. Each resource is referenced with a global identifier like uniform resource identifier (URI) in HTML. The REST architectural style is described by six constraints and leaves the implementation of the respective component design flexible [Fielding and Taylor, 2002]:

**Client-server** Server are not concerned with interfaces and the client is not concerned with data storage. Therefore the server is more scalable and the client code is more portable.

**Stateless** With each request a client sends all information necessary to service and holds the session state.



**Cacheable** Each response has to be defined by itself as cacheable or not. This helps to eliminate unnecessary client-server interactions, and therefore lead to an improved scalability and performance.

**Layered system** A client is unaware of connected intermediary servers. Intermediary servers or services can enforce better security or make the system more scalable.

**Uniform interface** To be decoupled, the architecture has to have a uniform interface for both server and client, allowing them to evolve independently.

**Code on demand (optional)** Client side scripts (e.g. JS) can be used by servers to temporarily alter the functionality of a client.

**Table 2.1:** REST data elements summarized (modified from [Fielding, 2000]).

Data element	Modern Web examples
Resource	The intended conceptual target of a hypertext (concept, the browser asks for a Web page representation of the concept) reference
Resource identifier	uniform resource location (URL), uniform resource names (URN))
Representation	HTML document, joint photographic expert group (JPEG) image
Representation metadata	Media type, last-modified time
Resource metadata	Source link, alternates, vary
Control data	If-modified-since, cache-control

## RESTful

REST describes the architectural paradigm whereas a service which is built using these paradigms are called *RESTful*. A *RESTful* Web service (*RESTful* application programming interface (API)) is implemented using hypertext transfer protocol (HTTP) and REST principles. Consequently, a *RESTful* web service is a collection of resources and representations which communicate through HTTP methods:

**Resource** Base URI, such as `http://virtualskeleton.ch/api/`.

**Representation** The supported Web media type by the Web API (e.g. JavaScript object notation (JSON)) which has to be a valid hypertext standard.

**Communication** The set of operations supported by the Web API using HTTP methods (e.g., GET, PUT, POST, or DELETE).

**API** The API must be hypertext driven (non-linear, inter-linkable)

Providing access to system resources through a *RESTful* API is a very flexible way to present formatted data to different kinds of applications in a standardised way. Complying with the REST constraints enables the service to show performance attributes like scalability, simplicity, modifiability, visibility, portability, and reliability.

### **Web distributed authoring and versioning**

Web-based distributed authoring and versioning (WebDAV) is an extension of HTTP. WebDAV adds the collaboration aspect of files stored on the WWW by making the Web a readable and writable medium. The WebDAV framework provides the possibility to edit, create, and move documents directly onto the server. The difference to the HTTP base protocol is the possibility to access the content of a Web server as network file system. The file system appears as additional disc of the local computer. Popular server side implementation are Sphorium WebDAV in C#, SabreDAV as PHP framework or the mod-dav module in the Apache webserver. The most important features of the WebDAV protocol are summarized in the following list:

- Namespace management deals with the ability to copy and move web pages within a server's namespace.
- Collections deal with the creation, removal, and listing of various resources (e.g. system directories).
- Locking of files for overwrite protection.
- XML properties, which facilitates operations (such as storage and retrieval) on metadata.
- The Distributed Authoring and Versioning (DAV) protocol, which enables property setting, deleting, and retrieving.
- The DAV searching and locating (DASL) protocol allows clients to access DAV-modeled resources through server-side search.

### **WebDAV tool comparison**

Many modern operating systems provide built-in client-side support for WebDAV. In general, two options are available. First, the built-in systems usually can mount the file system of the server as a network drive. Secondly, some independent software packages offer a file transfer protocol (FTP)-like interface with a local resource and a remote location (Figure 2.2) side by side. Additionally, command line applications (Cadaver, figure 2.1) and libraries (python-webdav-lib) are available for developers. They allow for complete customization of the interaction with the remote system.

```
Listing collection `/webdav/': succeeded.
Coll:  -Upload-                0  Dec 31  0
Coll:  MyData                  1368 Dec 31  0
Coll:  MyGroups                6  Dec 31  0
Coll:  MyProjects              9  Dec 31  0
Coll:  SharedFolders           4  Dec 31  0
```

Figure 2.1: Cadaver is a fast command line WebDAV client for Linux

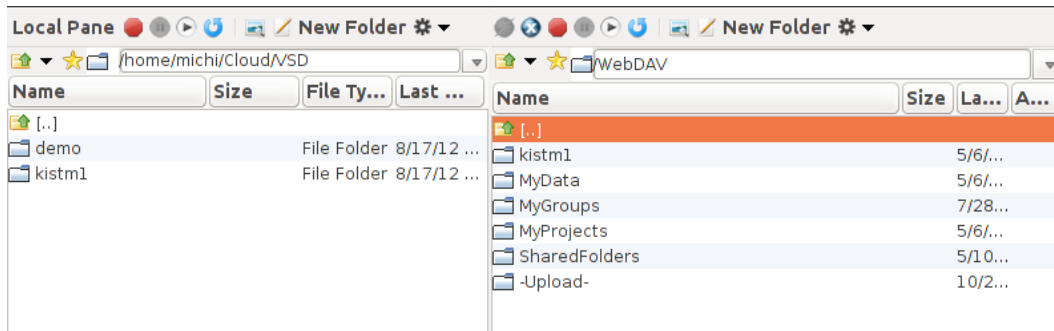


Figure 2.2: CrossFTP WebDAV client features the two panel view (local and remote location).

Table 2.2: Overview of available WebDAV clients and their functionality

Client	OS	Type	Caching	Price	Notes
CrossFTP	all, JAVA	both	yes	Commercial (free trial)	multi threads, scheduling, queue, log
Cyberduck	Win, Mac	File manager	??	free	log
Anydrive	all, JAVA	File manager	??	free	
Bitkinex	Win	File manager	yes	free	log
Webdrive	Win	File manager	yes	Commercial (free trial)	log
Transmit	Mac	mount drive	??	Commercial (free trial)	
Win explorer	Win	mount drive	yes	free	
Finder	Mac	mount drive	??	free	
Nautilus	Linux	mount drive	??	free	
Cadaver	Linux	cmd-line file manager	??	free	
Davfs	Linux	mount	??	free	

### 2.1.2 Database

Based on the relation model introduced by E.F Codd in 1969 the relational database management system (RDBMS) have become the standard to store information [Codd, 1970] in businesses and on the Web. The data in RDBMS is stored into tables which might be related to each other by key fields. These collections of tables are relying on operators to manipulate the stored data. The predominant query language (operator) for RDBMS is SQL. Alternative approaches like XML stores have never gained the same market share as RDBMS. In the new millennium, another type of database system collectively labeled as NoSQL databases surfaced. A distinct categorization of these databases is not available, since their approaches are often overlapping. Nevertheless, people agree that NoSQL databases are built on a data model. These NoSQL databases were developed to tackle the shortcomings of RDBMS like horizontal scalability, object-oriented programming, flexibility, efficiency, handling very large amounts of data (structures, semi-structured and un-structured), and to address the increased access frequency, performance and processing (Table 2.3).

**Table 2.3:** Comparison between RDBMS and NoSQL. Adapted from [MongoDB]

	<b>RDBMS</b>	<b>NoSQL</b>
Types	SQL database	variable
Examples	MS SQL Server, DB2, Oracle, Postgre, MySQL	Document: MongoDB, CouchDB Graph: Neo4J, HyperGraphDB Key-value: Riak, Redis Wide-Column: HBase, Cassandra
Data storage model	records stored in tables, connected tables	variable: two column tables, single documents, hierarchically
Data schemas	relatively fixed, changes require large interventions	typically dynamic
Scaling	vertically: software option, hardware demanding	horizontally - distribute to instances
Transactions	supported	in certain cases and at certain level
Data manipulation	quering language SQL	object-oriented API
Data consistency	strong consistency possible	product dependent

Despite these interesting options of NoSQL, RDBMS remain the most popular database systems (Table 2.4). The main reason for the success of RDBMS are manifold. During the last decades

the RDBMS reached a level of maturity which other systems lack. Not only the database itself but tools and addons of each RDBMS grew into powerful ecosystems where the development environment almost automatically suggest the corresponding RDBMS. For example, if .NET is used, developers choose predominantly Microsoft SQL servers whereas JAVA programmers work mostly with Oracle. RDBMS also provide a high level of security. Especially the security level of Microsoft's SQL server in terms of known security vulnerabilities is impressive, having only three vulnerabilities open for the 2008 R2 64bit version [Microsoft, 2013]. Two other aspects are important in the context of RDBMS. First, the concept of ACID (Atomicity, Consistency, Isolation, Durability) which describes a set of properties that ensure reliable database transactions processing:

**Atomicity** is the *all or nothing* concept: The entire transaction fails even if only one part fails, and the database is left unchanged.

**Consistency** property ensures that any transaction will not leave the database in an invalid state by validating the data written to the database against all defined rules.

**Isolation** property ensures that the parallel executions of transactions result in a system state that would be achieved as if their execution was processed in serial.

**Durability** means that once a transaction has been committed, it is definite. No power failure or error can prevent the transaction.

A second important concept of RDBMS is normalization. Normalization defines the efficiency of data organization, thus eliminating redundant data, and ensuring that data dependencies make sense. The normalization guidelines are split into normal forms where the subsequent normal form inherits the definitions of the previous form:

**First normal form** Eliminates repeating groups in individual tables. Creates a separate table for each set of related data. Identifies each set of related data with a primary key. For example, do not create Child1, Child2 fields in a single table. Create a table where the Children are stored, and put the key into the original table.

**Second normal form** Applies the rules of the first normal form, and creates separate tables for sets of values that apply to multiple records. It relates these tables with a foreign key. Now, the children live both in the same household, have therefore the same address. Instead of putting the address for both child twice, put the address into separate table and relate to it with a foreign key.

**Third normal form** Applies the second normal form and eliminates fields that do not depend on the key. Here, we replace values which can have multiple occurrences in a table and create an additional table for them. For example, the ZIP codes are independent of the primary key of the address and can occur in other addresses. Another example would be the category of the address, here probably labeled as *Home Address*. However, the third normal form is not always practical, and can therefore be ignored in specific cases.

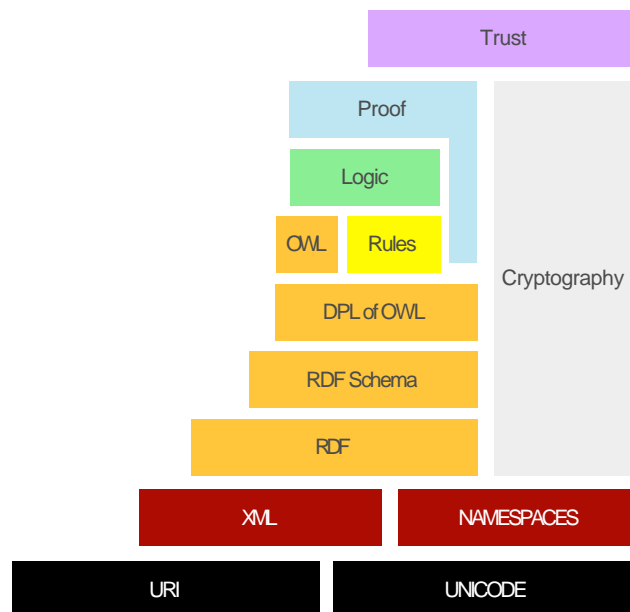
**Forth and Fifth normal form** Both are rarely applied in practical applications. Disregarding these rules may result in slightly less perfect database design without affecting the functionality of the database.

**Table 2.4:** Popularity ranking of database systems according to DB-Engines in November 2013 [Db-engines].

Rank	Name	Type	Score
1.	Oracle	RDBMS	1617.19
2.	MySQL	RDBMS	1254.27
3.	Microsoft SQL Serer	RDBMS	1234.46
4.	PostgreSQL	RDBMS	190.83
5.	DB2	RDBMS	165.90
6.	MongoDB	NoSQL (Document)	161.87
:	:	:	:
11.	Cassandra	NoSQL (Wide column)	57.58
13.	Redis	NoSQL (Key-value)	40.57
23.	Neo4j	NoSQL (Graph)	10.30

### 2.1.3 Semantic Web

The goal of the semantic Web is to enhance the current WWW with a standard to generate information that can be accessed and understood by computers. This should change the way humans find required knowledge. In contrast to the distributed hypertext system of the WWW (documents), the semantic Web should turn the WWW into a huge knowledge base (data). The World Wide Web Consortium (W3C) is leading the standardization to allow the sharing and re-usability of data across different boundaries. A short overview of the languages specifically designed for data in the semantic Web is outlined in figure 2.3.



**Figure 2.3:** Semantic Web stack - General Web technology to interact and integrate into the existing hypertext Web & semantic Web technology for semantic Web applications, adapted from [Horrocks et al., 2005]

**Identifier - URI** internationalized resource identifier (IRI) is a generalization of URI and therefore the unique identifier for semantic Web resources.

**Character sets - Unicode** for working with texts in different languages.

**Syntax - XML** for the creation of documents composed of structured data. The XML namespaces is used to refer to multiple sources within a single document.

**Data interchange - RDF** resource description framework (RDF) represents statements in so called triple-stores (subject, predicate and object). Information in the RDF format can be represented as a graph.

**Taxonomies - RDFS** resource description framework schema (RDFS) is the vocabulary of the RDF to create, as an example, hierarchies.

**Ontology - OWL** Web ontology language (OWL) is more advanced than the RDF, is based on description logic, and therefore allows for more reasoning of the data.

**Querying - SPARQL** SPARQL protocol and RDF Query Language (SPARQL) is used to query data stored in the RDF format and to retrieve informations.

**Rules - RIF** Rule Interchange Format (RIF) for describing relations that cannot be directly described in OWL.

These technologies are combined in order to provide descriptions of content of Web documents. The content itself can be descriptive data in a Web-database, can be markup included in documents or even be stored as pure XML. This content can be accessed and understood by machines, and rendered for human readers independently.

## Ontology

In Philosophy, the term ontology refers to the subject of existence. The modern ontology refers to the explicit specification of conceptualization. Conceptualization is an abstract, simplified view of a domain that we want to represent ([Gruber, 1995]). For researchers, an ontology defines the common terms and concepts needed to share knowledge in a specific domain. The ontology includes definitions and relations of basic concepts in the domain, in a machine-interpretable way. Originally a realm of Artificial-Intelligence laboratories [Levesque, 1984], ontologies are moving into the fields of domain exports and the WWW [Gruber, 1993]. The ontologies hosted online are used to categorized products and their features, to categorize Website in taxonomies or are used in the biomedical field to define the vocabulary of gene and gene products. Standardized ontologies are now developed to share and annotate data in their respective domain field. In medicine, SNOMED is a large, standardized collection of clinically used terms, codes, definitions for documentation, and reporting [Cornet and de Keizer, 2008]. Another example of a comprehensive taxonomy is the foundational model of anatomy (FMA) [Rosse and Mejino, 2003]. In a taxonomy, the classification of things is structured in a tree or lattice that represents subsumption relation. This means, the usage of classes is usually restricted in a taxonomy. In a taxonomy, classes are subsets of all possible instances in the domain. However, ontologies are not necessarily limited to such hierarchies. But, to realize a conceptualization, axioms that constrain the interpretation possibilities of terms may be needed.

The basic components of an ontology are:

**Instances** are specific examples of a class in a domain.

**Classes, concepts** are the explicit descriptions of concepts in a domain of discourse and build the focus of most ontologies.

**Slots, properties, roles, relations** are the properties of each concept describing various features and attributes of the concept. Slots are used to give classes relationships to other objects (object properties) or to definitive values (datatype properties). Properties combine the objects with a predicate.

**Facets, role restrictions, axioms** describe a property of a slot. This property can be a con-



straint on valid values that slot can hold like a standard value or a value type.

### **Anatomical terminology resources**

Terminologia Anatomica is [TA1, 1998] the international standard on anatomical terminology. Its purpose is to standardize anatomical terminology of macroscopic anatomical structures (7500 structures defined). While it can be used to consistently annotate anatomical macro-structures, the terminology represents only terms but not knowledge.

The FMA [Rosse and Mejino, 2003] is most complete ontology in the domain of anatomy with support for machine-based inferences. The comprehensive description of anatomical structures ranges from the complete human body to the smallest structure, a biological molecule. To describe the phenotype of the human body the FMA defines 75'000 anatomical classes which are arranged in a subclass hierarchy using the Protegé software. 130'000 unique terms, 200'000 frames and 174 slots complete the representation of the human body. 2.5 million relationship occurrences are modelled. About 1 million occur on classes, and 450'000 describe relations between classes. The FMA consist of four interconnected components:

**anatomy taxonomy (AT)** classifies anatomical entities.

**anatomical structural abstraction (ASA)** defines the spatial relationship between AT.

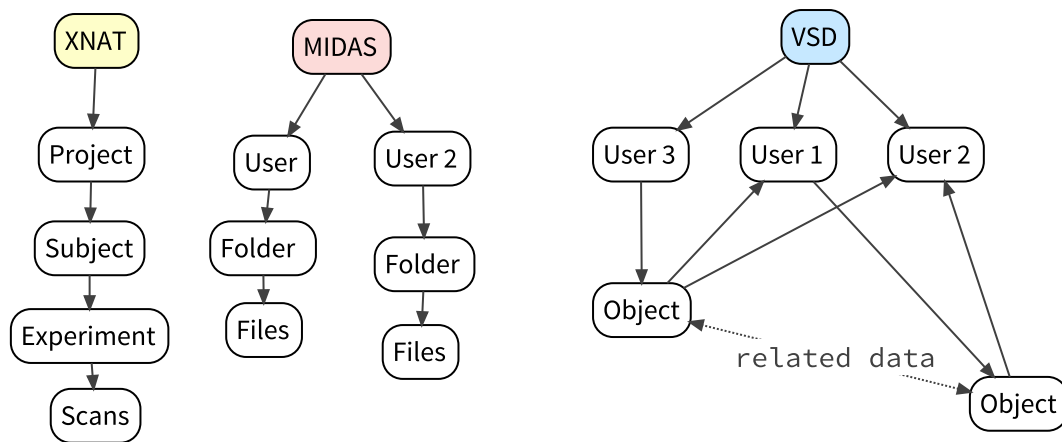
**anatomical transformation abstraction (ATA)** describes the prenatal/postnatal development of the AT entities.

**metaknowledge (Mk)** specifies the implementation principles of the entities in AT, ASA, and ATA and their relationships.

#### **2.1.4 Biomedical repository software**

Database systems play an important role in the organization of medical data collections since radiological acquisition devices like CT or magnetic resonance (MR) are generating digital images. In the clinical environment, PACS rapidly became the standard for local management of huge medical data collections. However, during the last decade, access to Internet resources changed the requirements of data management. While it is still essential for medical facilities to store their patient data offline in PACS, the importance of international access to medical image data for academic research is rising. First, generic data sharing solutions like Dropbox or Box provide a solid option to share data over the WWW. In parallel, dedicate software solutions to share medical image data haven been developed based on different concepts and functionalities (Table 2.5).

The differences between the three concepts are visualized in figure 2.4 and explained in the next paragraphs.



**Figure 2.4:** Conceptual differences of available biomedical Web repositories - The project/patient centric extensible neuroimaging archive toolkit (XNAT), the archive structure of midas and the object centric concepts of VSD

One option for such a repository software is to transfer the concepts of a PACS into a Web application. The Washington University School of Medicine has developed a software platform called XNAT which incorporates the patients specific structure of a PACS and additional options to store patient related informations on the Web. On XNAT, digital imaging and communications in medicine (DICOM) images are grouped into projects, subjects, and data acquisition sessions together with related research data. XNAT is an open source platform based on PostgreSQL, Oracle Java JDK, and Apache Tomcat.

Data centric computing is a second possibility to optimize the structure of commercial products, like Dropbox, for the needs of academic users. Kitwar Inc. developed a Web platform called Midas, which is freely available under the Apache 2.0 License and runs on an Apache Server. It uses PHP and either MySQL or PostgreSQL. In this free digital archive, stored data is organized into folders and items. Each file uploaded generates an item on the system, which is stored in a folder. This is very similar to the functionality of a file manager like Windows Explorer or Mac's Finder.

For the development of a research specific repository, a third strategy is to use generic objects as the core of the application. A generic object contains any number of object versions, which contain either one, two or any number of image file. In this concept the behavior and creation of object versions follow the definition of its specific type. Therefore, the system can only accept file types known to the system. A second part of this concept is to detach the objects from any binding

structure. To be more specific, the dataset is added to a catalogue of objects of the system and is available to all users if not specified differently. Each user can build his own project structure with objects available in the catalogue. This approach is used by the VSD and can be described in short as catalogue of data objects, similar to organizing songs into a playlist.

Table 2.5: Comparison of biomedical image repositories. Adapted from [NIC]

Client	XNAT	MIDAS	VSD
<b>Data transfer options</b>	DICOM via Web UI (HTTPS) DICOM browser tool XNAT batch uploading	DICOM via Web UI (HTTPS) MIDAS Desktop tool WebDAV	Via Web UI (HTTPS) Advanced Java Uploader WebDAV
<b>Queries</b>	Limited to a subset of DICOM tags (configurable)	Search by registered tags Full text search	Search by registered tags Full text search Anatomical search based on FMA ontology
<b>Controlled vocabulary</b>	-	NIH Mesh, Dublin Core	FMA Ontology for anatomical regions
<b>Sharing</b>	Yes	Yes	Yes
<b>Public access</b>	Yes	Yes	Yes
<b>Programming API</b>	WCF services RESTful	REST OAI-PMH	RESTful web services
<b>Supported data formats</b>	DICOM	DICOM (Any other files without information extraction)	DICOM ITK based formats HDF5
<b>De-Identification</b>	Yes	No, but can be realized using pre-storage filters	Yes
<b>Image processing</b>	No	Yes	Yes
<b>Core concept &amp; Data organization</b>	Project support collaboration system based on datasets	Multimedia storage system based on files	Research community platform based on objects (data catalog)
<b>Data organization</b>	Hierarchically in projects, subjects, experiments / sessions	Hierarchical folders for separated communities	Global object repository Private and shared folder hierarchies Linked objects
<b>Related data</b>	Folders	Folders	Object linking, folders
<b>Versioning</b>	unknown	On file level (user)	On object level (system)
<b>Collaboration, community</b>	No	Comments and Ratings	Comments Rating object discussions

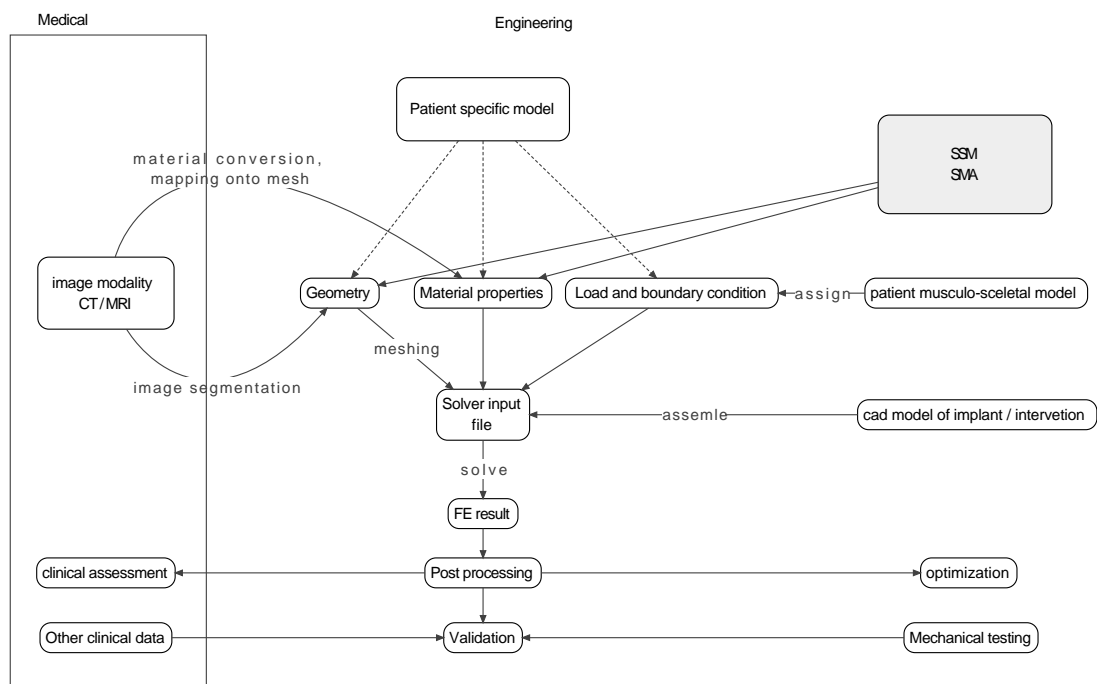
## 2.2 Patient specific finite element models in orthopedics

In general, engineering methods have always been part of the package to study musculo-skeletal disorders and in developing orthopedic implants to treat them. As a concrete example, the FEM has been able to improve the understanding of bone biomechanics like load transfer or fracture risk. The origins of FEM date back to the 1940's. Decades later it was introduced to the orthopedic field by Brekelmans in 1972. He used FEM to analyze stresses in a human femur under physiological loading conditions [Brekelmans et al., 1972]. During the next 30 years, FEM reached into different areas of biomedical research. FEM was used to perform stress analysis of bones, to study, to improve fracture fixation techniques and implant design, to extended to other biological tissues, and to process models [Huiskes and Hollister, 1993]. The availability of CT images allowed engineers to describe the geometry for the analysis with greater accuracy which finally established FEM in orthopedics [Prendergast, 1997]. Further advances in all aspect of FE modelling (compare to list in 2.2), and the availability of faster computers led to *patient-specific* FE models. These models can provide surgeons with additional informations or can help to interpret the clinical data. This knowledge can subsequently be used to optimize pre- and intra-operative planning. The main steps to create a *patient-specific* FE model are not different from other FE models. The difference to a general model is that the geometry, material properties, and loading conditions of a specific subject are used to create a valid model for this specific subject. The main steps to create a *patient-specific* FE model are described in detail in the following sections (Figure 2.5).

1. **Geometry** A set of nodal point spatial locations.
2. **Mesh** A set of elements connecting the nodal points.
3. **Material** Definition of the Mass properties.
4. **Constraints** Apply boundary conditions or restraints.
5. **Loading** Apply the loading function details.
6. **Analysis option** Definition the output parameters of the analysis.

### Image acquisition and patient geometry

CT's are best used for bone structures and density because of the high special resolution. But CT use a radiating source which can be harmful in high dosages. Therefore, Shim et al. [Shim et al., 2007] investigated the possibility of the reconstruction of a human dataset from spare image data. With a set consisting of only 7% of the original information, the root mean square error (RMSE) is 2 mm with an unacceptable high maximum of 1.5 cm. These errors suggest this method is



**Figure 2.5:** General FE modeling workflow

not suitable to create the geometry for patient specific FE models. However, in a subsequent study Shim et al. [Shim et al., 2008] tested the method against in vitro experiments for a simple load case. They compared the average RMSE of the strain prediction of the full dataset (15.8%, max. 29%), and the sparse dataset (mean 25.4%, maximum 48.4%) against the results of the experiments. These reported results suggest rejecting this approach of reducing the radiation for patient during the generation of a patient specific model building process.

MR images are ideal to provide doctors with high contrast resolution of soft tissue properties and geometries. Therefore, they are of less importance in biomechanics. However, advances in hardware and software of MR devices, make it possible to obtain high resolution MR images of trabecular bone [Majumdar et al., 1998]. Further advances would be very interesting for the biomechanical community since MR does not use an irradiating source [Poelert et al., 2013].

### **Mesh generation from images**

After image acquisition, the subsequent steps in the pipeline of *patient-specific* model are image segmentation and mesh generation. During image segmentation the anatomical structures are identified by labelling the corresponding grey values in the image. This process usually involves manual intervention and is therefore a time consuming process. Several (semi-)automatic segmentation algorithms are described in literature. The simple *intensity-based* segmentation algorithm is using pixel intensities to identify the structures of interest. However, they fail in case of image distortion, image artefacts or structure overlapping due to lack of appropriate spatial resolution of the acquired image. *Edge-based* segmentation is based on gradient fields and are sensitive to noise or structural gaps in the image. *Region-based* based algorithms can segment regions of a certain homogeneity. Other methods which use deformable algorithms morph an existing shape to the image data to ensure closed surfaces. Every method has its advantages and disadvantages, so they are often complementary and not competitive. Therefore, custom adaption and combination of different methods is the most effective way to obtain segmentations.

After the geometry is obtain through segmentation, a mesh can be generated. The mesh is called *voxel-based* if a predefined amount of voxels from the image source constitutes to one element. A *structure-based* mesh is created based on a surface model and is more flexible in its usage. More advanced meshes can be produced with *structure-based* models. For example, the elements density can easily be varied [Poelert et al., 2013].

## Material properties

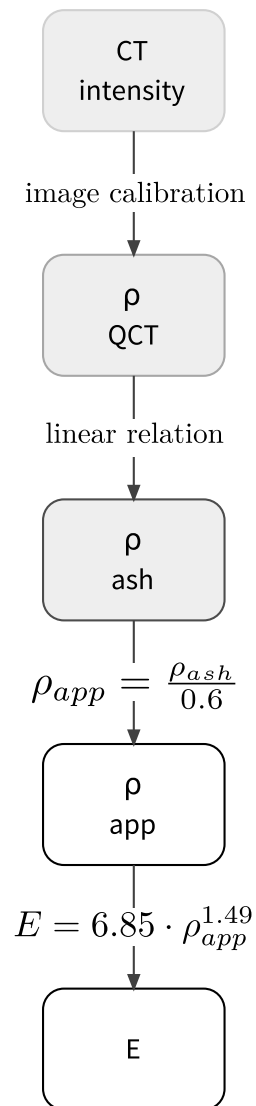
After mesh generation, the material property of each element has to be specified. Initially, the whole bone was considered homogeneous, isotropic and linear elastic. To account for the differences between cortical and trabecular bone properties, the most simple solution defines a cortical and a trabecular region and assigns individual Young's moduli to these regions separately. A more elegant approach uses the fact that local bone stiffness is directly related to the local bone mineral density. Therefore, the HU value of a voxel encodes the local stiffness of the bone represented by that voxel.

The mapping of material properties onto an element has different levels of difficulty. It is easy for voxel-based meshes. The average HU of a voxel cluster can be transformed using an appropriate density-modulus relationship [Keyak et al., 1990; Carter and Hayes, 1977]. For structured meshes, the HU can be extracted at the node positions in the image, transformed into Young's modulus and applied to the mesh element [Zannoni et al., 1998]. To account for the values in close proximity of a node, the surrounding values can be integrated over the volume of the element [Taddei et al., 2004]. And finally Helgason et al. showed that directly mapping mechanical properties to a node instead of an element lead to more accurate results if the partial volume effect is considered [Helgason et al., 2008b].

The accurate conversion of HU to bone mineral density (BMD), and to  $E$  can only be performed if the image is calibrated by a calibration phantom [Kalender et al., 1995]. After the calibration, the CT intensities can be translated to Young's modulus using different relationship between  $\rho_{QCT}$ ,  $\rho_{ASH}$ ,  $\rho_{APP}$  and  $E$  (Figure 2.6). Morgan et al. [Morgan et al., 2003] investigated the relationship between elastic modulus and density for trabecular bone with respect to the anatomical location. The reported relationships vary not only for anatomical structures but also by author. These published relationships haven been recently reviewed by Helgason et al. [Helgason et al., 2008a]. They found considerable differences between the investigated studies and were not able to fully relate these differences to the methodological inter-study differences.

The approximation of Young's models from HU assumes the bone to be isotropic. However, bone is considered to be an anisotropic material and is usually modeled as linear elastic instead of its slight viscoelasticity. To simplify the complex (discontinuous) micro-structure of bone, bone is treated as a continuum. A micro-FE model of the trabecular structure therefore might better catch the anisotropy. Such a model is computationally very demanding, and the required micro CTs are incompatible with clinical routine. Verhulp et al. [Verhulp et al., 2006] compared the effect of assumed isotropy between a continuum model and the corresponding micro FE model. They





**Figure 2.6:** Material property conversion: from image intensities to the Young's modulus

found little to now effect on the stress and strain distribution if anisotropy is excluded. On the other hand, micro FE models are better suited to model osteoporotic bone. It is still to be decided in which situations the modelling of anisotropy is required.

### **Loading determination**

Many studies can report good correlation between FE and in-vitro experiments if the load or displacement is predefined [Taddei et al., 2006b; Yosibash et al., 2007]. However, the loading conditions for simulation of in-vivo situations are more complex. There is currently no easy way to determine in-vivo forces, muscle insertion and force angle. In general, muscle forces are obtained indirectly by using a large scale musculoskeletal model while using inverse dynamics to determine muscle forces and moments [Glitsch and Baumann, 1997; Pedersen et al., 1997]. But still, the in vivo validation of these results remains challenging. Heller et al. [Heller et al., 2001] published a first direct comparison of musculoskeletal loading conditions computed from gait data with simultaneous measured hip contact forces [Bergmann et al., 2001]. They could show that computer models can predict the in-vivo data with an average error of 12% to 14% in four patients. It therefore seems possible to determine physiological-like musculoskeletal loading conditions that consider the interdependence of muscle and joint contact forces at the hip.

## 2.3 Population finite element models in orthopedics

As described in the previous section, the main challenges in achieving *patient-specific* models are the ability to obtain patient-specific information on anatomical shape, mechanical properties and boundary conditions. Instead of acquiring patient shape information from an image, the patient's shape and material property can be obtained by using SSM and statistical intensity model (SIM).

SSM were first introduced by Cootes and Tyalor in 1995 [Cootes et al., 1995] with the goal to capture the variability of shapes in a model. Such a principal component analysis (PCA) based model is able to describe a new shape because the variation of the model is captured. It can also be used to estimate how well a new shape fits the model. In medicine, with a SSM a 3D bone shape of an individual subject can be described with few modes of variation. Instead of acquiring 3D datasets, it seems possible to estimate a patient bone shape from simpler 2D modalities. A second option for SSM is to generate a large number of bone instances and to use these as the basis for FEA to analyze a large population. The SSM and SIM greatly depend on the number of the training data, which needs to be high for them to be of value. A statistical model (SM) is a tool to estimate population variability, learned from a set of  $n$  training data:

$$X = X^1, \dots, X^n$$

The following steps are required to successfully build a SSM.

1. Registration
2. Discretization
3. Normalization
4. Model building

### Registration

Accurate correspondence establishments between each training examples, are needed for the discretization. Failing to establish correct correspondences will result in a poor SM. Technically, registration is taking two sets of data, of which one is mapped into the space of the second in a way that similar patterns in each dataset are at the same position. Registration in medical image analysis is used for images, a set of points, surfaces, or meshes. The difficulty with this correspondence determination is its domain specificity. Therefore, many different image registration methods have been developed and classified in different ways [Maintz and Viergever, 1998; Pluim et al., 2003; Zitová and Flusser, 2003; Crum, 2004; Fitzpatrick et al., 2008; Sotiras et al., 2013].

Maintz et al. (1998) [Maintz and Viergever, 1998] categorize registration schemes into nine categories, [Fitzpatrick et al., 2008] Fitzpatrick et al. condensed it slightly to eight categories. Crum et al. [Crum, 2004] classified the registration methods into similarity measures, transformation models, and optimization strategies. Sotiras et al. [Sotiras et al., 2013] were using the same three categories (matching criteria, optimization methods, and deformation models) in their comprehensive survey on deformable medical image registration.

### Discretization

This aims to define a discrete shape domain,  $\Omega = \{p_1, \dots, p_N\}$ . The training shapes  $X^i$  are then approximated on this domain  $\Omega$  through the mapping function  $\phi^i$ :

$$X^i = (\phi^i(p_1), \dots, \phi^i(p_N)), \quad i = 1, \dots, N$$

where  $p_i$  are the coordinates and  $N$  the number of points describing the shape. In case of shapes, the domain is usually a 3D mesh function that maps each point to the corresponding point of an example shape. For images  $\phi_i$  assigns each point an image intensity.

### Normalization

After discretization, the shapes have to be rigidly registered using generalized Procrustes alignment. This is performed by optimally translating, rotating, and uniformly scaling ( $T$ ) the objects to minimize the shape and position differences between the shapes:

$$\sum |m - T_i(x_i)|^2$$

where  $m = \frac{1}{n} \sum T_i(x_i), \quad |m| = 1$

### Model building

After the registration, correspondence finding, and normalization, the set of training meshes consists of corresponding points and can therefore be used as input to PCA. Each shape  $X^i$  is now represented by a high dimensional vector  $x_i$  in the high dimensional space  $\mathbb{R}^{N \cdot d}$

$$x^i = (\phi^i(p_1), \dots, \phi^i(p_N)) \in \mathbb{R}^{N \cdot d}$$

The goal of the PCA is to reduce high dimensionality of the datasets into a set of organized uncorrelated components. PCA defines these orthogonal basis iteratively. These bases are aligned

with the principle directions (eigenvectors), order according to the importance of the component with respect to variance description (eigenvalues). Keeping only principle directions which are covering a defined proportion of the total variability reduces the dimensionality of the model. This is done using the mean shape  $\bar{x}$ :

$$\bar{x} = \frac{1}{n} \sum_{i=1}^n x_i \quad (2.1)$$

and the covariance matrix  $S$ :

$$S = \frac{1}{n-1} \sum_{i=1}^n (x_i - \bar{x})(x_i - \bar{x})$$

singular value decomposition (SVD) is used to decompose the covariance matrix:

$$S = UD^2U^T$$

The columns of  $U$  hold the principle components  $\phi$  and  $D$  contains the variance  $\lambda$  of each principle component in the diagonal.  $\lambda$  describes the amount of variance represented by the principle component:

$$D = \text{diag}(\lambda_1, \dots, \lambda_n) \quad (2.2)$$

$$x = \bar{x} + \sum_{i=1}^m \Phi_i b, \quad b = \lambda_i \alpha_i \quad (2.3)$$

where  $m$  ( $m < n$ ) is the number of principle components used. Each vector  $\alpha$ :

$$\alpha = \alpha_1, \dots, \alpha_m$$

defines a new unique shape instance. Usually,  $\alpha$  is considered to be a standard normal distribution where:

$$-3\sqrt{\lambda_i} \leq b \leq 3\sqrt{\lambda_i}$$

## Applications

Most SM only use SSM to include the shape variations. Only a few include a SIM to model material property information using image based [Querol] or mesh based [Bryan et al., 2010, 2012] approaches.

In 2006, Querol et al. presented a framework for statistical FEA [Querol] of the proximal femur. Their focus was on the design of orthopedic implants, which should perform best for a maximal

of the target population. They incorporated material properties and shape informations from a source of 11 non-rigidly aligned calibrate training CTs using PCA. From the SM, mesh instances were generated, intensities were sampled, converted to Young's modulus, and the biomechanical performance (bone stiffness) was analyzed using FEA.

Using the mesh based approach, Bryan et al. [Bryan et al., 2010] create a femur SM which generates meshes ready for FEA. The variations for both shape and material properties were captured in the SM based on 46 CT scans. To do this, a set of femurs was segmented with CT and the surface meshes were generated. The surfaces were registered to a selected reference mesh using an elastic registration scheme and the template volume mesh was morphed to fit the registered surface mesh. The image intensities were extracted from CTs and converted to Young's modulus using the density-elasticity relationship of Morgan et al. [Morgan et al., 2003]. This information was added to the vector of shape informations for the PCA. From this model, a population of 1'000 new femur instances was generated using a Gaussian sampling distribution of the weighting coefficients. The SM, the mesh quality, and instance generation were analyzed.

The same approach was used to investigate the femur neck fracture risk for a sideways fall [Bryan et al., 2009]. They sampled, using an adopted Monte Carlo approach, 1'000 femur instance with individual shape and material properties. In 2012, Bryan et al. [Bryan et al., 2012]. used the same model for a multi-femur FE study where they analyzed the impact of the femoral head resurfacing on load transfer in the proximal femur.

In her thesis [Bonaretti, 2012], Bonaretti compared both the image and mesh based approach for SM building and the subsequent FE mesh generation for a training set of femurs. Computational time, mesh quality, model compactness, and correspondence establishment differences were discussed. She concluded, that the image based approach has a better volume detection and produces a better FE mesh. The computational efficiency and topological mesh is superior in the mesh based pipeline. However, she did not give any definitive recommendation based on these findings.

Recently, SM are not only a tools to generate populations of instances but are also used to analyse and represent their FEA result in a compact way. Khalaji et al. used SSM to correlate anatomical morphology with mechanical measurements to predict the mechanical behavior of a new shape [Khalaji et al., 2009].

For the assessment of the individual fracture risk of the proximal femur, Schuler et al. created [Schuler et al., 2010] five SM for five regions of the femoral head from a training pool of 100 CT of human femur cadaver specimens. These models are then used to predict the fracture load of an

individual subject.

Fitzpatrick et al. combined probabilistic sampling and PCA for a multivariate sensitivity evaluation [Fitzpatrick et al., 2010]. They defined seven geometrical (alignment) and functional (loading) input parameters which were sampled using Monte Carlo and Latin Hypercube distribution. A FE model based on the MR of a healthy subject was created. The sampled input parameters were used to create a new FE model, and were analyzed using Abaqus explicit solver. To assess the influence of individual input parameters, they performed a PCA on the sampled input parameters. By varying the principal component (PC), the relationship between loading, alignment and mechanical prediction could be characterized. They tested the predictive capability of the SM on ten randomly generated new sets using a linear regression relationship.

Mousavi et. al. [Mousavi et al., 2012] applied a similar approach. Morphometric parameters obtained from a SSM were correlated with the results of FE simulation using artificial neural network (ANN) and PCA. With this technique, the full displacement field corresponding to a simplified 2D model of the prostate could be obtained without additional FE calculation.





## Chapter 3

### The Virtual Skeleton Database

This chapter deals with the first part of the project - the handling of image data for research on a large scale. The VSD, a web repository to store, share, and manage medical research data with focus on SSM is proposed as Web solution. In a second section, some technical aspects of the VSD are highlighted. Important concepts, and their consequences on the VSD processes are outlined. Additionally, the acquisition of the full body dataset collection is explained in detail and the technical aspects of an ontology based search are presented.

#### 3.1 The Virtual Skeleton Database: An Open Access Repository for Biomedical Research and Collaboration

M. Kistler (1), S. Bonaretti (1,3), M. Pfahrer (2), R. Niklaus (2) and P. Büchler (1)

- (1) Institute for Surgical Technologies and Biomechanics, University of Bern, Switzerland;
- (2) UCSF School of Medicine, University of California, San Francisco, CA, United States
- (3) Engineering and Information Technology, Bern University of Applied Sciences, Biel, Switzerland

##### 3.1.1 Abstract

**Background** Statistical shape models are widely used in biomedical research. They are routinely implemented for automatic image segmentation or object identification in medical images. In these fields, however, the acquisition of the large training datasets required to develop these models is usually a time-consuming process. Even after this effort, the collections of datasets are often lost or mishandled resulting in replication of work.

**Objective** To solve these problems, the Virtual Skeleton Database is proposed as a centralized storage system where the data necessary to build statistical shape models can be stored and

shared.

**Methods** The Virtual Skeleton Database provides an online repository system tailored to the needs of the medical research community. The processing of the most common image file types, a statistical shape model framework, and an ontology-based search provide the generic tools to store, exchange, and retrieve digital medical datasets. The hosted data are accessible to the community, and collaborative research catalyzes their productivity.

**Results** To illustrate the need for an online repository for medical research, three exemplary projects of the Virtual Skeleton Database are presented: (1) an international collaboration to achieve improvement in cochlear surgery and implant optimization, (2) a population-based analysis of femoral fracture risk between genders, and (3) an online application developed for the evaluation and comparison of the segmentation of brain tumors.

**Conclusions** The Virtual Skeleton Database is a novel system for scientific collaboration for the medical image community with a data-centric concept and semantically driven search option for anatomical structures. The repository has been proven to be a useful tool for collaborative model building, as a resource for biomechanical population studies, or to enhance segmentation algorithms.

### 3.1.2 Introduction

Beyond the obvious variability in appearance, a large anatomical variation among the human population exists. For example, even for similar looking people, the human skeleton has a large variability in bone shape, internal structure, and mechanical strength. Following the systematic use of modern imaging techniques in the medical routine, the interest in studying human variability grew in the medical research community. Roughly two decades ago, Cootes et al. [Cootes et al., 1991] introduced the first statistical model to quantify anatomical shapes [Cootes et al., 1994]. This technique became very popular in the medical image analysis community and has been used in a wide range of applications: novel implant design [Hawkes et al., 2005; Kozic et al., 2010], surgical planning [Zheng et al., 2009; Schumann et al., 2013], and improving image segmentation [Heimann and Meinzer, 2009; Bauer et al., 2013] and image registration [Albrecht et al., 2008]. More recently, these models have been extended to combine the description of the anatomical shape with mechanical information to analyze the risk of fracture in a population [Bryan et al., 2009, 2012] or to design orthopedic implants [Bou-Sleiman et al., 2011].

A recurrent problem that is faced when applying SSM to specific clinical indications is the large amount of data required to build a valid model. A repository for images and processed data is

therefore vital for the fast development of new applications or image processing algorithms based on this technology. However, the existing solutions for storing medical images are not appropriate for building statistical models. In the clinical environment, PACS was introduced in the 1980s to manage clinical images of patients [Liu et al., 2004; Hood and Scott, 2006]. The DICOM is the standard file format used in PACS, which ensures that the proper metadata concerning the patient and the image technique are available to the radiologist. This system is ideal for archiving clinical data but is ineffective if the user wants to retrieve a large amount of data corresponding to the same anatomical site. In addition, due to legal restrictions and data protection laws, it is not possible for researchers to freely access the large database of medical imagery stored in clinical institutions. Therefore, significant efforts are necessary to obtain data, to process them, and to build the models. However, even after this time-consuming process, collections of data are often lost or mishandled in research institutions, resulting in replication of work, even within the same institution. A centrally organized system can limit or even suppress these barriers, which hinder fast and innovative approaches in medical image research.

Inspired by PACS and institutional repository software [DSpace; Staples et al., 2003; EPrints], several projects have been developed for the biomedical research community. For example, the XNAT [Marcus et al., 2007] has developed an open source solution for the neuroimaging research community. Recently, the Midas media archiving platform [Jomier et al., 2009] was developed to extend the functionality of DSpace [DSpace] repository software. This platform aims to simplify the collaboration between researchers and to provide more flexibility on the supported file format and data structure. Several other projects are building infrastructures to host data collections in their respective research domain. For example, the Living Human Digital Library [tlh] aims to provide a collection of raw and processed data on the anatomo-functional characteristics of the human musculoskeletal system at dimensional scales spanning from the whole body down to the molecules. However, this system is limited to a small number of human bodies generated during the project and does not allow the user to upload their own datasets. The Internet Brain Segmentation Repository [ibs] provides manually guided expert segmentation along with magnetic resonance brain image data. All these projects provide extremely important data to the scientific community, but they either consider a limited number of subjects, are specific to a certain organ or pathology, or present a mix of patients and pathology. A general database where medical image datasets are stored and further processed toward statistical shape modeling is required to model the variability of the complete human anatomy.

The objective of the VSD is to provide and maintain an open access repository for scientific re-

searchers to archive, search, preserve, trace, and share data resources for statistical models. In this article, the authors describe the main concepts implemented in the system and demonstrate its operation on exemplary use cases.

### 3.1.3 Methods

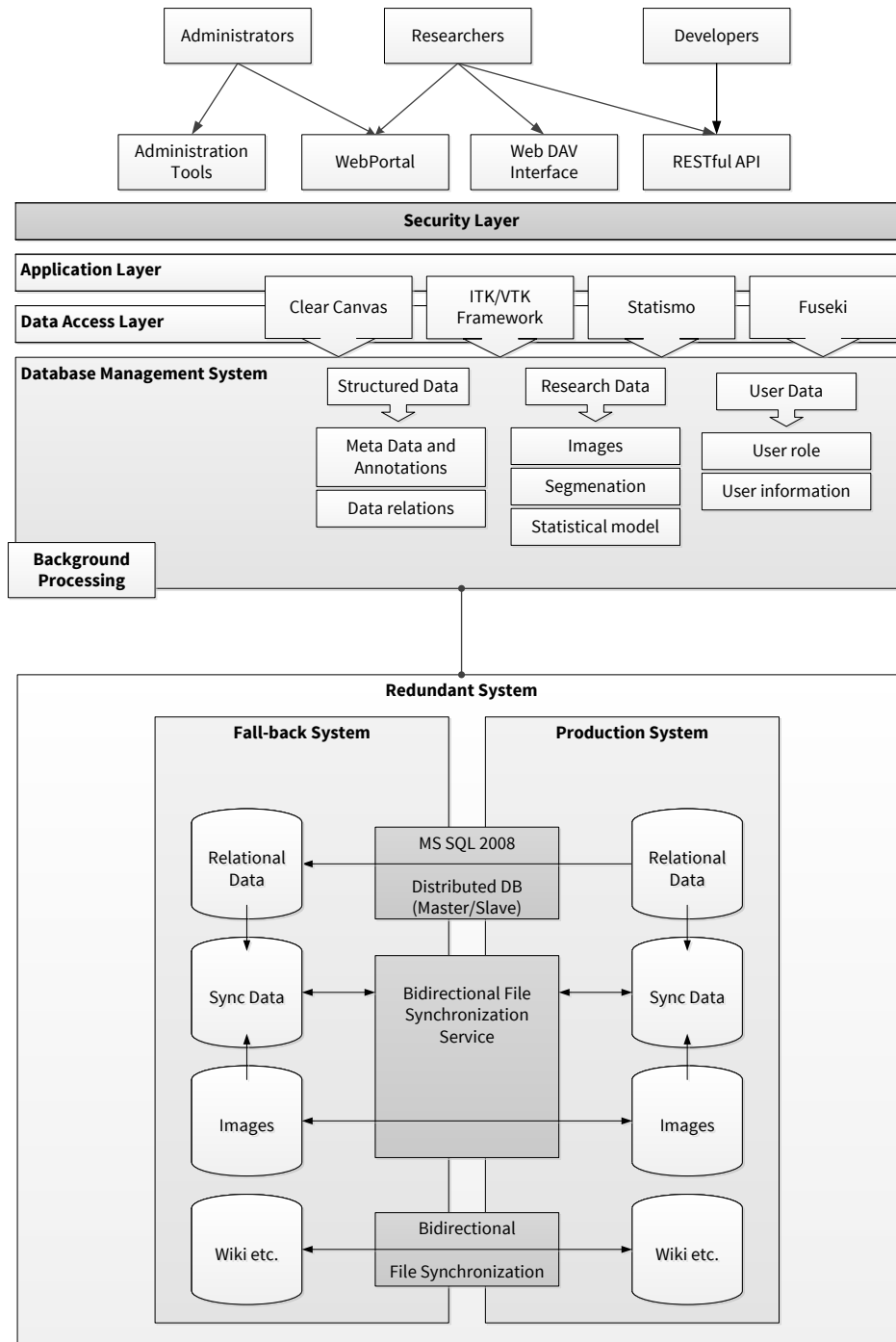
#### General Concepts

The VSD can be described as a catalog of data that is accessible and organized with a focus on, but not limited to, building statistical anatomical models. Therefore, the VSD was built around the concept of *data objects*, which constitute the basic element of the system. These data objects can be any type of image file, processed data, or models. This approach provides a large flexibility to the system in terms of data formats, data organization, and data collaboration. The design is intended to have the capacity to provide the same basic functionality as a PACS, but it is more flexible and can integrate additional research data, such as labeled images and statistical models.

#### Technology

The architecture of the VSD is based on the classical multitier architecture (Figure 3.1). The topmost layer provides multiple interfaces: the Web portal for managing and sharing the data, WebDAV for direct interaction with different file systems, and a REST API for interaction with other scientific applications while the administration functionality is provided through a Web application. The middle tier provides all the necessary application logic but also contains the functionality covering security aspects. Data storage and data access are provided on the next tier. Aside from the relational database system for storing the information, the system integrates other tools and frameworks for specific purposes; ClearCanvas is used to handle DICOM files, Insight toolkit (ITK)/visual toolkit (VTK) for image processing, Statismo for SSM, and Fuseki for the integration of ontologies. The scalable data layer (database and data) is equipped with a mechanism to provide a full synchronization between two functional redundant systems.

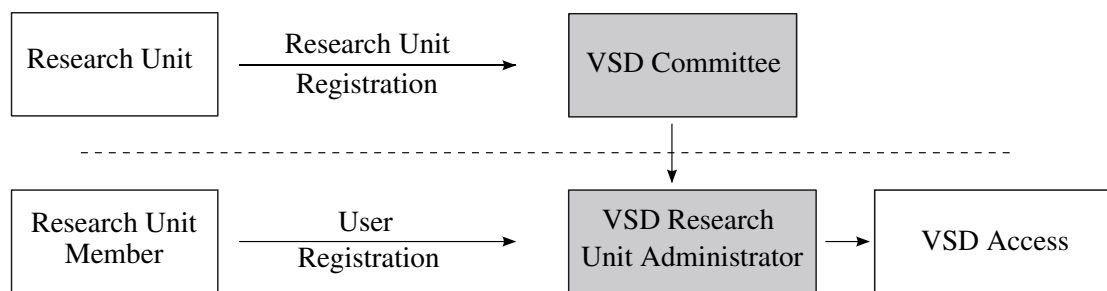
The development of the VSD was based mainly on Microsoft technologies. The system relies on a SQL database and the Microsoft internet information service (IIS) Web-server. For the application development, Microsoft Razor, which is built on the Microsoft .NET technology, was chosen to enable consistent development of a responsive Web service. The Razor application framework was complemented by the established frameworks Bootstrap [Bootstrap, 2013] and jQuery [jQuery, 2013] for a smooth and dynamic user experience on the website.



**Figure 3.1:** Schematics of the multi tier architecture of the VSD, which consists of different types of interfaces, an application logic and security layer, and data access and data storage.

## Registration

Standard user and object rights management is required to control access, visibility, and sharing of the objects stored on the VSD. But, since legal and ethical aspects play an important role when medical images are involved, a two-step registration procedure and user management were implemented. The system's registration procedure was designed to build the VSD as a research-only repository (Figure 3.2). In the first step, academic institutions can register as research units. After approval of the research unit by the VSD administrator, each research unit can administer their members and is responsible for controlling access to the research data and ensuring the proper rights and licenses are attached to their uploaded datasets.



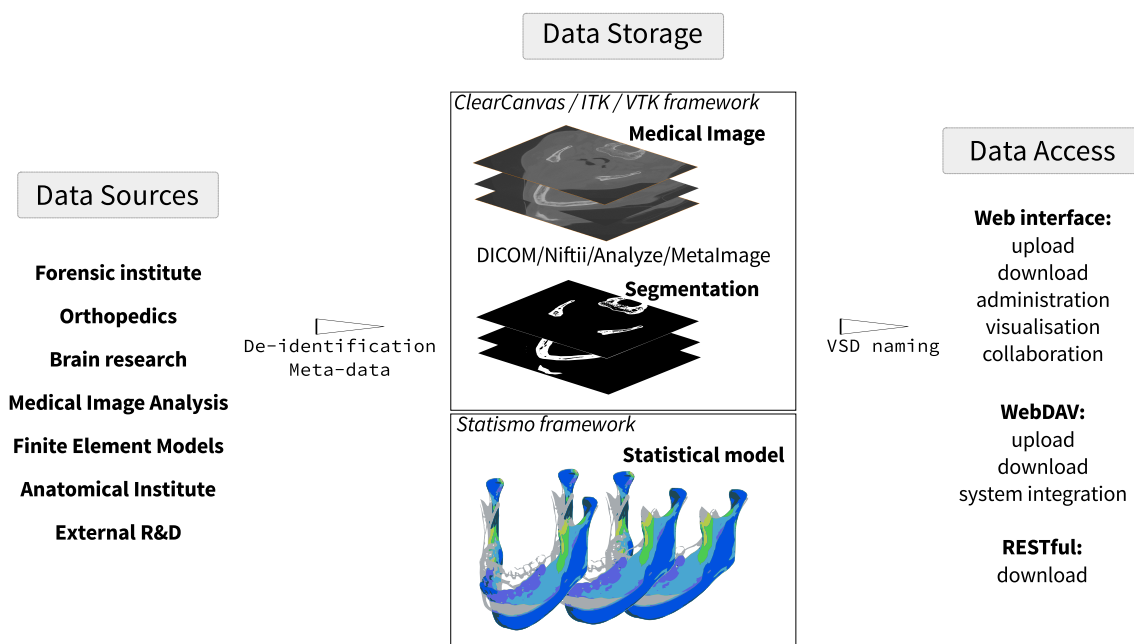
**Figure 3.2:** Registration process - Top: registration of a new research unit and appointment of a research unit administrator. Bottom: individual users can register to a research unit and have to be accepted by the respective administrator.

## Medical Images

The system provides the user with multiple options for the image upload. A standard Web upload form and a Java applet are available. While the standard browser upload is most convenient for small images, the Java applet is able to submit files larger than 2GB to the server. Additionally, if close integration in the local system is required, the VSD can be accessed through the WebDAV, which allows for customized upload workflows. The VSD integrates the most common image formats used by the medical image analysis community, but theoretically any kind of medical image format could be integrated. The VSD can read classical DICOM files through the ClearCanvas framework, and all image types recognized by the ITK library (MetaImage, Niftii, and Analyze) are accepted (Figure 3.3). During the upload process, metadata are extracted from the images, preview images are generated, and a de-identification of the medical image is performed. The de-identification consists of file type-specific header manipulation and the replacement of the original file name by a generic VSD file name, preserving the information only for the original contributor.

To keep the storage system efficient, the uploading functionality has mechanisms to avoid duplicated objects on the disk and supports multiple versions of the objects.

To assign proper and consistent metadata to the images, the VSD features a publishing concept where uploaded data have to be reviewed before they become available to the other users. During this process, the user is asked to review the uploaded dataset and to provide the missing information. First, the dataset has to be characterized by annotating the anatomical structure depicted in the image. For this metadata, the anatomical terms are taken from the comprehensive FMA ontology [Rosse and Mejino, 2003]. This ontology includes more than 75,000 anatomical terms and 450,000 direct relations between classes. Additional metadata like age, gender, and image modality can be filled to enrich the meta-information content of the image. If a related dataset already exists on the VSD, the user can reference this data by linking both datasets together. For example, different image modalities of the same patient and anatomical structure can be linked and therefore grant a direct access between both datasets. As a last step, a Creative Commons (CC) license can be attached to a dataset to specify the intended offline usage. To control the sharing of the data on the website, predefined permission sets are available to specify the access rights. After a final activation, the data are accessible to other users of the VSD.



**Figure 3.3:** Conceptual overview of the Virtual Skeleton Database - data from various sources are stored in the VSD and can be accessed, organized, and downloaded.

## Data Organization

Users can search the available online data catalog to find the datasets relevant for their projects (Figure 3.4). The system allows the creation of virtual folders to organize the available datasets, which provides the user with the flexibility to freely create their personal workspace. Data objects are not physically moved or duplicated, but the system creates a reference to the data object, retaining the original file permission and ownership. For collaboration or other purposes, the user can share parts of their workspace by changing the permission of the folder accordingly. To simplify the collaboration within a research unit, the system provides a default shared group folder, which is accessible and manageable by all members of the research unit.

Several functions provide additional information to the users and help them identify the relevant datasets. Each dataset can be rated for quality and tagged with personal comments. To comment on the object publicly, a discussion thread can be initiated in the integrated VSD forum. Additionally, the search function allows users to find specific metadata including ontology terms. The ontology search is using SPARQL, which queries the semantic information contained in the ontology. This feature enables a powerful search where anatomical substructures can be identified within stored data objects. For example, a user can search for images containing the body part *Leg*. With a conventional index-based search, only data annotated as *Leg* can be retrieved (zero search results in the VSD). With the semantics of the ontology, the VSD will find and return data that are or contain the *Leg* (69 datasets found in the VSD).

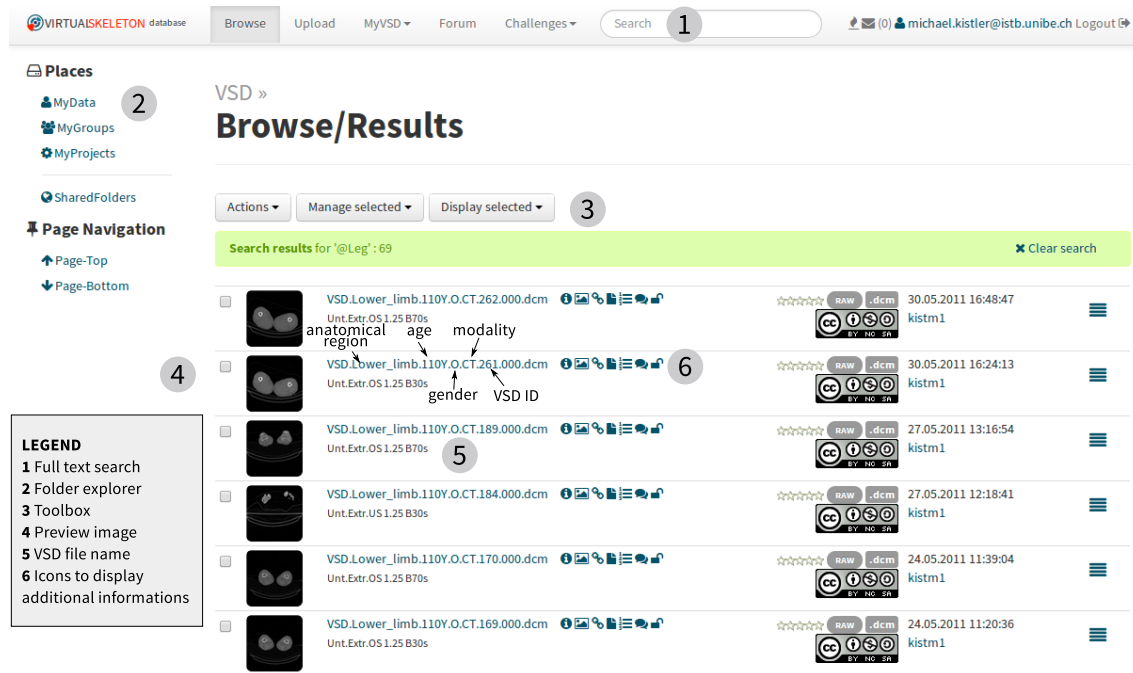
## Retrieve Images

An individual dataset as well as a folder structure can be downloaded from the VSD for processing on a local machine. The data are wrapped for download into a compressed archive file to reduce file size and to preserve the folder structure from the VSD. For local access to folders on the VSD, the user can mount the WebDAV folder as a network drive on their computer.

## Segmented Images

Images that contain segmentation labels can be uploaded the same way as medical images. The system identifies how many anatomical structures are labeled in the segmentation image, the de-identification is performed, and the thumbnail images for preview are extracted. During the review process, all the labels of anatomical structures have to be specified and the segmentation technique can be described. The uploaded segmentation data can then be linked to original medical images





**Figure 3.4:** VSD Web interface to browse data with folder explorer: MyData=Location of the user's uploaded data; MyGroups=Default collaboration folder accessible to all group members; MyProjects=Folders to organize data into personal projects; SharedFolders=Folders of other VSD members which are shared to the user.

or to other segmentations of the same structure, which have been performed using a different technique.

## Statistical Models

To standardize the building and storage of shape models, the open source library "Statismo" has been developed [Lüthi et al., 2012]. An important aspect of this library is that it proposes a simple file format to store shape model, based on the hierarchical data format (HDF5). The VSD recognizes shape models stored in HDF5 and is able to extract important information about the model, such as the datasets used or the registration technique used. After the upload, the review process is similar to that of the images, asking the user to annotate the anatomical region and to specify the license and access rights.

Three exemplary projects using key functionalities of the VSD are presented. First, the creation of a statistical model of the cochlea for surgery and implant optimization is described. As a second example, a statistical appearance model of the femur is used to analyze fracture risk within a population. Finally, an online segmentation challenge hosted by the VSD is presented.

### 3.1.4 Results

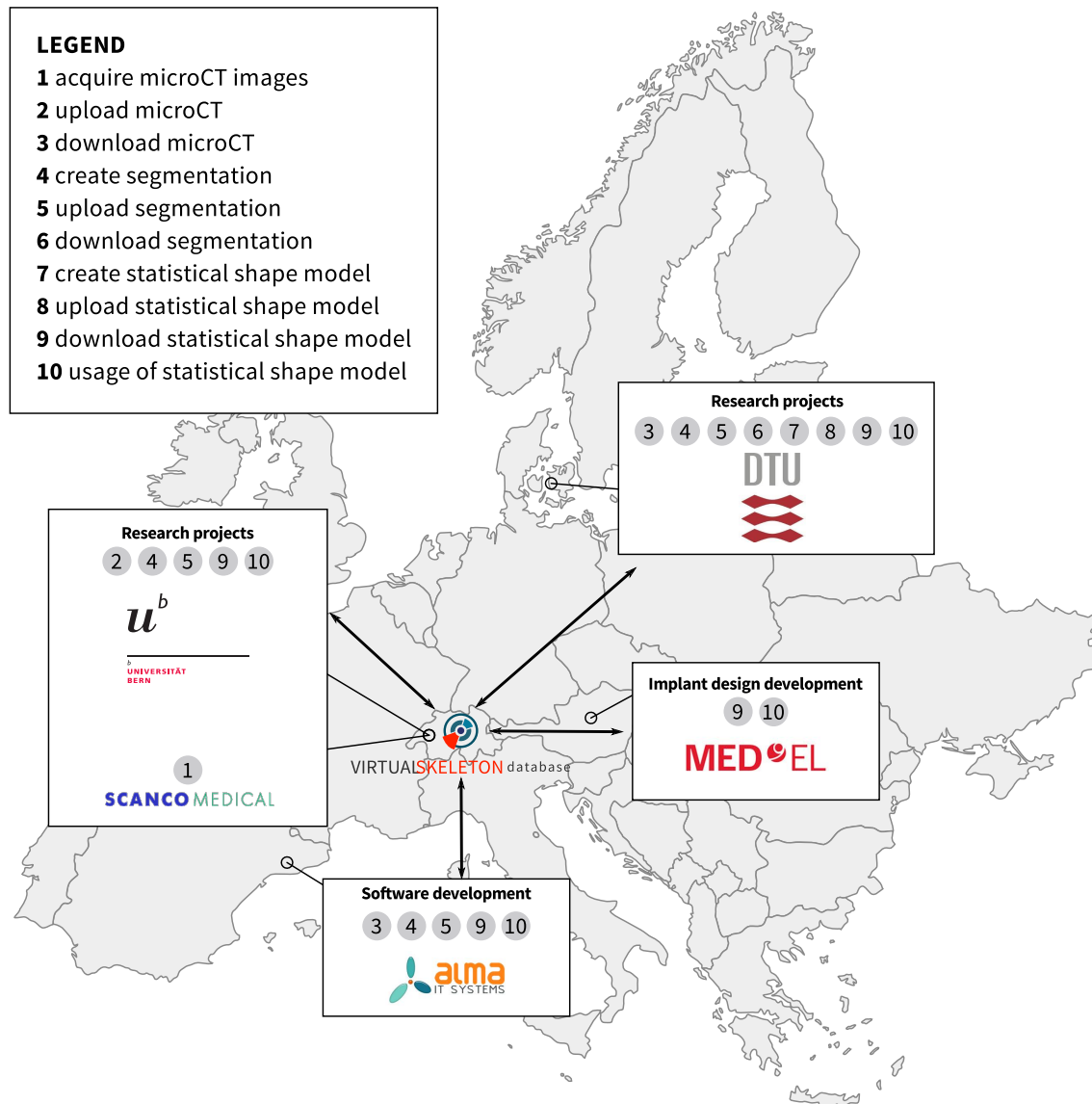
#### International Collaboration on Statistical Shape Model of the Cochlea

The goal of this international collaboration project, the Hear-EU project [Gonzalez], is to improve cochlear implants. This surgical procedure tries to overcome hearing loss by implanting a device that accesses the cochlea of the inner ear. Clinical expertise and detailed information about critical structures close to the surgical site are needed for such a surgery. Since this surgical intervention is very complex and a vast variety of patient anatomies exist, the project hypothesizes that a comprehensive knowledge of the involved anatomical structures would enable improvements for implant design and for surgical planning. In this context, the VSD acts as a data hub (Figure 3.5; map adapted from [Dalet, 2013]) to assist the building of a statistical shape model of both the middle and the inner ear. High resolution CT images with a data size of over 5GB are uploaded to the VSD and will be processed by different institutions across Europe. The resulting segmentation images will be subsequently re-uploaded to the VSD. Having both the images and processed data available will enable the Technical University of Denmark to create a statistical shape model of the regions of interest. Finally, the shape models will be available on the VSD and can be used by different teams to optimize surgical procedure as well as the functional outcome of the surgery on a patient-specific basis.

#### Biomechanical Femur Population Study

The authors searched the VSD for available lower extremities datasets to conduct a study on the fracture risk on this population. A total of 72 female and 72 male subjects were isolated and retrieved together with their available metadata. The population consisted mainly of Caucasian (114) supplemented with Asian (28) and African (2) subjects. The female subpopulation's body mass index (BMI) (mean 26.4, SD 5.5) was slightly higher compared to the male (mean 25.5, SD 4.9) subjects, while the male represented an older subpopulation than the female group.

For each gender, the statistical appearance model was calculated using the image-based approach described by Bonaretti et al [Bonaretti, 2012] and polyaffine demons [Seiler et al., 2011]. From both appearance models, 1'000 instances were created and biomechanical finite element simulations were performed with a loading situation corresponding to normal walking [Heller et al., 2001; Speirs et al., 2007]. The bone intensity values were converted into material properties [Morgan et al., 2003; Schileo et al., 2007] and mapped onto each node of the FE mesh of the second order tetrahedral elements.



**Figure 3.5:** Collaborative network, interactions, and workflows for the Hear-eu project on cochlear implants.

The relationships between the fracture risk in the femoral neck and morphometric measurement was performed (Table 3.1). Six geometrical measures were identified [Bergmann et al., 2008][Gray, 1985] (Figure 3.6) as possible risk predictors. As a mechanical parameter, the average Young's modulus in the femoral neck was calculated. All predictor parameters were centered and normalized to perform the regression and evaluate their influence in femur fracture risk.

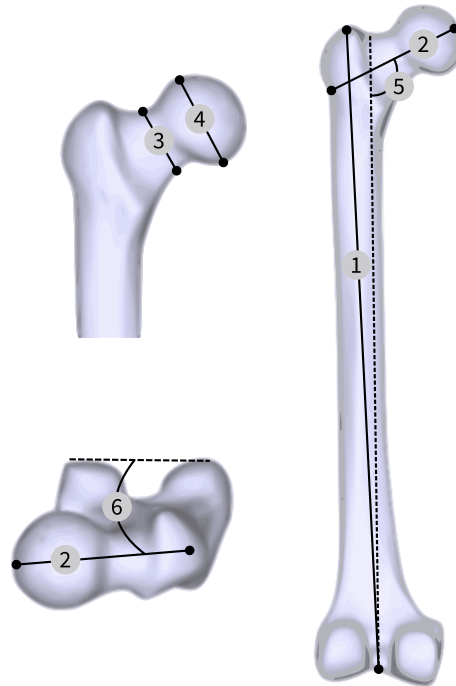
For both genders, body weight was identified as the most relevant predictor for fracture risk while the mechanical measures showed a lower influence of fracture risk in general. In contrast, among geometrical parameters, the neck-shaft angle could be identified as playing a predominant role for both populations, whereas the order of importance of the parameters shows clear difference between men and women. The complete study results are presented in [Bonaretti, 2012].

**Table 3.1:** Measured bone geometry and bone mechanical properties for men and women.

<b>Parameter</b>	<b>Male, mean (SD)</b>	<b>Female, mean (SD)</b>
Femur length, cm	42.6 (2.9)	40.8 (2.5)
Neck length, cm	10.5 (0.8)	9.9 (0.5)
Neck width, cm	3.9 (0.3)	3.6 (0.2)
Head width, cm	5.0 (0.5)	4.5 (0.5)
Neck-shaft angle, degree	128 (4)	130 (4)
Anteversion angle, degree	15 (7)	19 (7)
Young's modulus, GPa	2.7 (0.7)	3.4 (0.5)
Body weight, kg	64 (14)	60 (14)

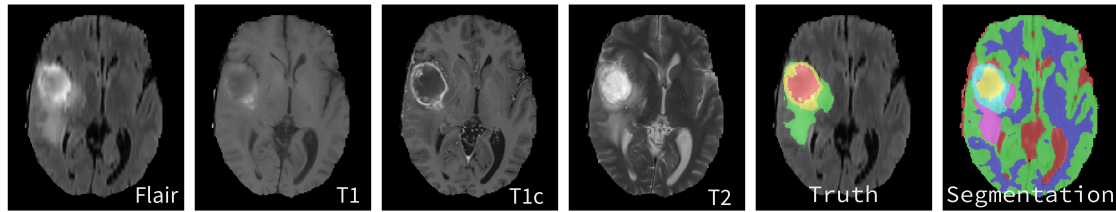
### Segmentation Challenge for Brain Tumors

The VSD was chosen by the multimodal brain tumor segmentation (BRATS) challenge organizer to host their data and challenge. The data were publicly available to any team around the world to develop and train their segmentation algorithms. In addition, the VSD was used to evaluate the submission of the competitor during the challenge, which took place during the annual conference of the medical image computing and computer assisted intervention (MICCAI) Conference 2012. Hosting such a challenge required several functionalities, which illustrates most of the features of the system. The VSD hosted multicenter MR imaging sets and their related ground truth, which were defined by inter-reader agreement from clinicians. The clinical segmentations were used to determine the accuracy of the segmentation of tumor subregions. A total of 80 brain MR and segmentations were available to the competitors for training purposes (Figure 3.7). An additional 30 challenge datasets that consist only of MR data were available for download. Their



**Figure 3.6:** Geometrical measures: (1) femur length, (2) neck length, (3) neck width, (4) femoral head width, (5) neck-shaft angle, (6) anteversion angle.

respective ground truth segmentation was hosted on the VSD but the download was protected through appropriate file permission. The users uploaded their segmentation through the Web interface, reviewed the uploaded segmentation, and started an automatic evaluation process. The VSD automatically identified the ground truth corresponding to the uploaded segmentations. The evaluation of the different standard parameters used to evaluate the quality of the segmentation (such as Dice coefficients) runs in the background and takes less than 1 minute per segmentation. Individual and overall results of the evaluation were automatically published on the VSD webpage and were downloadable as a comma separated values (CSV) file for further statistical calculations. The VSD has evaluated more than 3'000 segmentations and had over 80 registered users for the BRATS 2012 group. The service was successfully used for the challenge in 2012 when around 700 evaluations were handled by the system within the last 2 hours of the competition. The results were presented in the proceedings of MICCAI 2012 [Menze et al., 2012], and the data are now open to anyone who wants to evaluate new segmentation tools against previous BRATS evaluation sets. So far, around 15'000 additional segmentations have been successfully benchmarked by the VSD.



**Figure 3.7:** Exemplary multimodal MR images of a high-grade Glioma patient 0001 with truth and label result from an automatic segmentation of a BRATS participant (red=cranio spinal fluid, green=gray matter, blue=white matter, yellow=necrotic, turquoise=active tumor, pink=edema).

### 3.1.5 Discussion

#### Principal Findings

The VSD features various innovative approaches to provide an efficient and easy-to-use open access repository to the medical image and modeling community focusing on the creation of statistical models. The standard image and segmentation file types (DICOM, MetaImage, Analyze, and Niftii) can be read and stored by the system. Additionally, the Statismo framework with a standard file type for statistical models has been included, which allows statistical models to be shared, hosted, and collaborated on via the VSD. The complete data used in the process of building a statistical shape model can be stored and tracked through the related data information in the VSD. Built in as generic a way as possible, the VSD hosts a catalog of data objects, which can be individually organized by users according to their needs. The anatomical structures are annotated using a comprehensive ontology allowing the integrated search algorithm to identify anatomical structures within datasets, which is not possible with a standard index-based search.

Access to the VSD is open to research units and their members. Users are invited to contribute by uploading images and processed data, which will increase the data pool available on the VSD. By adding their data to the VSD, the users profit from the permanent accessibility provided through the Web service. This approach supports the current trend towards open access and re-usability of research results, which should be accompanied by the policy of scientific journals. This facilitated access to data should enhance productivity and research quality through competition and stimulate improvements by the research community. The three example projects presented highlight the benefits of the VSD and its contribution to statistical model building, population-based research, and object identification in medical images.

### **International Collaboration on Statistical Shape Model of the Cochlea**

With the VSD, it is possible to streamline the process of SSM building for accurate population-based models in a multidisciplinary project setting. All parties have access to the same dataset and the metadata. The individual processing tasks can be distributed while the research data is stored on the VSD. An institution that has access to high resolution medical data can provide researchers with medical image analysis background with data for segmentation. Once these segmentations are available on the VSD, the SSM can be engineered and provided through the VSD. The statistical model then can be implemented into surgical planning, segmentation algorithms, or implant design improvements. Since every processing step is stored on the system, this approach ensures a high level of reproducibility of the model building and quality control.

### **Biomechanical Femur Population Study**

The VSD provides a service to overcome the limitation of the small number of available subjects in mechanical studies by promoting statistical shape model, hosting the respective images and processed data. This approach enables population-based studies. These population-based investigations allow not only study of the mechanical behavior of a large amount of bones, but also the comparison among different groups of populations. They allow study of the shape and volumes of anatomical structures and, consequently, clinically relevant parameters. As presented, for geometrical parameters of the femur, the neck-shaft angle plays a predominant role for fracture risk of both genders. Additionally, differences between men and women could be identified due to the use of a population-based model. Similar approaches could be used to perform virtual evaluation of orthopedic implants and optimize their design to market-specific needs.

### **Segmentation Challenge for Brain Tumors**

Accurate segmentation is a critical step in visualization for treatment planning or later to monitor the therapeutic outcome. Manual segmentation from experienced experts is generally considered to contain the most reliable information. However, a lot of effort goes into the development of algorithms to automate this process. But, for almost every anatomical structure, those algorithms have to be adapted or trained. As a consequence, these techniques have to be constantly enhanced. To catalyze the innovation, researchers need image data and the opportunity to compare their results. The VSD provides the data repository and an evaluation platform, which are both needed to enhance those algorithms. The usefulness of such a platform in order to improve the sensitivity and specificity of the identification of glioblastoma is documented by the activity and registration

numbers on the VSD. Due to the object-centric architecture of the system, the VSD is able to host any similar setup for other anatomical structures.

### **Limitations and Further Directions**

Although already populated with an initial set of data, the collection still needs to grow significantly. Constant efforts are being made to increase the amount of data, which are also expected to increase with the dissemination activity and number of users. Additionally, the VSD is expanding the supported file type based on requests from users. Finally, an additional interface to exchange data with the system is planned based on the REST interface, which will allow for online preparation of statistical models.

To deal with the delicate aspect of data privacy, the VSD provides automatic tools such as de-identification, metadata stripping, and file name replacement. However, these tools cannot prevent the possible identification of a patient associated with objects visible in the medical images themselves. In some case, a special plate or implant, a rare malformation, or the image of the head is sufficient to recognize the subject. Therefore, the owner of the data is responsible for ensuring that they have the right to share the images and that a proper anonymization has been performed by removing identifiable regions of the image. However, the functionality on the VSD to give the data a two-level control (permission and license) allows the user to ensure that images are accessible only to individuals allowed to work with their data.

### **Conclusions**

The VSD allows users to very flexibly manage and organize their data and online workspace. The VSD provides researchers with access to a growing community-filled data repository. The authors showed a novel system for scientific collaboration in the medical image community with a unique object-centric concept and semantically driven search option for anatomical structures for medical images, processed data, and statistical models. However, the clientele is not limited to these communities since the system can and will deliver functionality for other file types and their applications, for example, finite element models. We have presented three applications that benefit from such a Web application. The VSD is a valuable solution especially in the context of the growing needs of open access, re-usability, and reproducibility of scientific work.



## 3.2 Technical aspects of the VSD

In this section, several technical and conceptual solutions, which would have exceeded the papers scope, are presented in detail. The ontology integration and data collection are presented. In the last part, some engineering details of the VSD are outlined.

### 3.2.1 Ontology

As described in section 3.1.3, the FMA ontology terms are used to annotate the datasets. This controlled annotation of the anatomical regions allows to use the semantics of the underlying FMA ontology. Its semantics allows querying anatomical structures within anatomical regions. In context of the VSD, the user specifies an ontology term like *Leg* in the search field on the VSD Web interface. The server maps the term to the identifier (*FMAID*) of the FMA. This identifier, a Fuseki service [Fuseki, 2013], and a dedicated SPARQL query is used to search for anatomical structures which match the search term *Leg* or contain the *Leg* according to the semantics of the ontology (Figure 3.8a). The FMA is available in different formats: Protégé and MySQL versions, several OWL conversions, and a open biological and biomedical ontologies (OBO) version. Since the goal is to query the ontology with SPARQL queries, the OWL version of FMA, version 3.2.1 (Listing 3.1) is used by the VSD.

**Listing 3.1:** Source of the used FMA version

```
version fma-3.2.1.owl.gz
url      https://code.google.com/p/fma-in-owl/downloads/list
```

To actually use the ontology with the Fuseki server, the OWL file has to be converted to another RDF serialization (a Turtle format) via a command line tool called *tdbloader* available from the Jena Tdbloader [2013] project (Listing 3.2).

**Listing 3.2:** OWL to RDF conversion

```
tdbloader --loc=FMA
          --graph=http://virtualskeleton.ch/data/fma
          fma-export.ttl
```

This port of the initial FMA database can be queried if loaded by the Fuseki server. The original FMA ontology has a direct relationship for *is\_a* and *part\_of*. Unfortunately, the available converted RDF format does not have this direct *part\_of* relation. It is divided into *regions\_part\_of*, *constitutional\_part\_of*, *systemic\_part\_of*, and *member\_of*. Therefore, a new graph representation

had to be created where these relations are explicitly modelled (Listing 6.1). Loading the inferred and the full RDF representation of the FMA into the Fuseki service, the SPARQL query in listing 3.3 is used to search the ontology for anatomical structures which match the original anatomical term (Example term *Leg* with *FMAID* 24979).

**Listing 3.3:** SPARQL query to find anatomical structures containing the search term (Leg)

```
SELECT ?uri ?label
FROM <http://virtualskeleton.ch/data/fma>
FROM <http://virtualskeleton.ch/data/fma/inference>

WHERE {
  <http://bio2rdf.org/FMA:24979 >
  (<http://www.w3.org/2000/01/rdf-schema#subClassOf>|
  <http://virtualskeleton.ch/vocab/part_of>)* ?uri .
  ?uri <http://www.w3.org/2000/01/rdf-schema#label>?label .
}
```

The exemplary results for the *Leg* are listed in table 3.2. With the list of retrieved identifiers, the SQL database can be queried to search for matching datasets, and can finally be displayed to the user (Figure 3.9).

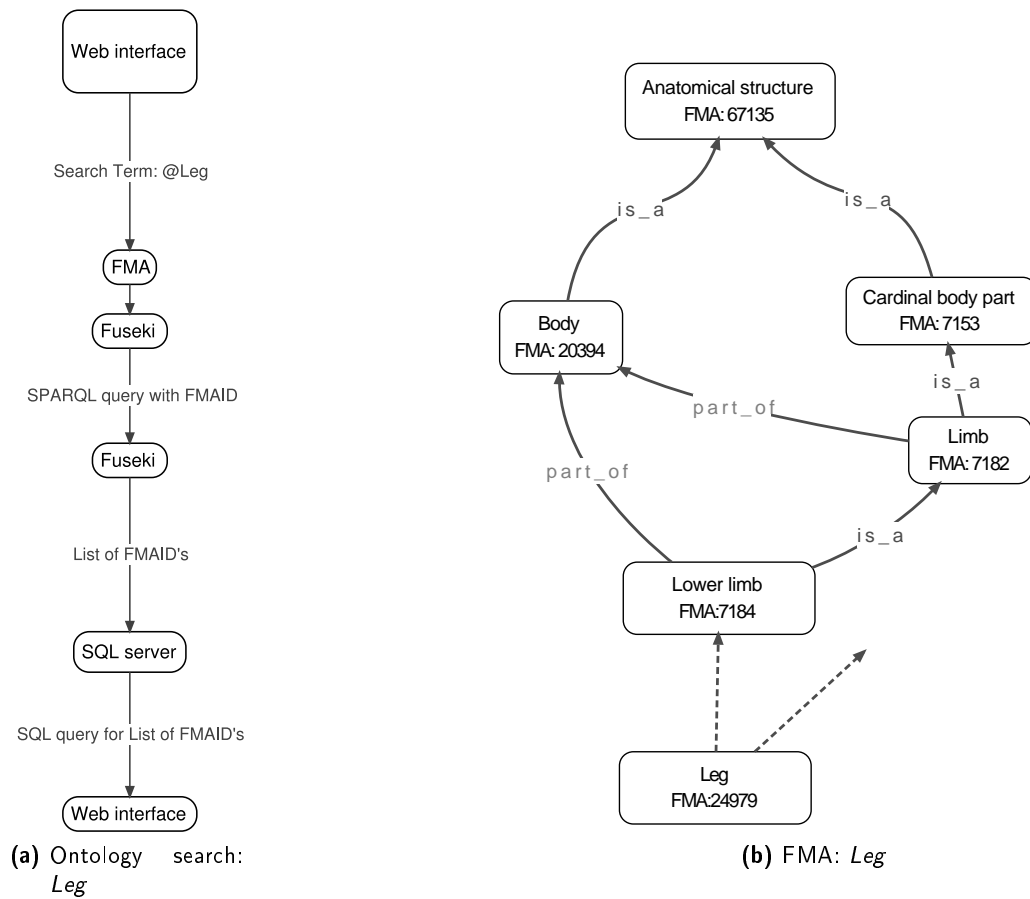
### 3.2.2 Data acquisition

A project with the goal to create a data repository and the acquisition of patient data has to answer some legal questions raised. The collection of post mortem full body CT and their usage for research purposes touches the Article 2, Section 2 of the cantonal regulation on research studies on humans (FoV) on medico-ethical aspects [Bern, 1998] and are obliged to the data protection law, where Article 15 specifically regulates the handling of data for research purposes [Bern, 1986]. And finally, the research ethical aspects have to be discussed.

**Data protection** Data can be used for research if the data is anonymized or de-identified and if the repository keeps the data secure.

**Research ethics** The cantonal ethics committee (KEK) is responsible for ethical aspects in research. The committee detects no research ethical question in the collection of post mortem full body datasets.

**Medico-ethical** These aspects of the FoV are not directly related with the database. If anything, medico-ethical rules apply for the acquisition of medical images. However, from a medical



**Figure 3.8:** (a) The process for a generic ontology search. (b) Graphical representation of the Leg. Only a sub-graph is presented.

VIRTUASKELETON database

**Places**

- MyData
- MyGroups
- MyProjects

**Page Navigation**

- Page-Top
- Page-Bottom

**VSD » Browse/Results**

Actions Manage selected Display selected

Search results for '@Leg': 70 [Clear search](#)










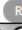




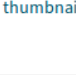









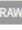
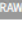




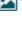
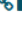





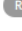







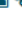
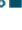
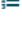



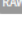
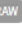
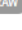













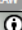












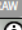













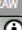































<input type="checkbox"/>		VSD.Body.090Y.F.CT.20087.000.nii 003 - Registered Full Body (Bern)	    	    	 	02.10.2013 17:48:55 kistm1	
<input type="checkbox"/>		VSD.Body.056Y.M.CT.5955.000 vsd z002 body without head	    	    	 	02.11.2012 19:27:10 kistm1	
<input type="checkbox"/>		VSD.Body.089Y.M.CT.5909.000.nii 001 - Registered Full Body (Bern)	    	    	 	30.10.2012 14:27:36 buchp1	
<input type="checkbox"/>		VSD.Body.075Y.M.CT.5907.000.dcm vsd z001 body without head	    	    	 	30.10.2012 11:44:59 kistm1	
<input type="checkbox"/>		VSD.Lower_limb.064Y.F.CT.568.000.dcm lower leg, Unt.Extr.OS 1.25 B30s	    	    	 	28.02.2012 11:25:09 kistm1	
<input type="checkbox"/>		VSD.Lower_limb.064Y.F.CT.567.000.dcm lower leg, Unt.Extr.OS 1.25 B70s	    	    	 	28.02.2012 11:09:50 kistm1	
<input type="checkbox"/>		VSD.Lower_limb.064Y.F.CT.564.000.dcm upper leg, Unt.Extr.OS 1.25 B30s	    	    	 	28.02.2012 10:42:40 kistm1	
<input type="checkbox"/>		VSD.Lower_limb.064Y.F.CT.563.000.dcm upper leg, Unt.Extr.OS 1.25 B70s	    	    	 	28.02.2012 10:30:10 kistm1	
<input type="checkbox"/>		VSD.Lower_limb.032Y.M.CT.556.000.dcm Upper leg 1.25 B30s	    	    	 	27.02.2012 19:07:30 kistm1	

Figure 3.9: The VSD Web interface with the first nine search results for the *Leg*

**Table 3.2:** Result of the SPARQL query for *Leg*: Anatomical regions containing the *Leg*

URI	Anatomical region
<http://bio2rdf.org/FMA:24979>	Leg
<http://bio2rdf.org/FMA:83016>	Middle free limb segment
<http://bio2rdf.org/FMA:83017>	Cardinal free limb segment
<http://bio2rdf.org/FMA:241863>	Free limb segment
<http://bio2rdf.org/FMA:9661>	Limb segment
<http://bio2rdf.org/FMA:67504>	Subdivision of cardinal body part
<http://bio2rdf.org/FMA:67135>	Anatomical structure
<http://bio2rdf.org/FMA:67165>	Material anatomical entity
<http://bio2rdf.org/FMA:61775>	Physical anatomical entity
<http://bio2rdf.org/FMA:62955>	Anatomical entity
<http://bio2rdf.org/FMA:24879>	Free lower limb
<http://bio2rdf.org/FMA:24875>	Free limb
<http://bio2rdf.org/FMA:7182>	Limb
<http://bio2rdf.org/FMA:7153>	Cardinal body part
<http://bio2rdf.org/FMA:7184>	Lower limb
<http://bio2rdf.org/FMA:20394>	Human body
<http://bio2rdf.org/FMA:256133>	Body of vertebrate
<http://bio2rdf.org/FMA:256135>	Body

point, the radiation during post mortem CT acquisition is irrelevant and a routine procedure required for a full forensic assessment.

The consequences for the VSD are:

**Data protection** The VSD has to provide mechanisms to de-identify the metadata of uploaded datasets. Additionally, the VSD is a research repository and provides a registration procedure where the VSD gives access to the individual research units, while the research units control their members. This mechanism should keep the VSD a research repository and limit the misuse (Section 3.1.3).

**Research ethics** The answer of the KEK required no adaptations of the VSD concept.

**Medico-ethical** It is impossible for the operator of a data repository to control all contributions. Therefore, the VSD hands this responsibility to its users. The user uploading the data is responsible for ensuring that they have the right to share the images, and that the data acquisition, and the content of the data, is in harmony with legal regulations.

In collaboration with the Forensic Institute of the University of Bern and Forensic Institute of the University of Zurich, a total of 107 post mortem full body CT datasets together with their

demographical data (100 complete, 7 incomplete information) were collected. The goal was to collect datasets from a broad demographical range (Table 3.3). Only a few selection criteria were defined. Datasets with a polytrauma or decomposed bodies, bodies with multiple implants, and children datasets were excluded from the collection for the VSD.

**Table 3.3:** Demographical data of the full body CT datasets

Gender	CT n		Age year	Height cm	Weight kg	BMI kg/m <sup>2</sup>
Bern datasets						
Female	18	mean (SD)	60 (21)	165 (6.86)	63.34 (17.77)	23.08 (5.88)
		range	19-95	152-180	32-90	11.90-31.89
Male	24	mean (SD)	55 (25)	175 (9.60)	77.71 (14.15)	25.34 (3.05)
		range	17-89	155-189	54-110	19.60-31.46
Total	42	mean (SD)	57 (23)	171 (9.65)	71.55 (17.18)	24.37 (4.57)
		range	17-95	152-189	32-110	11.90-31.89
Zurich datasets						
Female	15	mean (SD)	52 (15)	168 (5.42)	59.78 (14.81)	21.12 (4.91)
		range	30-75	154-180	37-85	11.54-28.30
Male	43	mean (SD)	53 (19)	178 (7.47)	78.85 (17.13)	24.84 (4.85)
		range	21-95	164-195	49-111	15.67-35.83
Total	58	mean (SD)	55 (19)	175 (8.13)	74 (18.48)	23.95 (5.15)
		range	21-95	154-195	37-111	11.54-35.83
Combined datasets						
Female	33	mean (SD)	56 (19)	167 (6.41)	61.72 (16.55)	22.18 (5.54)
		range	19-95	152-189	32-90	11.54-31.89
Male	67	mean (SD)	54 (21)	177 (8.35)	78.52 (15.92)	25.08 (4.27)
		range	17-95	155-195	49-111	15.67-35.83
Total	100	mean (SD)	54 (20)	173 (9.05)	72.97 (17.90)	24.13 (4.90)
		range	17-95	152-195	32-111	11.54-35.83

To ensure the subjects privacy, the soft tissue of the head scans was manually stripped (Figure 3.10), and the metadata was anonymized by the Forensic Institute before the transfer to the VSD. Furthermore, the European spine phantom (ESP) ([Kalender et al., 1995]) was scanned to ensure the datasets usability to the biomedical community. The reference dataset of the ESP allows to calibrate the full body scans, and is needed to subsequently translate the image's gray values to material properties.

The scanning protocol for the full body datasets of Bern required the scanning table to be rotated. Therefore, all scans were performed with the body embedded in a vacuum mattress to

ensure a fixed position. The Bernese datasets (Table 3.4) consist of a fused Thorax-Abdomen (T1 vertebra to tuber ischiadicum) set, a combined Leg (Crista iliaca to the feet) scan and the masked head part (Top to the C7 vertebra). The datasets from Zurich (Table 3.5) required no rotation as their CT device is able to scan the body in one go. Again, the head was scanned separately and manually masked for the reason of privacy protection (Figure 3.10).

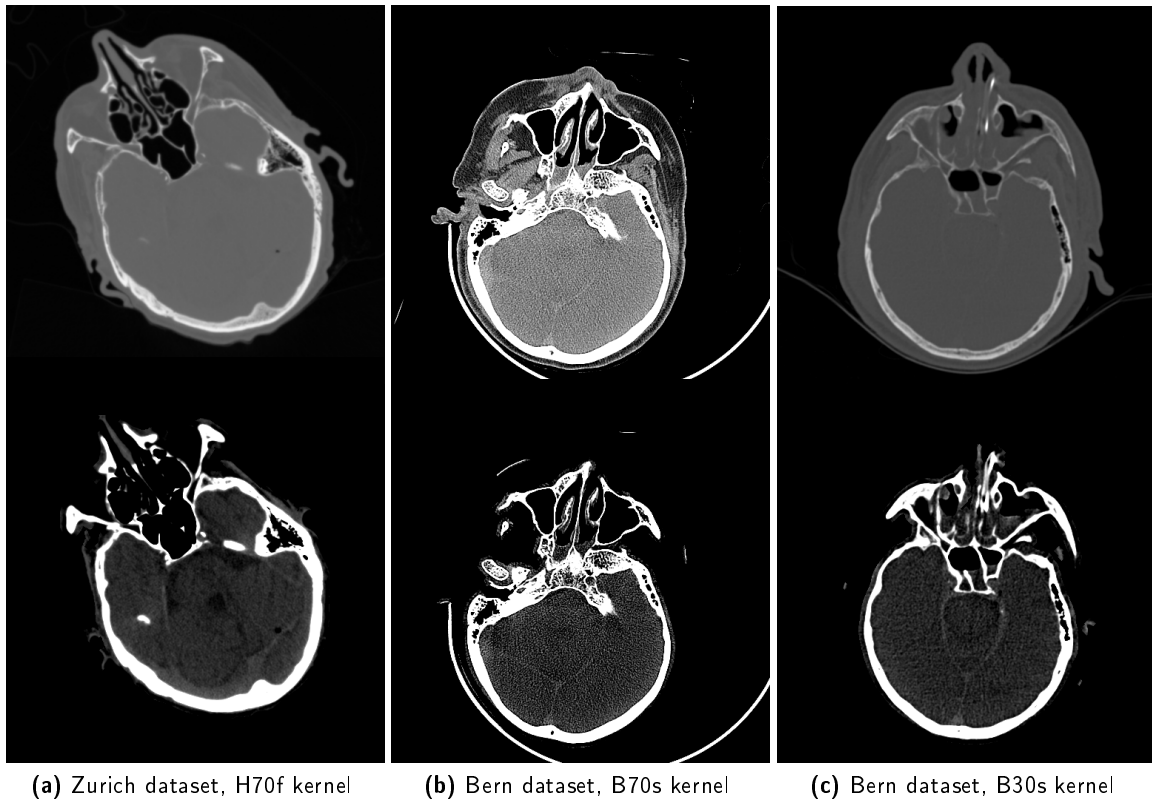
**Table 3.4:** Technical data of the full body CT datasets of Bern

Parameter	Phantom	Body data	Head data
Convolution kernel	B70s	B70s, B30s	B70s, B30s
Slice thickness, mm	0.63	1.25	0.6-1.25
Slices spacing, mm	-	0.7	0.7
Image size, px	512x512	512x512	512x512
Pixel spacing, mm	0.49x0.49	0.97x0.97	0.46x0.46- 0.50x0.50
Rescale intercept	-1024	0	0
Rescale slope	1	1	1
Calibration function	a: -1024	a: -32768	a: -32768
( $y = a+bx$ ), "Gray Value"	b: 1	b: 1	b: 1

**Table 3.5:** Technical data of the full body CT datasets of Zurich (\* Phantom data not provided yet)

Parameter	Phantom*	Body data	Head data
Convolution kernel	-	B70f	H31s
Slice thickness, mm	-	1.00	0.75
Slices spacing, mm	-	-	-
Image size, px	-	512x512	512x512
Pixel spacing, mm	-	0.92x0.92	0.44x0.44
Rescale intercept	-	-1024	-1024
Rescale slope	-	1	1
Calibration function	-	a: -1024	a: -1024
( $y = a+bx$ ), "Gray Value"	-	b: 1	b: 1

In addition, efforts were made to identify the datasets available at the institute for surgical technology and biomechanics (ISTB). More than 600 head datasets with mandibular and orbital segmentation, 150 cone beam computed tomography (CBCT), and more than 800 CT and segmentation of the lower extremities are stored on ISTB discs. Additional data include about 50 mid-face CT scans, 160 pelvis of which about 110 were segmented, 9 liver datasets including CT,



**Figure 3.10:** Example of masked head datasets. Top row is showing the original slice, bottom row presents the masked version available on the VSD

3D ultrasounds and segmentation, 10 MR of scoliotic spines including segmentation of about 6 levels around the apex of the curve, 10 angio-MR of the leg at two flexion positions including segmentations of bones and arteries as well as 6 angio-CT of the leg of patients with arterial calcifications. About 20 brain MR of glioma cases are available as well as 10 knee MR including segmentations of the bony structures.

### 3.2.3 The VSDUploader logic

The general concepts of the VSD had a strong influence on the implemented upload logic of the VSD. The VSDUploader has to be compatible with different types of files and has to work independently of the upload technology. The upload logic has to ensure minimal storage usage, the handling of thousands of files on the file system, and has to be able to create dataset versions if required. The VSD has to handle confidential metadata of images and has to guard the ownership of the uploaded data. Additionally, the number of files in a medical images dataset can consist of multiple, exactly two or a single file. Therefore, the VSDUploader not only has to include routines



to read the different file type extensions but also to handle these cases individually. The different aspects are discussed in the following paragraphs.

### **Minimal storage**

Although hard drive storage is relatively cheap, one goal of the VSD is to minimize storage usage. Therefore, a unique file is exactly stored once. To reduce the size of the SQL database, the database design follows the principles presented in section 2.1.2 as much as possible .

### **Persistent data**

In a large repository with data interconnections (related data), with the possibility to organize datasets of different users and inhomogeneous file types, deletion of objects would require a lot of housekeeping or would even be impossible to do. On the other hand, the advantages of the possibility to remove datasets cannot be neglected. To be able to remove unwanted data increases the confidence in the system, and the content of the VSD is of better quality. Therefore, the VSD allows the deletion of files in the *Unvalidated Data Folder* but not after the validation step.

### **Ownership protection**

With the VSD, the user who uploads a dataset is the *Owner* of the data. He can share, modify, and administer his owned files. To prevent the re-upload of shared data by another user, the VSD rejects data if an validated version is already owned by another user. However, it is possible to upload existing data as long as the object is unvalidated (data in the *Unvalidated Data Folder*). In short, the system grants a user ownership rights on data in the *Unvalidated Data Folder*. But only validating objects (make them visible for other users) protects the data from re-upload.

### **Privacy protection**

The system automatically performs various de-identification tasks. In general, all metadata fields containing a name or similar entry are removed. Additionally, the birth date is erased after the calculation of the age. Another important source of information leakage are the filenames. The filenames are not only labelling the files themselves on the disk but can be written into the file itself. Therefore, the VSD introduced a filename convention (Listing 3.4) which replaces all filenames on the VSD, keeping the original filename only visible to the *Owner*. The filenames of the VSD not only protect the privacy of a dataset but also directly reveal important information to the user, especially after the download when the researcher is working offline without all the information

visible on the VSD. For example, the filename *VSD.Body.089Y.M.CT.5909.000.nii* describes the full body CT dataset of an 89 years old male subject, stored on the VSD with the id 5909 as a Niftii file.

**Listing 3.4:** VSD filenames template

```
VSD.AnatomicalRegion.Age.Gender.Modality.VSDID.FileNr.extension
```

### Upload process

In general, the upload logic has to perform several steps before the file is finally stored on the disc and the related information is stored in the database. The generic procedure is depicted in figure 3.11. First, the file is identified by its calculated secure hash algorithm (SHA-1) value. Subsequently, based on the file extension, the object's category and file format (List 3.1) is defined and the file is passed to the correct *Uploader*.

**List 3.1:** object categories and file types of the VSD

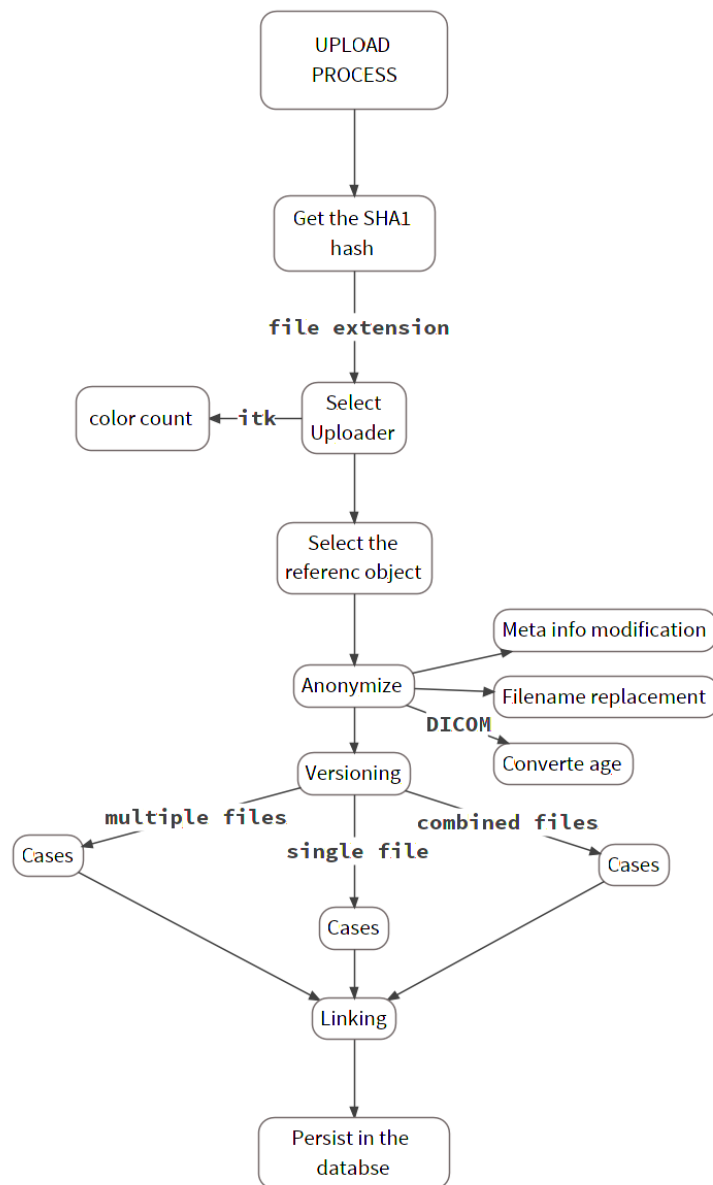
**Raw image** DICOM, Analyze, MetaImage, Niftii  
**Segmentation** DICOM, Analyze, MetaImage, Niftii  
**Statistical Model** HDF5  
**undefined** rejected

The system can automatically distinguish between raw images and segmentations based on the number of unique gray values in the images. Segmentations are defined as image masks (labels) and therefore contain a limited number of colors, typically less than ten.

The reference object is retrieved based on the selected *Uploader*, and is required for object versioning (Figures 3.12, 3.14). Subsequently, the anonymization tasks are performed. Versioning depends on the file type structure (multiple file stack, combined files, and single files). For each file type different schemes control the versioning (Figures 3.13, 3.15a, 3.15b, 3.16). In a final step, the system links a new dataset to an existing one if its filename follows the VSD filename convention with the *VSD ID*, or according to the patientID in the DICOM

**List 3.2:** File type categories and associated file types

**Multi file stack** DICOM  
**Combined files** MetaImage, Analyze  
**Single file** HDF5, Niftii, MetaImage, DICOM

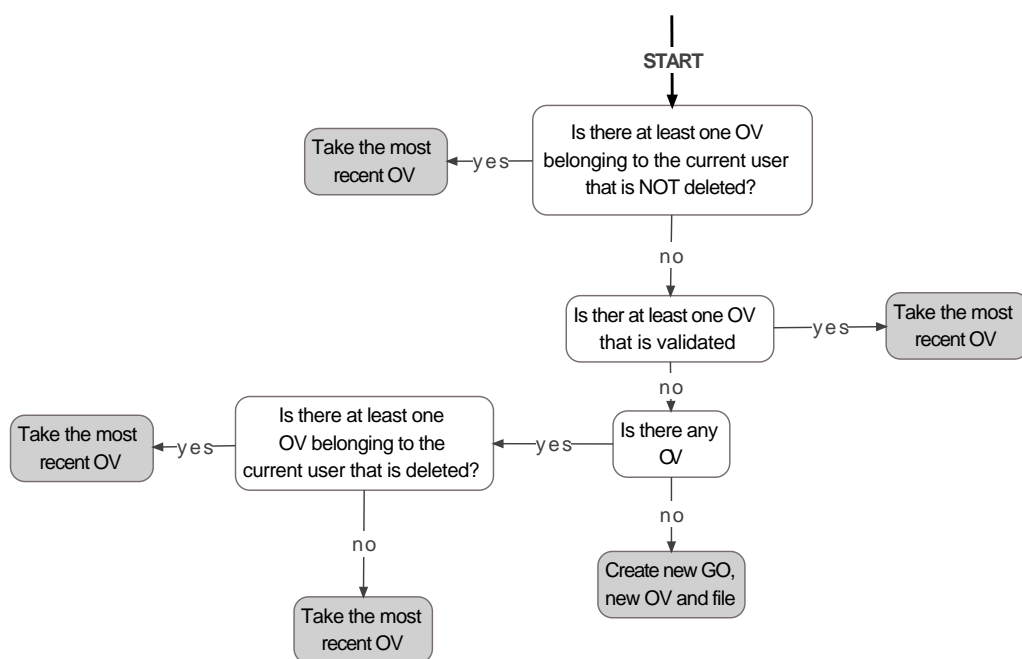


**Figure 3.11:** Schematic of the general behavior of the VSDUploader

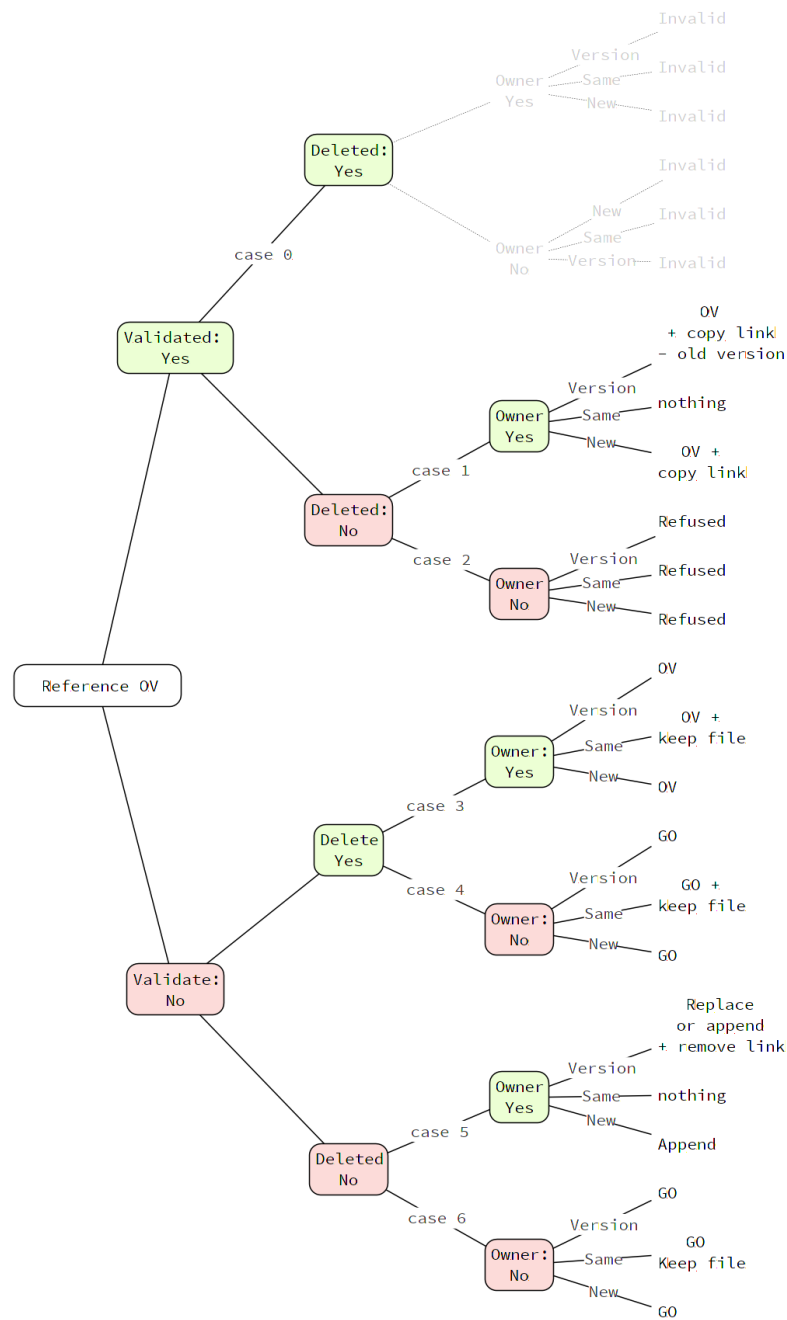
**Multifile objects**

The stack is characterized by a series of images which build a dataset. However, the stack has no machine readable start and end tag. Therefore, the system requires the user's input to mark the stack as complete.

The VSDUploader of the multi file dataset has to generate, when receiving the first file of a stack, a new object version (OV), and has to append subsequent files of the DICOM stack (case 5 in figure 3.13). The order of the file upload can be random, and simultaneous uploads of users with the same files are possible. Normally, following the concept defined in 3.2.3, such a case (cases 5 & 6 in figure 3.13) would require the system to store the same file multiple times. Alternatively, the system would create two incomplete datasets which would be unsatisfying for the user. The *Inbox* concept of the VSD resolves this issue. Both users get an independent generic object (GO) and a OV which point to the same images on the file system. Both *Owner* can control the access rights and manage the metadata of their dataset independently.



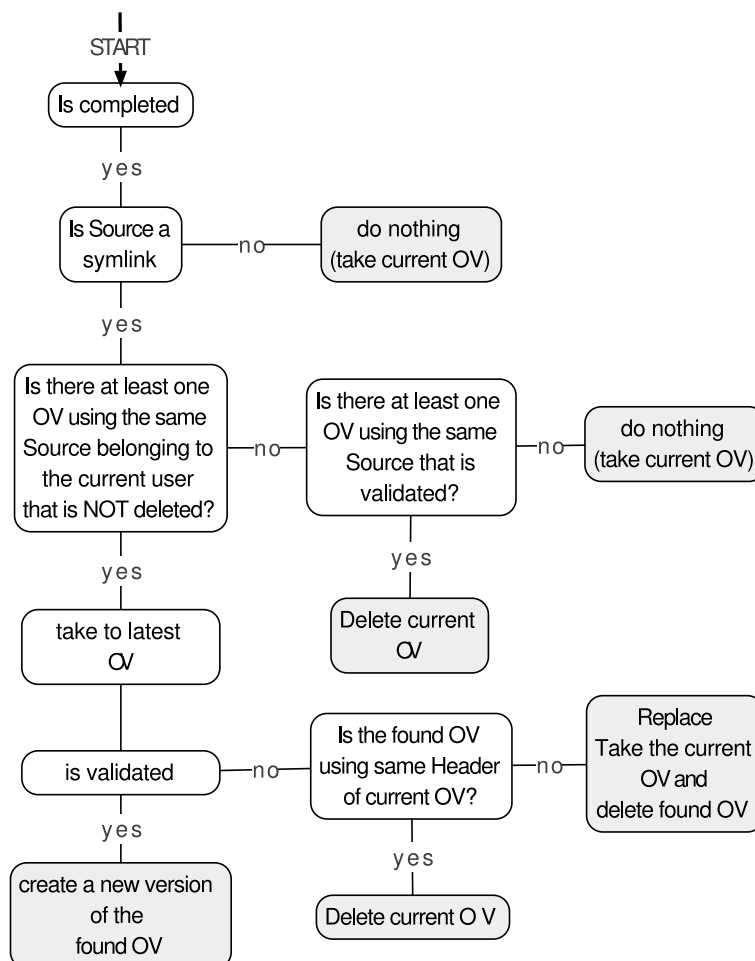
**Figure 3.12:** Decision tree to find the reference object version. If no reference object exists, a new object is generated, otherwise the found OV is used to select the appropriate case for the versioning (in figure 3.13).



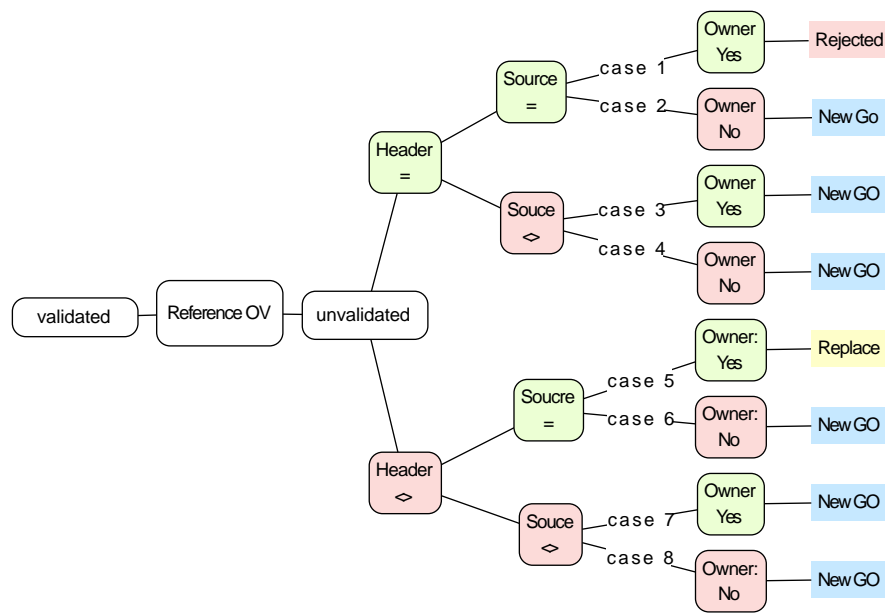
**Figure 3.13:** Multi file versioning. The multi file VSDUploader is using the reference object, the validation state, the status of the data (delete/active), and the ownership status to decide the action on the file. The default result for a new file is *Append* (case 5).

### Combined objects

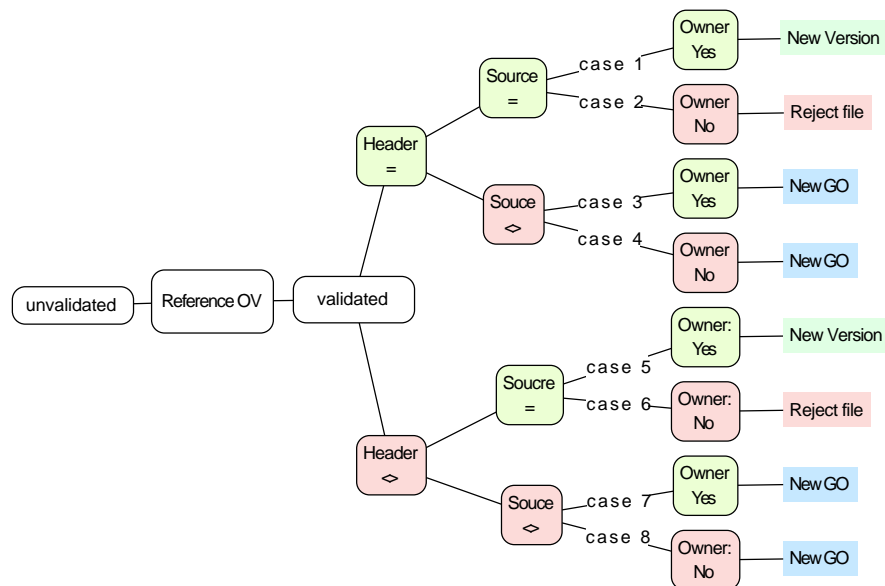
The combined files consist of a header (information) and a source part (images). Therefore, for a combined object to be valid, both files have to be present. Only if both files are uploaded, the object can be validated on the VSD. There are two options for a header file to find the corresponding source. Either both files need to be stored in the same location or the path to the source file is referenced in the header file. Since the header contains no image material, the VSD treats the two files differently. The information stored in the header can easily be similar and hence their SHA-1 value is equal. As a consequence, only a source file invokes ownership on the object. These facts required the development of a different reference object OV finding scheme (Figure 3.14), an adapted versioning behavior (Figure 3.15b, 3.15a), and the usage of symbolic links to avoid duplicated source files on the data storage.



**Figure 3.14:** Decision tree to find the reference OV for the combined objects.



(a) un-verified



(b) verified

**Figure 3.15:** Versioning scheme for combined objects. Legend: <> files not equal, = files are equal.



### Singlefile objects

The images are stored (compressed) in one single file. The versioning (Figure 3.16) and reference object localization is straight forward. In fact, their versioning scheme is only invoked if exactly the same file is uploaded.

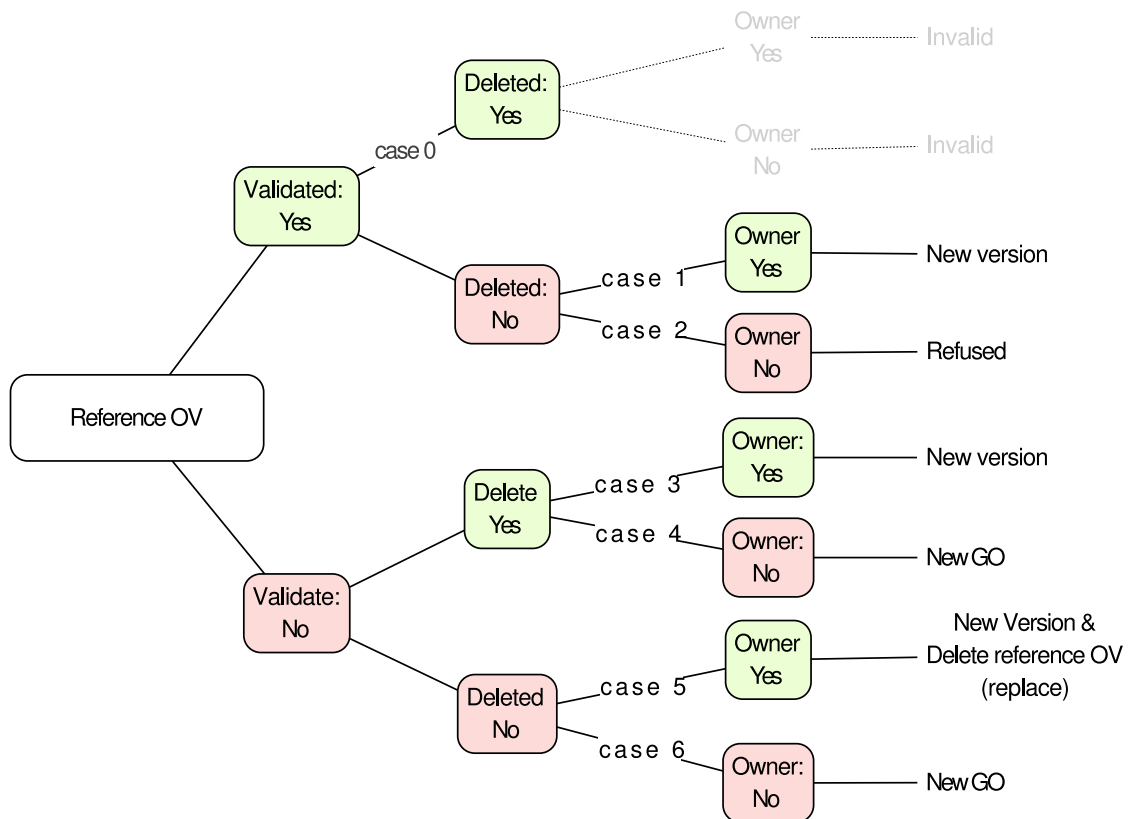


Figure 3.16: Single file decision tree



## Chapter 4

### Femur prediction model

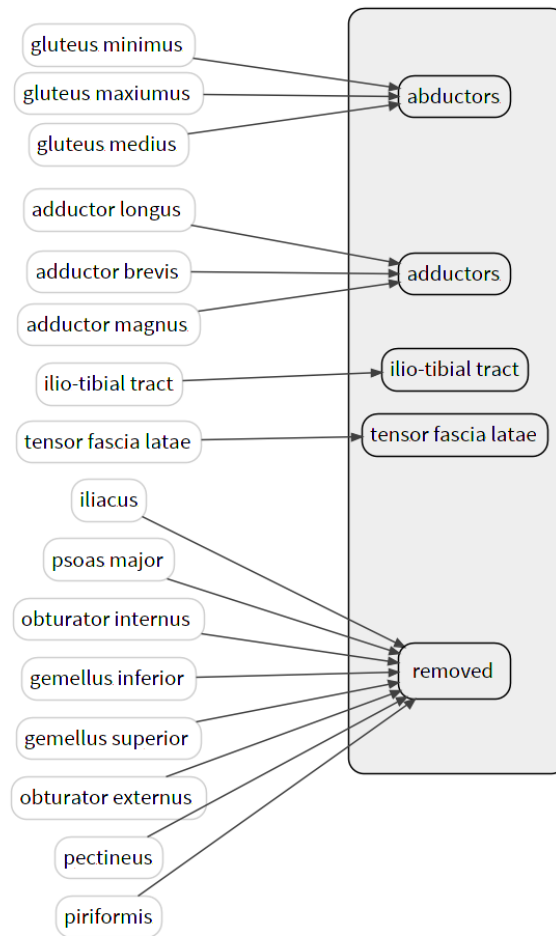
In this chapter, the incremental steps of the development of a femur model are presented. These steps include the FE femur model, a first SSM, and a linear regression model of limited validity. The models was then extended with a statistical appearance model (SAM) of the femur to predict peak stresses in three femur regions. The subsequent prediction model for secondary output variables was then extended in a final study to predict primary output parameter like the stress tensor and displacement vector. Additionally, this prediction model was not only tested on synthetic bone but on patient data.

#### 4.1 Finite element model of the femur

##### 4.1.1 Introduction

FE model building in the biomedical field often faces the problem that material properties, geometries, boundary constraints and muscle forces are difficult to define. In biomechanics, accurate in vitro measurements of muscle forces are rarely available and most likely not available for *patient-specific* modelling. Luckily, Bergmann [Bergmann et al., 1993] did implant force sensing and transmitting femoral prostheses during a total hip arthroplasty (THA) in four patients. From the data of this patients, Heller et al. [Heller et al., 2001] could show that, using individual musculoskeletal models from imaging (CT, X-ray) one can calculate hip contact forces and is able to predict the peak force with a mean error of  $\pm 12\%$  during walking. Heller simplified this model (Figure 4.1) by grouping involved muscles in the hip joint into functional muscle units [Heller et al., 2005]. They finally derived a load profile from the four patients and four muscles units for the maximum hip joint loading during walking. The reported 10% error for a typical THA patient is in the same range as the model in the previous publication. This suggests that a simplified model performs as good as the full model. The load profiles are reported as percentage of the bodyweight in the local coordinate system of the femur described by Bergmann et al. [Bergmann et al., 1993]

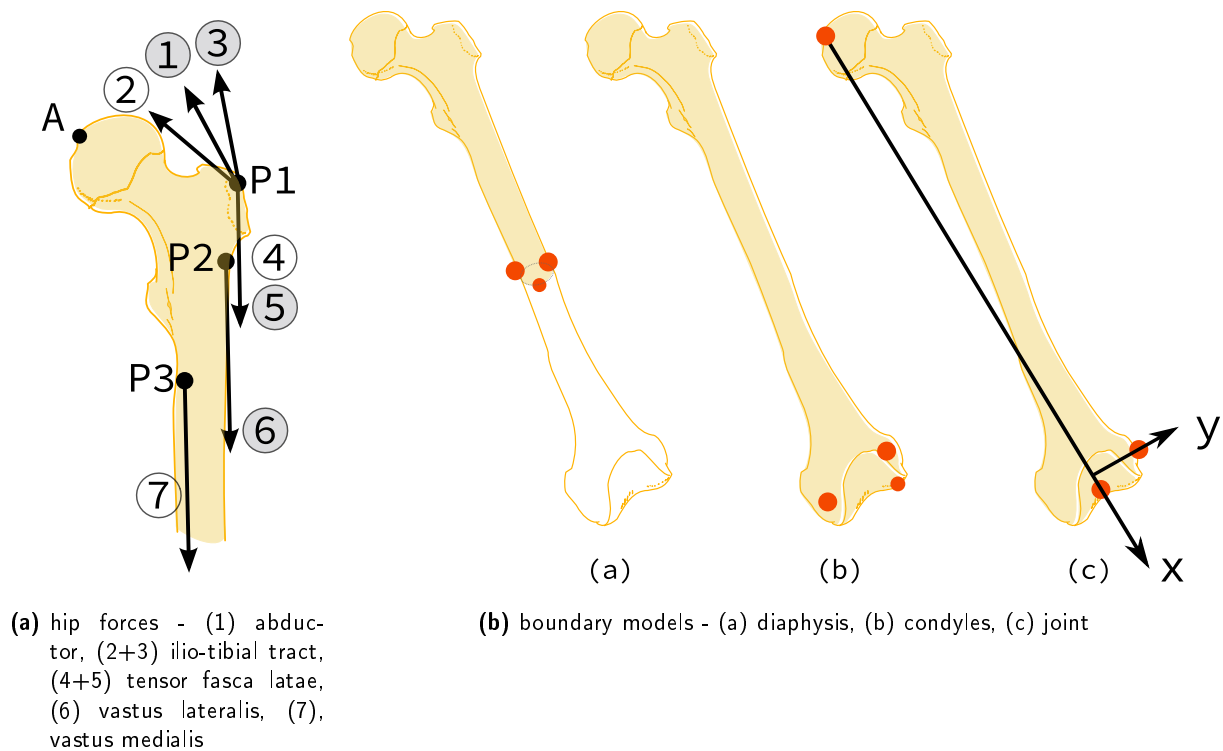
(Table 4.1) which makes them useful for other researchers.



**Figure 4.1:** Muscle of the complex model on the left were simplified to four groups on the right side (adapted from [Heller et al., 2005]).

The constraining of rigid body motion is a central aspect in every biomechanical FE model. Several approaches have been used to apply constraints to the femur on at least six degrees of freedom (DOF). A common method is to constrain nodes at the mid-shaft. They are, however, not particularly physiological. The distal condyles can be constrained to achieve a more physiological behavior at the knee. This simulates the passive soft tissue structure of the knee region [Taylor et al., 1996; Duda et al., 1998; Polgar et al., 2003; Kleemann et al., 2003]. Both approaches do not constrain the femoral head. Speirs et al. [Speirs et al., 2007] introduced a third option where the femoral head is constrained in its motion so that it only deflects along an axis toward the knee centre. These boundaries were combined with the previously mentioned muscle models of Heller et al.. In his study, Speirs compared five combinations of load cases and boundary sets. The body

weight was 860N in all simulations. The standard femur model (SFM) served the geometry for the FE model and consisted of 4 mm second-order tetrahedral elements. The cortical part was assigned a Young's modulus of 17 GPa, and the elastic modulus of the trabecular region was set to 1 GPa. The Poisson's ratio for both parts was 0.3. Analyzing the five models revealed constant high reaction forces at the hip contact for both the diaphysis and the condyle model. Only the newly introduced physiological "*joint*" model combined with the muscles from the complex model of Heller was in agreement with deflections measured in a one-legged stance X-ray.



**Figure 4.2:** Selected load and boundary models from the literature. (4.2a) adapted from [Heller et al., 2005] and (4.2b) from [Speirs et al., 2007].

The aim of this section is to establish a new femur model by combining the simplified muscle model of Heller with the physiological boundaries of Speirs for a normal walking situation.

#### 4.1.2 Method

##### Geometry

The SFM V4 from [Viceconti et al., 1996] was imported as a Parasolid and slightly adapted in Solidworks to receive nicer patches in the computer aided design (CAD) solid model. The SFM

is a CAD model of a standard femur used for experimental in-vitro testing and is available in the public domain. The SFM has been validated in several studies [Polgar et al., 2003; Polgár et al., 2003]. It does not represent a mean of a specific population but is widely accepted in biomechanical simulation and modelling. The available SFM consists of a cortical bone shell, and a distal and proximal trabecular bone part (Figure 4.3). The femur model was meshed in Abaqus with 40'579 second-order tetrahedral element (C3D10 type) and a total of 66'841 nodes. According to values given by Speirs, cortical bone was assigned a Young's modulus of 17 GPa and a Poisson ratio of 0.3 while trabecular bone was set to 1 GPa and 0.3.



**Figure 4.3:** Imported standardized femur model

### Loading

In the 1980's Bergmann introduced an universal coordinate system for the femur femur coordinate system (FCS) where the ideal longitudinal axis defines the z-direction [Bergmann et al., 1984]. The x-axis is define by the two epicondyles (knee axis), and the sagittal plane defines the y-axis. The forces given by Heller are defined in this FCS. Therefore, the femur was transformed to match the FCS to the global coordinate system (GCS), and the loads of the normal walking profile were

added and scaled with the body weight of 836N (Table 4.1).

**Table 4.1:** Forces used in the femur model [Heller et al., 2005]. All values in % of body weight. LCS = local coordinate system, GCS = global coordinate system (femur coordinate system)

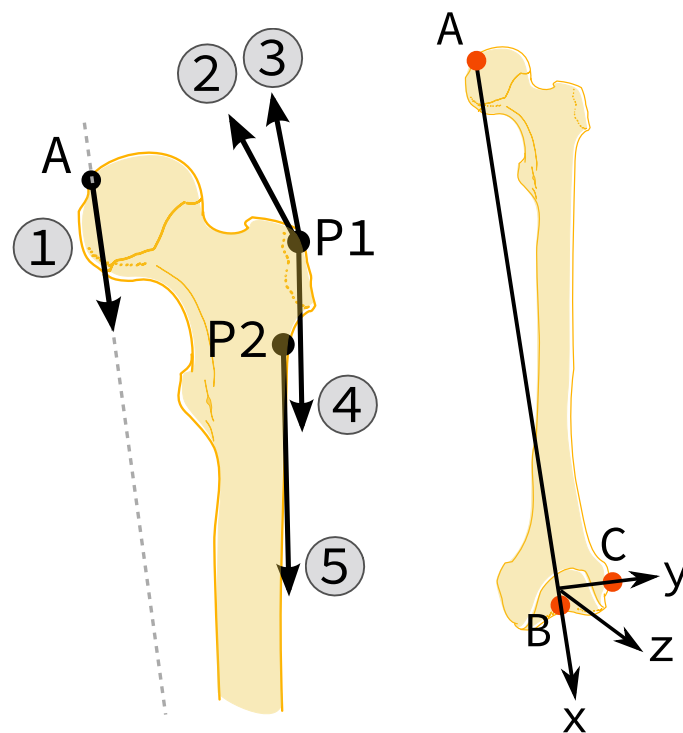
Muscle	x	y	z	Coord. System	Point
1 Hip contact	1987.85 (Magnitude)			LCS	A
2 Abductor	-484.88	-35.95	723.14	GCS	P1
3 Tensor fasc. latae, proximal part	-60.19	-96.98	110.35	GCS	P1
4 Tensor fasc. latae, distal part	4.18	5.85	-158.84	GCS	P1
5 Vastus lat.	7.52	-154.66	-776.64	GCS	P2

### Boundary conditions

First, the coordinate system of the SFM was defined to match the universal coordinate system proposed (FCS) by Bergmann. The FCS was then aligned with the GCS to define the loading profile for normal walking. A second coordinate system was introduced to apply the boundary condition (BC) at the constraining nodes *A*, *B*, and *C*. This local coordinate system (LCS) was defined by an x-axis from the hip contact point *A* towards the centre of the knee *B* (Figure 4.4b). The y-axis is defined by point *B* and *C*. The normal on this x-y plane defines the z-direction. This LCS is needed to constrain the magnitude of the joint contact force to point down the x-axis, and to constrain the hip contact node to move only in x direction. Point *B* is fixed in all three translational DOF, and the node at Point *C* is preventing anterior-posterior motion of the distal femur in the LCS.

### 4.1.3 Results

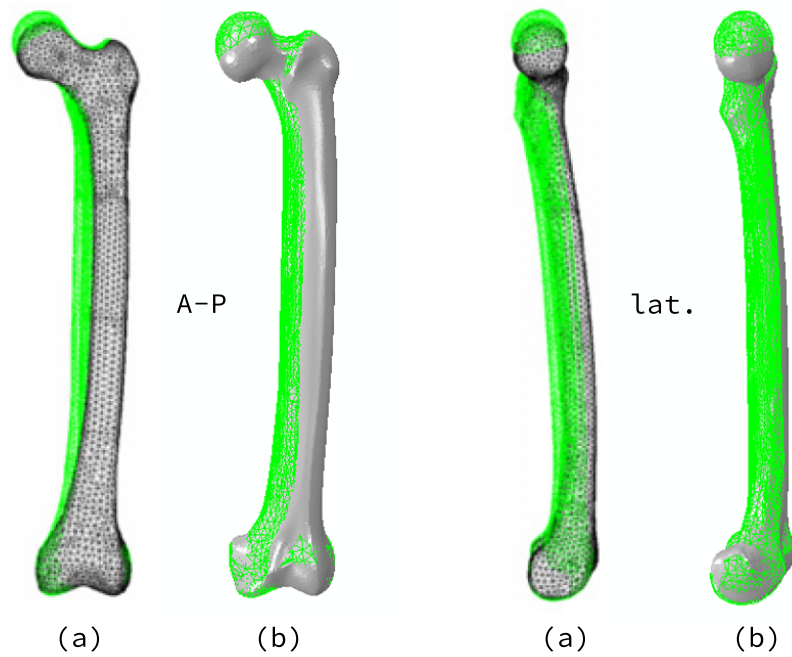
The presented femur model with walking BC was validated against the results from A.D Speirs. The model showed the same behavior as the published data of Speirs (Figure 4.5). The average displacement for the full femur was 1.62 mm compared to 1.8 mm in the complex joint model of Speirs. The femoral head deflection in the model of Spears was 3.2 mm compared to 2.11 mm in the model used in this study. In addition, the deflection in the shaft showed only a small difference of 0.1 mm (Kistler: 2.6 mm, Speirs: 2.5 mm). Secondly, the maximal principal strain along the bone shaft was in agreement with the published curve of Speirs (Figure 4.6).



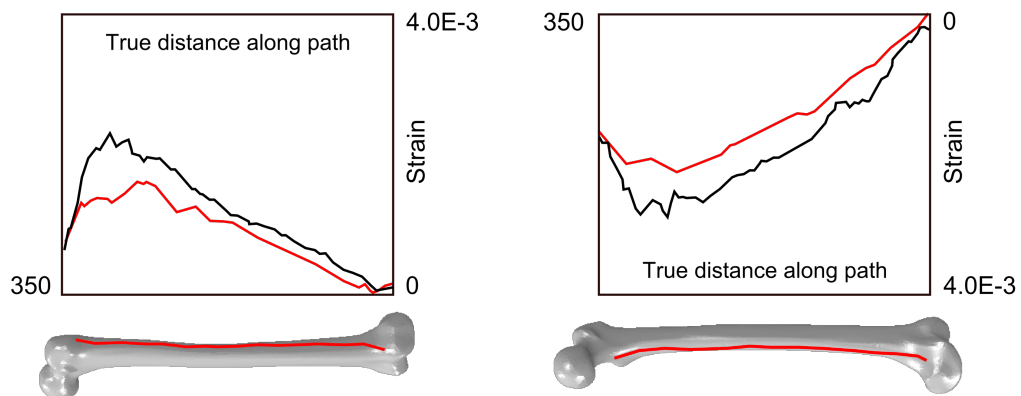
(a) hip forces - (1) hip contact, (2) abductor, (3+4) tensor fascia latae, (5) vastus lateralis (b) joint boundary model

**Figure 4.4:** Final setup of forces for normal walking and joint-boundaries





**Figure 4.5:** Qualitative comparison of the A.D Speirs result (a) and the presented model (b) initial state (green) and loaded (gray). Displacement magnified five times.



**Figure 4.6:** Comparison between maximal principal strains on the lateral (left) and medial (right) sides as calculated by Speirs (black line) and in the present model (red line) [Distance in mm].

#### 4.1.4 Discussion

The description of the full complex model from Heller was not available in this work, only the simplified model with loading profiles for the pooled muscle group were accessible. The simplified model from Heller promised to be in the same accuracy range as a full muscle model. The work of Speirs indicated that the joint BC setting is the only viable option for the femur model. This work aimed to combine these two best effort solutions and evaluated this combination on published results of Speirs. However, this combination was included by Speirs and therefore our combined model had to be compared against the closest available option: the *joint contact force and all muscle included* muscle model, and the *joint* boundary model. Both models were based on the same geometry and material properties, boundary conditions, and second order tetrahedral elements were used. However, the exact muscle insertion were unknown, and there was a difference of 24N for the body weight.

The qualitative assessment of the femur deflection confirmed that the presented model shows a similar physiological behavior as the full complex model. The mean average deflection error for the full model supported this findings with a difference of 0.18 mm. Additionally, a small maximum mid-shaft deflection error of 100  $\mu\text{m}$  could be observed. The difference in the deflection of 1.1 mm in the femoral head can be explained by the higher body weight used by Speirs and inconsistent muscle attachments (especially of the hip force point A). These model variances influence the principle strain behavior in terms of magnitude but not the general behavior itself.

In conclusion, a femur model for a normal walking situation which combines components previously validated by other researchers [Bergmann et al., 1993; Heller et al., 2005; Speirs et al., 2007] was presented. The model is in good agreement with the published data and behavior of the model from Speirs and Heller. Without being dramatically complex, the defined femur model shows physiological results for a normal walking situation. This model can be used to analyze the general behavior of a femur in a normal walking scenario.

## 4.2 Statistical Shape Models to Accelerate Finite Element Calculations in Biomechanics: A Preliminary Study on Femoral Bones

M. Kistler (1), C. Boichon (2), M. Rochette (2) and P. Büchler (1)

(1) Institute for Surgical Technologies and Biomechanics, University of Bern, Switzerland;

(2) ANSYS Inc., France

### 4.2.1 Summary

Over the last decades, the biomechanical community invested efforts to develop *patient-specific* models. The objective is to enable the surgeon to plan the surgery, select the appropriate implant and position or optimize the surgical techniques. However, results of these development failed to spread widely into medical practice due to the large amount of time required to setup the numerical model and to perform the FE calculations. The purpose of the present work is to propose a possible technique to reduce the computational time for *patient-specific* models. The method relies on a combination of SSM and FEA. Preliminary results based on a limited training data set indicates that this approach could be a valid alternative to the current procedure.

### 4.2.2 Introduction

FE models developed from CT data are commonly used to evaluate the mechanical performance of the bone [Hernandez and Keaveny, 2006; Taddei et al., 2004] load transfer from implant to bone [Farron et al., 2006], bone–cement interface mechanics [Mann and Damron, 2002], and evaluation of fracture risks [Cody et al., 1999; Schileo et al., 2008b]. However, the construction of a numerical model for a specific patient involves many steps and is time consuming. The generation of such a model requires segmentation and parametrization of the relevant patient structures, generation of a volume mesh, allocation of appropriate material properties and boundary conditions to finally solve the FE problem. This limitation prevents a day-to-day use of biomechanical findings in the clinical routine, and limits this approach to a limited number of specific cases.

Statistical shape analysis has been used to represents human bone anatomy. This method enjoys a remarkable popularity within the medical image analysis community. Since its invention, many groups worldwide started to investigate the capabilities of these techniques to study human

anatomy and to model its variability. SSM are widely used for both, as basis for image segmentation, and to study and interpret complex anatomical structures.

In this work, we propose to combine SSM with FE to reduce the time required to obtain *patient-specific* FE calculations. First, a SM of the anatomical structure is developed. The model is then used to generate new bone instances representing a known percentage of the target population and subsequently to perform FE calculations on this generated models. Finally, the database of pre-calculated FE results is used to estimate the stress distribution of a *patient-specific* bone.

### 4.2.3 Methods

The first step is to build a SSM of the anatomical structure of interest. Six post-mortem full body CT image data sets from three male and three female subjects of age between 22 and 90 years (22y, 56y, 77y, 88y, 89y, 90y) were used. The subjects left femurs were segmented out of the image stack using AMIRA (Visage Imaging) in a semi-automatic procedure. The resulting bone segmentations were then exported to 3D STL objects. One reference bone from the training data set was meshed with linear tetrahedral elements. The reference mesh consisted of 26'435 elements and 42'145 nodes.

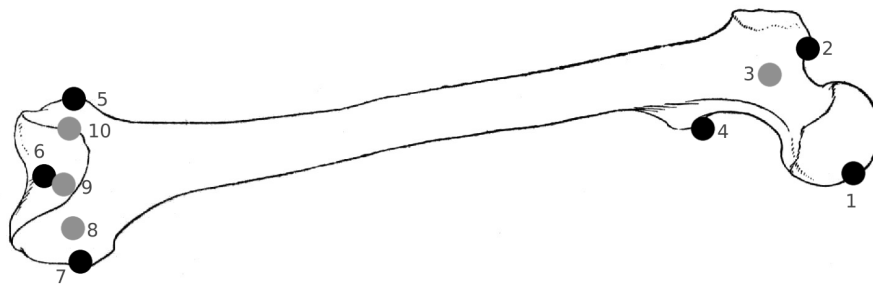
A morphing procedure was used to establish correspondence between the bones of the training data set. For each femur, a set of ten anatomical landmarks was recorded (Figure 4.7). The landmarks were used by the Morpher tool, which uses radial basis function (RBF) in 3D and projection on the STL surface for morphing, for the non-rigid alignment and shape vector generation [Hraiech, 2010]. Subsequently, the generated volume meshes with established correspondences were aligned using Procrusters analysis. The SSM was constructed from five femur using PCA [Cootes et al., 1992]. Seven new femur instances were generated from this shape representations using equation 4.1:

$$X = \bar{X} + \sum b_i \sqrt{\lambda_i} \phi_i \quad (4.1)$$

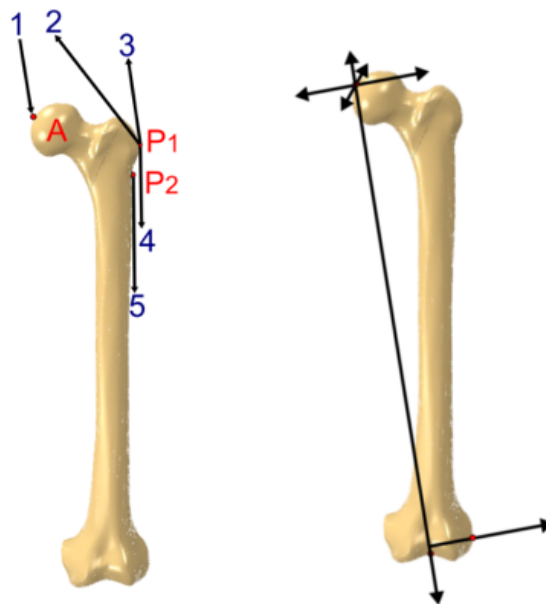
First, five femurs instances were generated along the first principle mode of variation with shape parameter ( $b = -0.6, -0.3, 0, 0.3, 0.6$ ). In addition, a control femur with a first mode parameter ( $b = 0.4$ ) was generated.

A FE model of the femur with a loading situation corresponding to a normal walking was designed according to the literature [Bergmann et al., 1993; Heller et al., 2005; Speirs et al., 2007] (Section 4.1). The model included a hip force of 836N, muscle forces for the abductor group, the tensor fasciae latae and vastus lateralis [Heller et al., 2005] (Table 4.1). To define directions of the

BC and loadings a LCS was introduced according to Speirs [Speirs et al., 2007] where the x-axis of this local coordinate system goes from the hip contact point of application towards the center of the knee. This coordinate system is used to constraint joint contact force to be applied toward this axis (Figure 4.8). The bone material was considered homogeneous and purely elastic ( $E = 5 \text{ GPa}$ ,  $\nu = 0.3$ ).



**Figure 4.7:** Landmark locations: 1 femoral head, 2 trochanter maj., 3 fossa intertrochanterica, 4 trochanter min., 5 epicondyle lat., 6 facies patellaris, 7 epicondyle med., 8 condyle med., 9 fossa intercondylaris, 10 condyle lat..



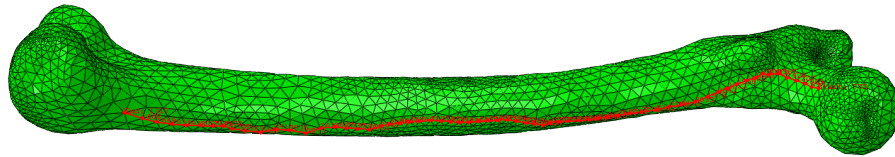
**Figure 4.8:** Loading situation (left side) and local coordinate system introduced (right side). (1) hip contact force, (2) abductor, (3+4) tensor fasciae latae, (5) vastus lat..

The results of this FE calculations form the database of numerical results are used to obtain fast FE results for new bone instances. In order to evaluate the predictive power of the method, the

prediction of the model for a the control bone was compared to the results of a direct FE calculation on the same bone instance. A path along the femoral neck and medial shaft was used to record stress and displacement. The results for the five generated femur instances were combined by interpolation and polynomial fitting to a statistical finite element model (SFEM). To assess the SFEM, the result from the control femur were compared to the corresponding predictions along the path.

#### 4.2.4 Results and Discussion

The calculated prediction from the SFEM of Mises stress along the medial shaft (Figure 4.9) and femoral neck were in good agreement with the result of the FE calculation (Figure 4.10 - 4.11). The maximum relative error occurred in the region of highest deflection and was about 12.7% and with an absolute error of 4.26 mm magnitude.

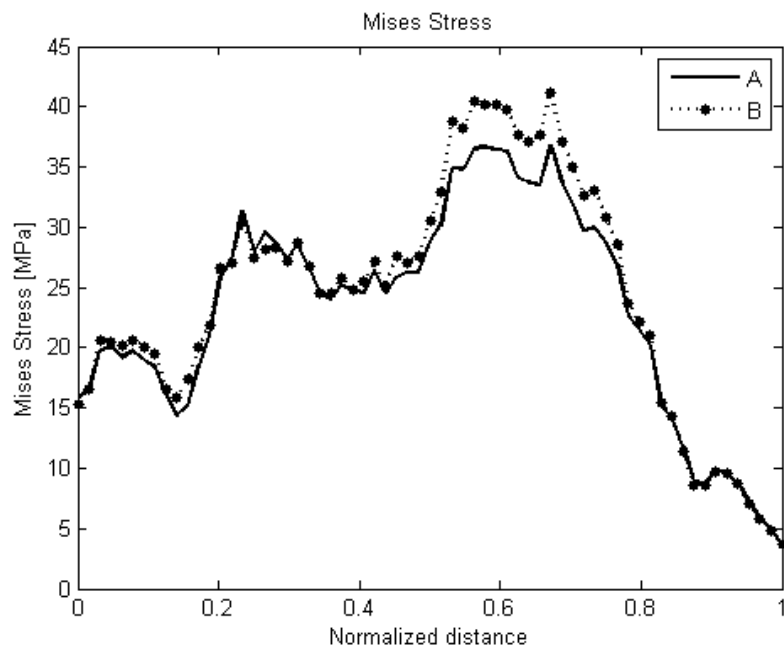


**Figure 4.9:** Path along the medial femur shaft

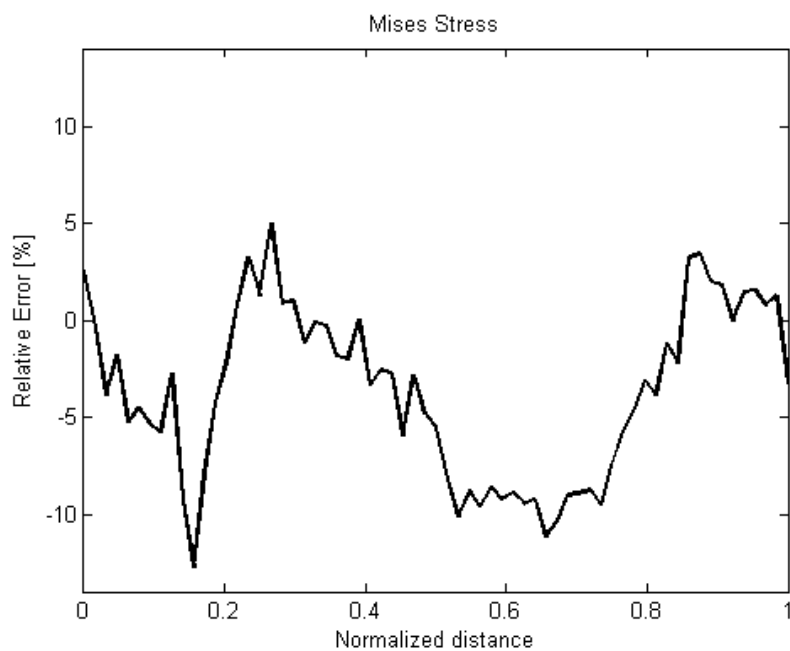
The femur model itself has limited validity because of constant young modulus and relatively low number of linear tetrahedral elements. However, efforts can be made to increase training set, assign intensity based material properties to the nodes, and elevate the number of elements to create a valuable femur model. Despite the limited training data for the SFEM, these preliminary results indicates the feasibility of the method to predict bone stresses. Additionally, this method can be extended to non-linear cases by use of more advanced interpolation techniques like ANN. The major benefit of this approach is that it shifts the calculation effort in a early phase of the development. This very time consuming task can be achieved in advanced using parallel high computational resources. On the user side, the calculation effort is minimal resulting in real time output, which is appropriate for clinical application.

#### 4.2.5 Conclusion

In this work, we proposed a feasible method for a pre-computed *patient-specific* model, hence, reducing time and complexity for future applications. We believe that this method has the potential



**Figure 4.10:** Mises stress along the path: Calculated values (A) and the simulation results (B)



**Figure 4.11:** Relative error along the normalized path

to bring recent advances in biomechanics to clinical practice.



### 4.3 Methods to accelerate finite element calculation in biomechanics using a statistical database of pre-calculated simulations: Von Mises and displacement

M. Kistler (1), S. Bonaretti (1), C. Boichon (2), M. Rochette (2) and P. Büchler (1)

(1) Institute for Surgical Technologies and Biomechanics, University of Bern, Switzerland;

(2) ANSYS Inc., France

#### 4.3.1 Abstract

FE models developed from CT data are commonly used to evaluate the mechanical performance of bones or orthopedic implants. However, the construction of a numerical model for a *patient-specific* involves many steps, which is time consuming and limits this approach to a small number of cases. In this work, we propose to combine a SAM with pre-calculated FE calculations to reduce the time required to obtain *patient-specific* mechanical simulations. A SAM was built from a training set of 72 CT of female femurs. The SAM was used to generate 1'000 FE models, covering 75% of the variability of the training population. Calculated stresses and displacements were used to build a database of numerical results. nonlinear iterative partial least squares (NIPALS) method was used to predict stresses and displacements for new bone instances without additional FE calculations. The accuracy of the predictions was evaluated on 25 bones samples. The method failed to predict bone response if only shape and material properties are considered. By including the loading scenario, the predictions error was about 0.5 MPa for stresses and 0.001 mm for displacements.

#### 4.3.2 Introduction

Over the last decades, the biomechanical community invested efforts to develop patient specific models. A popular approach to create such models is the FEM. FE models developed from CT data are used to evaluate the mechanical performance of bones, load transfer from implant to bone, bone-cement interface mechanics and fracture risks [Querol; Bonaretti et al., 2008; Bryan et al., 2009]. FE models are build out of CT scan data by first label the desired bony structure (segmentation), followed by the creation of the 3D representation of the anatomical structure from the segmented CT data, and by the creation of a FE mesh to solve the mechanical problem. However, the construction of a *patient-specific* numerical model and solving the FE problem is time

consuming, which limits this approach to a small number of cases. In addition, most analyses do not account for the wide variation in material properties and geometry that may occur in natural tissues. They do not include manufacturing imperfections in synthetic materials because the underlying information came from only a limited number of anatomical structures. Recent work started to include this variability into biomechanical analyses; Taddei et al. [Taddei et al., 2006c] proposed a method based on Monte Carlo simulations to include geometric and material uncertainties in FE simulations. The technique was improved by Laz et al. [Laz et al., 2007] who proposed a probabilistic platform to account for the uncertainties in the mechanical properties for fracture risk predictions. Khalaji et al [Khalaji et al., 2009]. proposed to combine FE calculations with SSM. SSM has also been used to represent human bone anatomy [Bianz et al., 2004] [Cootes and Taylor, 2001] [Rajamani et al., 2007]. This method was extended to include bone mineral content in a combined SAM [Bryan et al., 2009], which includes both anatomical and mechanical information.

The purpose of the present work is to propose a technique to reduce the computational time to build and solve *patient-specific* models. The proposed method relies on a combination of SAM and FEA.

### 4.3.3 Methods

#### Statistical model of appearance

The SAM was built from a training set of 72 female left femur CT image series. First, the femurs were manually segmented in Amira (Visage Imaging Inc., USA) and the surface mesh was created. Subsequently, correspondence and non-rigid alignment between the 72 training instances was established using a morphing approach developed by ANSYS Inc., France. The ANSYS Morpher takes as input a generic template mesh and a subject's geometry. Additionally, ten anatomical landmark points on both meshes were recorded. Using these inputs, the algorithm matches the template mesh onto the subject's geometry based on radial basis function, and generates a new volume mesh of the subject geometry with corresponding number of nodes and elements [Hraiech, 2010].

PCA [Cootes and Taylor, 2001] was used to create the SSM from the volumetric meshes. A second SM for the intensities of the CT images (SIM) was created using again PCA. Since the mineral content is related to the image intensity, this model corresponds to a SMM of the bones. Both models were combined to build the SAM. The SAM was used to generate 1'025 femur mesh instances, using the first five modes covering 75% of the variability of the training population.

1'000 bones were used to build the training population for the FE predictions, and 25 cases are used for the model validation.

### Finite element model

An FE model was built for each femur of the dataset with a loading situation corresponding to normal walking (Section 4.1). The magnitude of the forces was scaled according to the subject's body weight. To account for the individuality of each subject, the body weight was generated based on the subject's femur length [Bryan et al., 2009] and on the training population's BMI ( $26.36 \pm 6.01$ ). The image intensity values were converted into material properties ( $0.05 \text{ GPa} < E < 17 \text{ GPa}$ , Poisson ratio = 0.3) [Morgan et al., 2003] [Schileo et al., 2008a] and mapped onto each node of the FE mesh which consisted of 129'600 C3D10 elements and 191'532 nodes. For the calculations, the commercial software package ABAQUS was used. Mises stress and magnitude of displacement for all nodes were collected from all simulations.

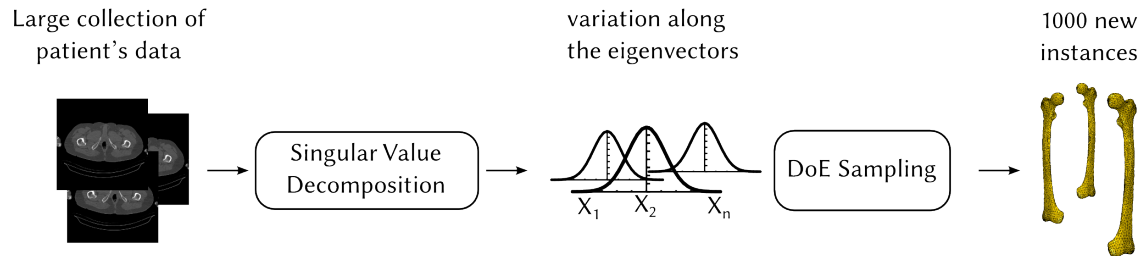
### Predictive model

The extracted stresses and displacements were used to build their respective database of numerical results by using SVD. NIPALS regression was used to establish a relationship between the model input parameters (geometry, mechanical properties, and loading) and the numerical FE predictions. For the predictions, a representation of 98% was used for both stress and displacement models. The displacement model showed higher compactness than the Mises stress prediction model. Finally, the accuracy of the model's predictions was evaluated on 25 bone samples. (Figure 4.12).

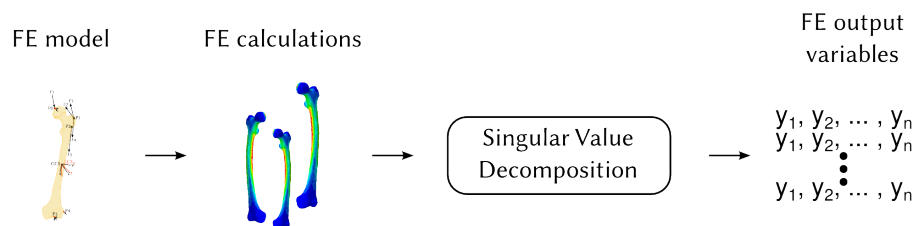
#### 4.3.4 Results

For a first prediction, which included femoral head displacement and maximum Mises stress in three regions, the response of the bones could be calculated by an average relative accuracy between 1.1% and 16%, with a negligible calculation time (a few milliseconds). The accuracy increases drastically by including the loading scenario in the predictive model as well as when more components are used in the partial least square (PLS) regression (Figure 4.13). In a second step, the prediction of the full response of Mises stress and displacement magnitude for all 25 was carried out (Figure 4.14). The average absolute prediction error for the Mises stresses was  $0.01 \pm 0.46 \text{ MPa}$  and for the displacement magnitude  $0.001 \pm 0.05 \text{ mm}$ .

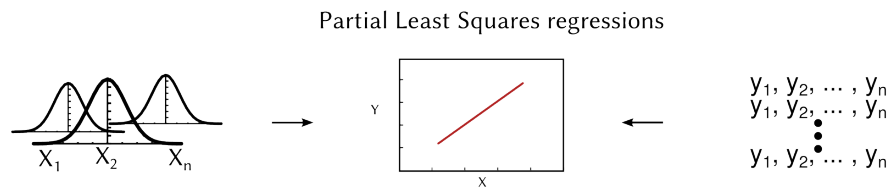
### 1. Building the Statistical model of appearance



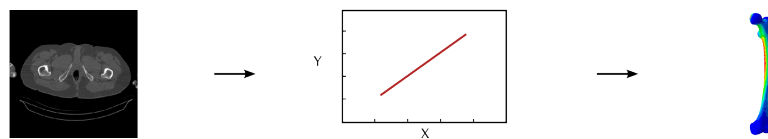
### 2. Construction of the pre-calculated database



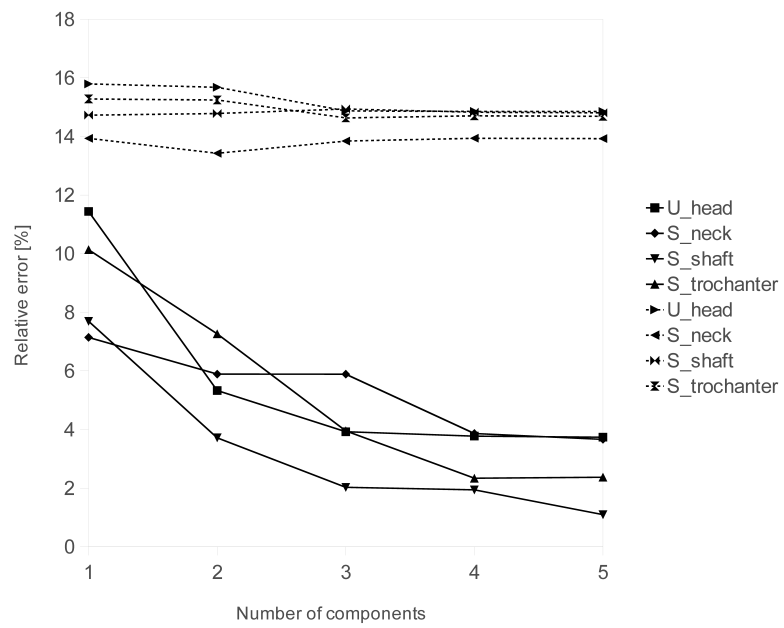
### 3. Simplified predictive model



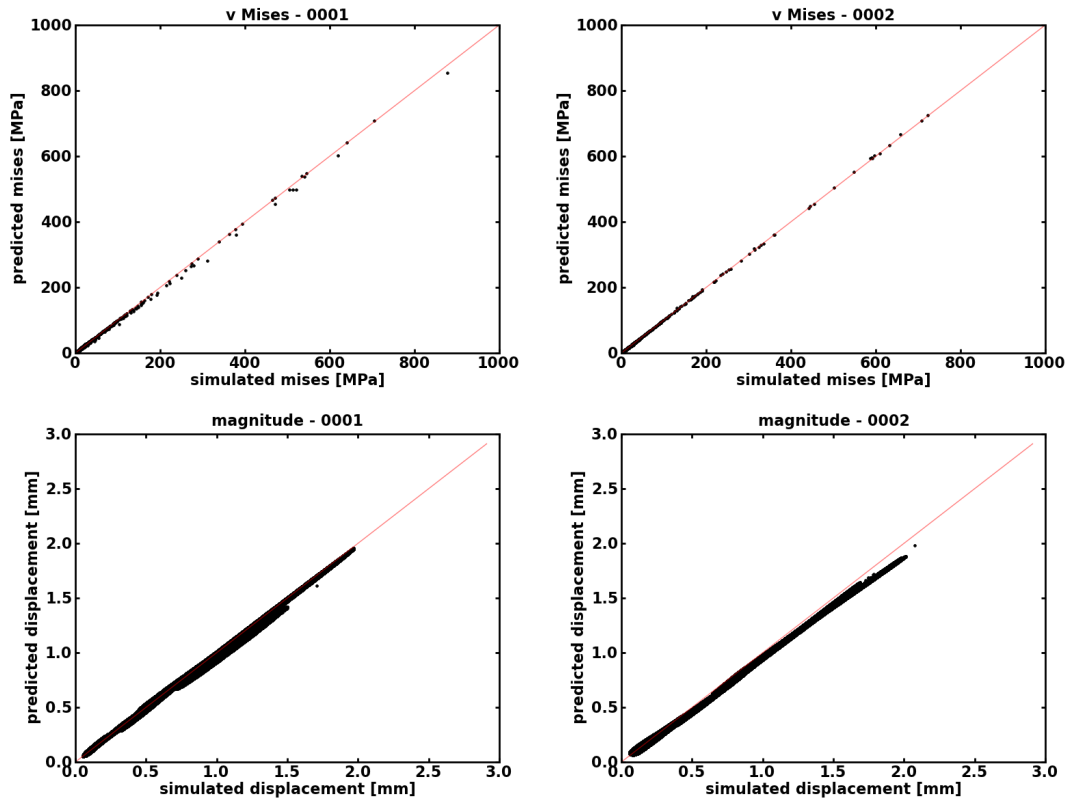
### 4. Prediction of the mechanical response



**Figure 4.12:** Pipeline to create a predictive model: (1) PCA is used to create a SMA model from which new bone instances are created. (2) another PCA decomposition is used to combine results form the simulations. (3) NIPALS relates the input model parameters to the numerical FE predictions and constitutes a predictive model. (4) The predictive model is used to instantly deliver the result for a new subject.



**Figure 4.13:** Prediction error with the mechanical loading included (solid line) or excluded (dashed line) from the predictive model for a single case. Measurements: femoral head displacement and Mises stress in the femoral neck, trochanter region, and the shaft of the femur.



**Figure 4.14:** Absolute prediction errors for Mises stresses and for the magnitude of displacement of two patients: Top row (Patient 0001)  $0.02 \pm 0.37$  MPa,  $-0.014 \pm 0.023$  mm, bottom row (Patient 0002)  $0.07 \pm 0.27$  MPa,  $-0.062 \pm 0.033$ mm.

#### 4.3.5 Discussion

The model fails to predict the bones response if only shape and material properties are considered. Hence, a SSM, which includes bone shape, material properties, and boundary conditions is required for reliable predictions. By incorporating mechanical parameters, the model is able to predict Mises stress with error of 0.5 MPa which is small compared to the failure strength of bone.

Some prediction outliers can be observed at nodes with high forces (e.g. muscle insertion point). This could be optimized by a FE model which distributes the loads over an area instead of a single node. Additionally, the model's capacity for predictions, for example fracture risks, is currently limited because the raw CT images were not calibrated.

However, we were able to show the power of this method to avoid additional FE calculations by combining SAM, FE, and a regression model to predict FE outcome. The accuracy of this method is already suitable for several clinical applications.

## 4.4 Methods to accelerate finite element calculation in biomechanics using a statistical database of pre-calculated simulations

M. Kistler (1), S. Bonaretti (1), C. Boichon (2), M. Rochette (2) and P. Büchler (1)

(1) Insitutte for Surgical Technologies and Biomechanics, University of Bern, Switzerland

(2) ANSYS Inc., France

### 4.4.1 Abstract

FE models of anatomical structures reconstructed from medical datasets are commonly used to evaluate the mechanical performance of bones or orthopedic implants. However, the process to build the numerical model and run the FE calculations is time consuming and prevents the clinical acceptance of *patient-specific* simulations. To solve this time constrain, we propose to combine a statistical description of bone shape and mechanical properties with pre-calculated FE calculations in order to obtain *patient-specific* mechanical information without additional time-consuming simulations. The proposed method was evaluated with a model of the femur loaded according to normal walking (Section 4.1). The accuracy of the predictions was evaluated on 25 bones samples. Results showed that the proposed method is able to instantaneously provide the distribution of bone stresses with a prediction error below 0.1MPa and of nodal displacements with an accuracy of less than 70  $\mu\text{m}$  for the in-silico data.

### 4.4.2 Introduction

FE simulations have been introduced in biomechanics about 40 years ago. Since then, this technique has been very successful in providing a deeper understanding of the human mechanical behavior, and optimizing implant design or surgical procedures [Hansson, 2003; Terrier et al., 2005]. With the increasing availability of computational power and the constant improvement of the numerical simulation tools, *patient-specific* numerical models have been proposed to predict the surgical outcome of a wide range of clinical procedures and to find the optimal treatment for each specific patient [Reggiani et al., 2007; Wittek et al., 2007; Little and Adam, 2011; Roy and Dupps, 2011]. Although these models have been successful in proving the feasibility of using biomechanical models for *patient-specific* simulations, to the best of our knowledge, to date, no *patient-specific* biomechanical model has been introduced in the daily clinical routine. One of



the main challenges in achieving this objective is the ability obtaining patient-specific information on the anatomical shape, mechanical properties and boundary conditions. Furthermore, clinical applications require automatic building of *patient-specific* FE models and near real-time results must be provided to physicians. The complexity of the FE modeling currently requires trained experts to build the numerical models through the processes of: including image segmentation, definition of appropriate boundary conditions and material properties, FE calculation and analysis of the numerical results. The additional time required to perform these steps is not acceptable for the physician, which prevents the diffusion of the FE method in the clinical environment.

During recent years, SSM has been introduced in biomechanics. This technique has initially been proposed by Cootes et al. [Cootes et al., 1995] to capture the anatomical variability in a given population and has been widely used in medical image analysis to study human anatomy [Lamecker et al., 2002; Lötjönen et al., 2004; Baldwin et al., 2010], perform model-based segmentation [Blanz et al., 2004; Fritscher et al., 2007; Schmid and Magnenat-Thalmann, 2008] or to enable 2D/3D reconstruction [Benameur et al., 2003; Deligianni et al., 2006; Zheng et al., 2009; Väänänen et al., 2012]. An initial study combining shape models and FE simulations has been published by Querol et al. in 2006 [Querol] comparing bone stiffness for different instances generated with a statistical shape model. Since then, SSM have been used to assess the risk of neck fracture in the population of 1'000 femurs [Bryan et al., 2009] and to study the impact of femoral morphology on the mechanical behavior of resurfacing implants [Bryan et al., 2012]. This approach is very useful in providing a deeper understanding of the biomechanical behavior across a given population, but doesn't provide *patient-specific* information. Some authors used SSM to correlate anatomical morphology with mechanical measurements [Khalaji et al., 2009]. The correlation model can then be used to make *patient-specific* mechanical predictions [Fitzpatrick et al., 2010]. More recently, Mousavi et al. [Mousavi et al., 2012] applied a similar approach and correlated morphometric parameters, obtained from a SSM of the prostate, with the results of FE simulation. With this technique, the full displacement field corresponding to a simplified 2D model of the prostate could be obtained without additional FE calculation. However, they did not include mechanical properties or loading conditions in the prediction model. To the best of our knowledge, no existing work considers all aspects required to perform accurate biomechanical calculations (ie. bone shape, mechanical properties and loading conditions) in order to predict a full stress or displacement response of a FE model.

The aim of this study is to assess the accuracy of combining a SM and FE simulation to predict bone stress and deformation fields for a realistic loading scenario. Such a model will enable

real-time prediction of the FE response of the mechanical structure based on *patient-specific* information.

#### 4.4.3 Methods

##### Statistical model of appearance

The SAM was built from a training set of 72 female left femur CT image series (Table 4.2). The resolution of the images was between 0.61 mm x 0.61 mm and 1.171 mm x 1.171 mm, with a slice thickness of 1 mm. The femurs were manually segmented out of the CT datasets with the commercial software Amira 4 (Visage Imaging Inc., USA), and the surface meshes were created. Subsequently, correspondence and non-rigid alignment between the 72 training instances were established using a morphing approach developed by ANSYS Inc., France. This mesh morphing techniques relies on a template FE mesh of a reference instance, which is projected on the surface model of the target femur. In order to ensure the quality of the anatomical correspondences established between the bone instances, ten easily identifiable anatomical landmarks were manually selected on all bone instances. The morphing algorithm uses RBF to deform the template mesh onto the subject's geometry [Hraiech, 2010]. The morphing process results in equivalent FE meshes for all of the femurs in the database having the same number of corresponding element and nodes. Finally, the meshes were rigidly aligned using the Procrustes algorithm in order to prepare them for PCA.

**Table 4.2:** Demographics of the femoral data collection used to build the statistical model

Parameter	Unit	Mean	SD
<b>Age</b>	<i>y</i>	64.28	15.60
<b>Height</b>	<i>cm</i>	162.92	6.05
<b>Weight</b>	<i>kg</i>	69.95	16.03
<b>BMI</b>	$\frac{kg}{m^2}$	26.36	6.01

PCA applied to the nodal positions of the FE meshes was used to create the SSM [Cootes et al., 1995]. With this approach, each shape can be described by a linear combination of modes of deformations in a basis of orthogonal vectors using equation 4.2:

$$x = \bar{x} + \Phi_s b_s \quad (4.2)$$

where describes the shape of a femur,  $\bar{x}$  is the mean femoral shape and the bone shape is fully

defined by its representation . The same approach was used to build a SM of the bone intensity at each node using equation 4.3:

$$g = \bar{g} + \Phi_g b_g \quad (4.3)$$

Finally, both models were combined to build the SAM (bone shape and intensity) as proposed by Cootes et al (Cootes and Taylor 2001) and described in equation 4.4-4.6:

$$a = \begin{pmatrix} W_s b_s \\ b_g \end{pmatrix} = \begin{pmatrix} W_s \Phi_s^T (x - \bar{x}) \\ \Phi_g^T (g - \bar{g}) \end{pmatrix} \quad (4.4)$$

$$a = \phi b_a \quad (4.5)$$

$$a = \begin{pmatrix} \phi_s \\ \phi_g \end{pmatrix} \quad (4.6)$$

where  $a$  represents the combined parameter matrix of one instance of the dataset,  $\phi_s$  represents the shape component, and  $\phi_g$  the intensity component of the combined model. The matrix  $W_s$  is used to scale the shape and intensity values to a similar magnitude using equation 4.7:

$$W_s = rI \quad (4.7)$$

where  $r$  is the square root of the ratio between the total variation obtained from the SIM and the SSM and  $I$  is the identity matrix. The SAM was used to generate new bone instances. The number of modes retained in the combined model was able to represent 75% of the variability of the training population. New bone instances were generated using equation 4.8 and 4.9.

$$x = \bar{x} + \Phi_s W_s \phi_s b_a \quad (4.8)$$

$$g = \bar{g} + \Phi_g \phi_g b_a \quad (4.9)$$

Each value given in the vector  $b_a$  defines a new bone instance. 500 new synthetic femurs were generated using this model. The weighting parameter  $b_a$  was defined using Latin hyper cube sampling.

### Finite element model

A FE model of the femur corresponding to a normal walking situation has been developed. The loading conditions were obtained for the forces in the abductor muscle group, the tensor fasciae latae muscle, the vastus lateralis muscle and for the force on the femoral head from data previously published by Heller et al. [Heller et al., 2005]. In order to provide realistic loads for each subject, the magnitude of the forces were scaled according to the subjects' body weight. This adaptation of load has been performed by first calculating the BMI of the bone population used in our study ( $\text{BMI } 26.36 \pm \text{standard deviation (SD) } 6.01, n = 62$ ). Based on the normal distribution, a BMI was randomly assigned to each subject and converted to the body weight using the direct correlation between the bone length and the subject's height [Bryan et al., 2009]. The loading was combined with the *joint* constraints configuration from Speirs et al. [Speirs et al., 2007] where node constraints were selected at the femoral head, the intercondylar femoral notch and the lateral epicondyle of the femur (Figure 4.15).

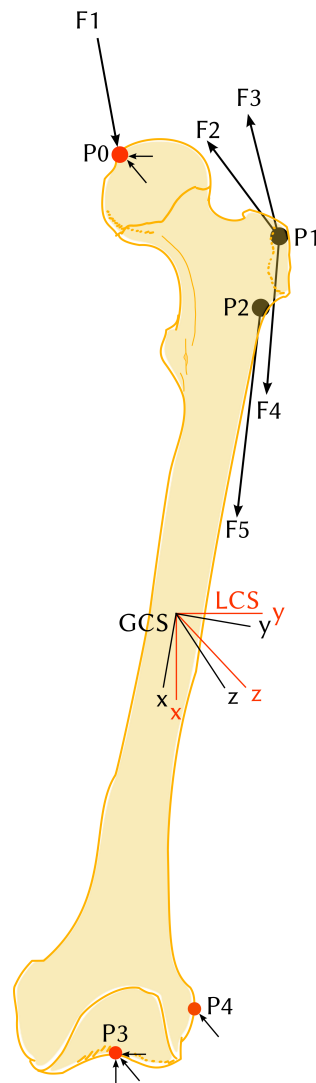
The Hounsfield values of the bone given in the CT images were converted into material properties ( $0.05 \text{ GPa} < E < 17 \text{ GPa}$ ,  $\nu = 0.3$ ) [Morgan et al., 2003; Schileo et al., 2008a] and mapped onto each node mesh. The FE model consisted of 129'600 quadratic tetrahedron (C3D10) elements and 191'532 nodes. For the calculations, the commercial software package ABAQUS (Abaqus, v6.10EF, Dassault Systems, Providence, RI, USA) was used. Stress tensor and displacement vector for all nodes were recorded.

### Prediction model

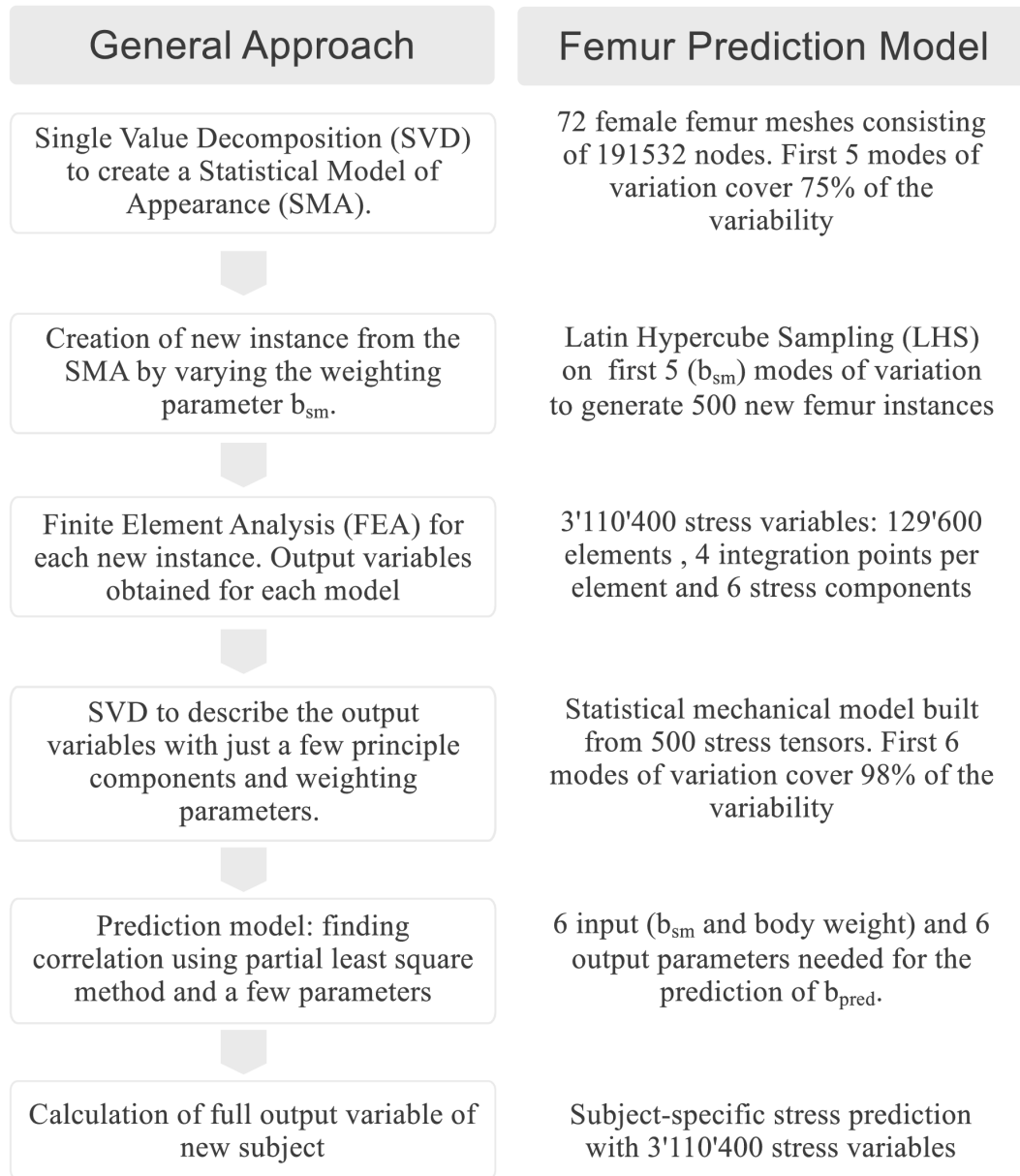
Numerical simulations were performed on 500 synthetic femurs. The displacement vector at each node of the model and the stress tensor for each integration point of the mesh were extracted. This data was used to build a SMM of the femur stresses and displacements. For the prediction models, the number of modes required to achieve a representation of 98% of the mechanical variability for both stress and displacement were retained.

NIPALS regression was used to establish a relationship between the model input parameters (geometry, mechanical properties and loading) and the numerical FE predictions parameters to build the prediction model (Figure 4.16).

To evaluate the prediction models, 25 additional samples were generated with the SAM. The mechanical state obtained by the direct FE solution of the problem was compared to the results obtained with the simplified predictive model. The comparison was performed on the full stress and displacement fields.



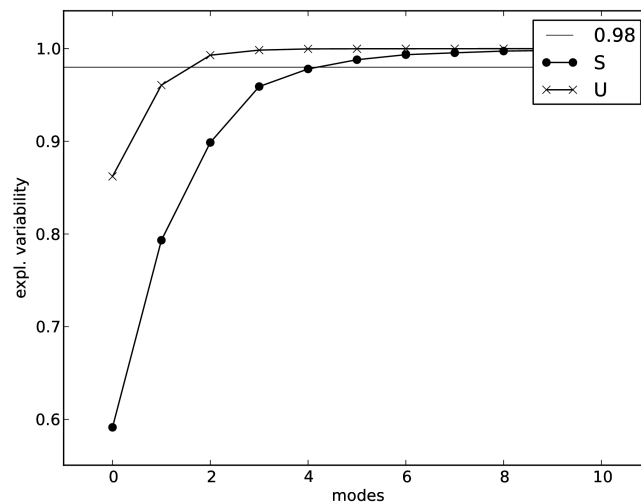
**Figure 4.15:** Boundary conditions applied on the FE model for a normal walking situation. The BC at P0 constrained the femoral head to move along the mechanical axis. The intercondylar femoral notch (P3) was constrained in three degrees of freedom and the lateral epicondyle (P4) was modeled to prevent anterior-posterior motion. The hip contact force (F1) was applied on the humeral head at P0, muscle forces were applied at P1 for the abductor (F2), and tensor fasciae latae proximal(F3) and distal (F4). The force corresponding to the vastus lateralis (F5) was applied on P2. The GCS was aligned to the anatomical femoral shaft axis and the LCS to the mechanical axis of the femur.



**Figure 4.16:** Schematic description of the workflow used to develop a prediction model and its application on a human femur.

#### 4.4.4 Results

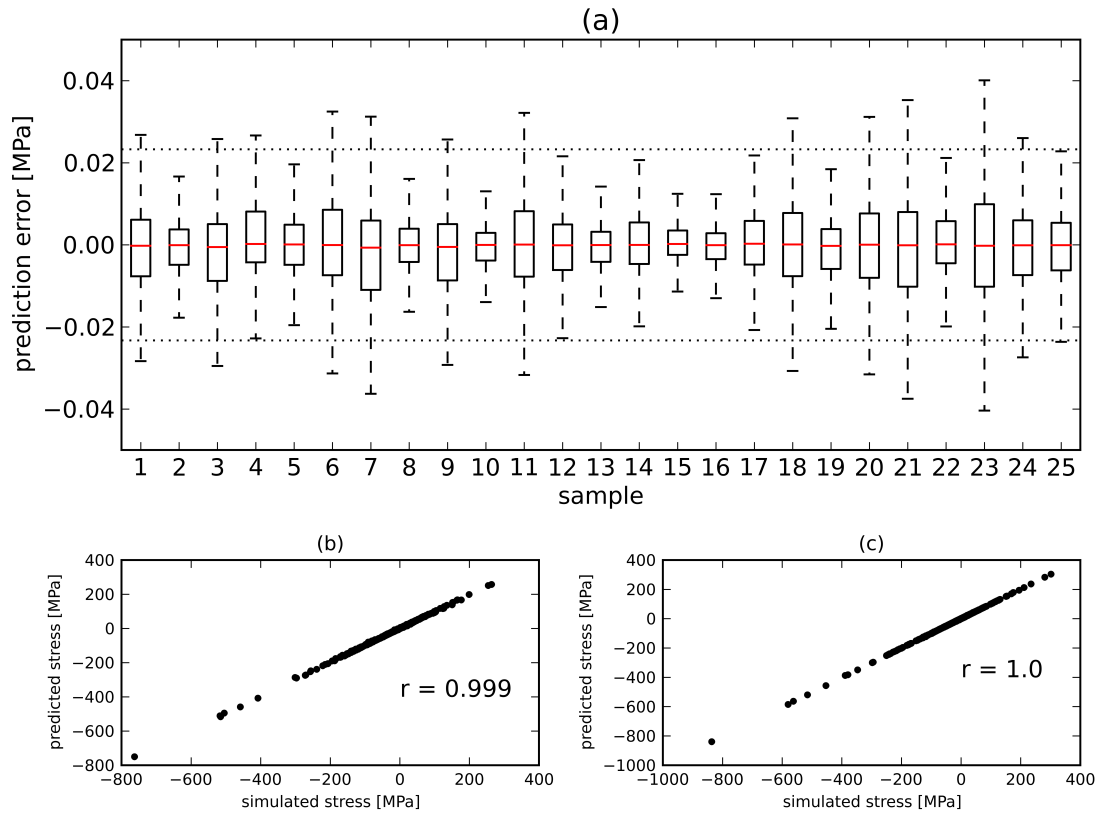
Two separate prediction models for the primary mechanical variables (stress tensor and displacement vector) were developed, and their accuracy's tested on 25 synthetics femur bones. PCA was used to represent the shape and intensity in a compact manner. Five modes were sufficient to reproduce 75% of the variability in the population. This result indicates that five modes combined with a mechanical weighting number (e.g. body weight) are able to fully describe 75% of the bones in a given population. Similarly, both the statistical stress tensor model and the statistical displacement vector model were able to represent the full training data in a compact way, where 98% of the variability is covered by the first six modes for the stresses and three modes for the displacements (Figure 4.17). As a direct consequence of this compact representation of the data, the PLS regression was able to establish a correspondence between the input and output parameters with a coefficient of determination of the prediction ( $R^2$ ) of 0.97 for stress and 0.87 for the displacement.



**Figure 4.17:** Compactness of the statistical stress tensor model (red line), and the statistical displacement vector model (blue line). Threshold was set to 98%.

The displacement vector as well as the stress tensor was calculated at each location of the FE mesh using two independent methods; first with a traditional FE solver and second using the proposed statistical approach. The predicted values were compared at each node and integration point for all 25 samples. The results showed no statistical difference between the stresses ( $p = <0.0001$ ) and displacements ( $p = <0.0002$ ) predicted with the two models. The average MAE across all samples was  $0.025 \text{ MPa} \pm 0.11 \text{ MPa}$  (Limits:  $-38.61 \text{ MPa}$ ,  $59.64 \text{ MPa}$ ) for the stress

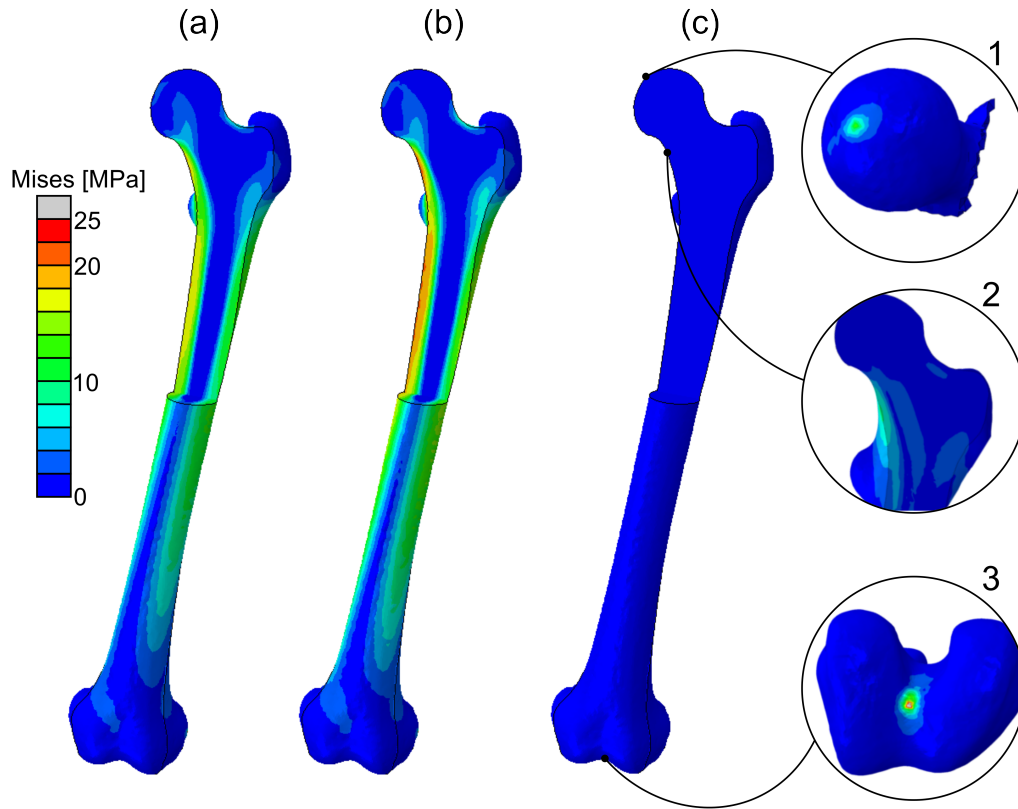
tensor and  $0.04 \text{ mm} \pm 0.05 \text{ mm}$  (Limits:  $-0.45 \text{ mm}$ ,  $0.31 \text{ mm}$ ) for the displacement vector. The quality of the predictions were also evaluated by calculating the regressions of the FE stresses and displacements of the solver respectively; the Pearson regression coefficient was above 0.99 for all 25 samples (Figure 4.18). The main difference between results obtained from the two methods are localized in the regions of stress concentration next to where the boundary conditions were applied, as well as in the regions of high stress values (Figure 4.19). In these cases, the difference can be up to 65 MPa, but this only represents a small percentage of the stress value at this location.



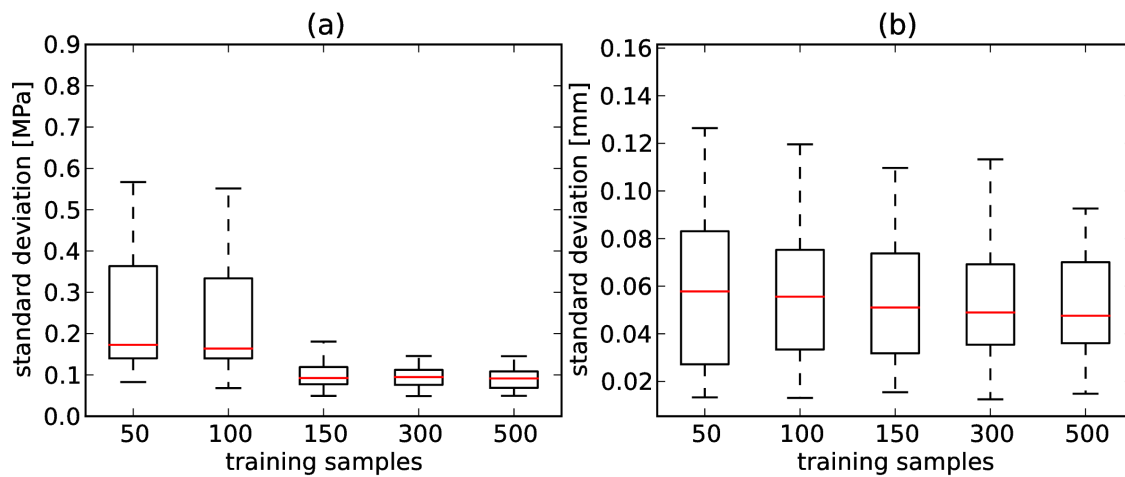
**Figure 4.18:** Prediction error of the stress tensors of all 25 test samples (a). Each box represents the error distribution of a single test sample. The area between dotted lines represent the  $\pm 2$  SD covering 95%. Simulated vs. predicted stress for sample 15 with mean absolute error  $0.005 \pm 0.052 \text{ MPa}$  (b) and sample 23 with a mean absolute error of  $-0.015 \pm 0.231 \text{ MPa}$  (c).

The influence of the size of the training dataset on the prediction accuracy was evaluated by building prediction models composed of 50, 100, 150, 300, and 500 training bones. Results showed a transition of the accuracy of the prediction at about 150 samples. Increasing the number of training data doesn't significantly improve the prediction accuracy (Figure 4.20).





**Figure 4.19:** Comparison of the Von Mises stress obtained with the FE prediction model (a) and from the simulation (b). The absolute error distribution (c) and regions with higher errors (1-3) are shown using the same color scale.



**Figure 4.20:** MAE using the prediction model with 50, 100, 150, 300 or 500 training data sets for the stress tensor (a) and displacement vector (b).

#### 4.4.5 Discussion

Simulation of the mechanical performance of bone is conventionally performed using the FE method, which implies a time consuming procedure to build the model, apply the boundary conditions, assign the mechanical properties and solve the numerical equations. The aim of this study was to evaluate the use of a database of pre-calculated FE simulations to accelerate the time required to obtain *patient-specific* results. Results showed that the mechanical state of the bone obtained with the statistical predictions is similar to results achieved with a full FE calculation, with the benefit of having the mechanical information available immediately. The presented method is able to determine the distribution of stresses and displacements over the bone volume to an accuracy of about 0.1 MPa for the stress and 65  $\mu\text{m}$  for the displacements, which is negligible compared to the failure strength of the bone.

PCA has been used to reduce the dimension of the problem. This reduction is necessary to be able to establish a simple correlation between input and output parameters. In the case of the femur, it was possible to limit the problem to finding the correlation between six input parameters describing the femoral shape, mechanical properties, and loading condition to a maximum of six output variables describing the mechanical stress distribution. These outputs should be compared to the number of elements in the femur models, consisting of about 130'000 triangular elements. In the present study, all important biomechanical parameters were included in the input of the predictive model, which constitutes a statistical biomechanical description of the problem. It can be shown that if one of these aspect is omitted (ie. bone shape, mechanics or load) the quality of the prediction decreases [Kistler et al., 2012].

The accuracy of the prediction achieved on the primary mechanical variables (stress tensor, displacements) allows the calculation of other mechanical quantities such as other descriptions for the stress, forces or strains. For example, the Von Mises stress in the femur calculated based on the stress predictions was not statistical different from the Von Mises calculated with the FE approach (Figure 4.19). However, if the focus of a specific model lies in the level of Von Mises stresses, the method of choice would be to directly generate a statistical predictive model for this variable instead of deriving it from the primary variables. Adapting this method to other output variables is straightforward, which makes it attractive for many areas within the biomedical field.

Prediction outliers can be observed at nodes with high forces (e.g. muscle insertion point and displacement boundary conditions), which indicates that the presented approach has a lower accuracy localized close to the loaded nodes. However, these localized stress concentrations represent numerical artifacts and the FE results are in most scenarios not relevant. If precise stress values

are required in these regions, a FE model with loads distributed over a larger area to represent the muscle insertion zone would optimize the prediction and limit the prediction outliers. Another factor that could explain the inaccuracy in region of stress concentration is the linear nature of the predictive model. Non-linear approaches such as ANN could provide more precise results.

One limitation of the presented study is that the bone instances used for the validation were generated with the SSM, which does not exactly correspond to the situation of *patient-specific* simulation. An additional step is required to establish the correspondence between new femoral instances and the template bone mesh. This registration step is the same as the mesh morphing used to build the SSM, however, it is used to project the new bone within the space of eigenvectors used to describe the training population. Once completed, the parameters describing the new bone within the orthogonal space of eigenvector are known and can be used for the predictions. However, the quality of representation of the bone in the PCA space will be bound by the number of modes retained to describe the training population, in our case five modes to represent 75% of the training samples. Nevertheless, the objective of this study was to evaluate if a simplified SM can replace the FE calculation. Therefore, although increasing the number of modes used in the model is technically straightforward, the investigation on the effect of the number of modes on the representation of new bone shapes is outside the scope of this study.

The combination of a SSM and a pre-calculated database of FE simulation can predict *patient-specific* mechanical responses with an accuracy and calculation time suitable for clinical situations. However, to ensure accurate results a SMM which includes bone shape, material properties, and BC is required. The presented method does not reduce the amount of work to obtain mechanical results, but shifts the calculation time to a pre-processing step where a mostly automated process can run a large numbers of FE simulations. Based on these pre-calculations, it is possible to obtain instantaneous FE results offline, which paves the way for FE applications to enter the daily clinical routine.



## 4.5 Patient-specific fe predictions

The previous sections demonstrated the possibility of the prediction method. So far, the methods were only tested on bone instances generated with the model which is used to initialize the prediction model and the test instances alike. Therefore, four CT datasets from the VSD and the SFM were chosen to test the prediction method on bones from outside the generated SSM in a *patient-specific* settings.

### 4.5.1 Methods

The prediction method was tested against the SFM [SFM, 2010] and four patients CT data available on the VSD to evaluate the accuracy of the model on subject specific data (Table 4.3).

The stress and displacement of these five *patient-specific* models were calculated in the same way as the 25 synthetic bones in section 4.4. However, an additional step is required to establish correspondence between new femoral instances and the template bone mesh. This registration step is the same as the mesh morphing used to build the SSM, however, it is used to project the new bone within the space of eigenvectors of the training population. The average mechanical properties of SAM were assigned for the SFM.

**Table 4.3:** Demographics of the four VSD subjects

Subject	Unit	VSD 2	VSD 3	VSD 8	VSD 14
<b>gender</b>		female			
<b>Age</b>	y	78	90	60	30
<b>Height</b>	m	1.62	1.57	1.54	1.65
<b>Weight</b>	kg	75	41	45	65
<b>BMI</b>	$\frac{kg}{m^2}$	28.58	16.63	18.97	23.88

### 4.5.2 Results

Again, the accuracy of the same prediction models as presented in section 4.4 were tested for all five samples. For all samples, both the traditional FE solver and the proposed method were used to calculate the displacement and stress at each location of the FE mesh. The predicted values were compared to the results from the FE solver at each node and integration point. Additionally to the stress tensor and displacement vector, the Von Mises stress and the displacement magnitude were calculated and compared.

The average MAE across all samples was  $2.04 \text{ MPa} \pm 3.64 \text{ MPa}$  (Max.:  $370.09 \text{ MPa}$ ) for the Von Mises stress (Table 4.4) and  $1.21 \text{ mm} \pm 0.38 \text{ mm}$  (Max.:  $4.72 \text{ mm}$ ) for the displacement magnitude (Table 4.5). The average MAE of the stress components was  $0.62 \text{ MPa} \pm 1.32 \text{ MPa}$  (Limits:  $-365.85 \text{ MPa}$ ,  $397.18 \text{ MPa}$ ). The average MAE of the displacement vector was  $0.77 \text{ mm} \pm 0.43 \text{ mm}$  (Limits:  $-2.73 \text{ mm}$ ,  $4.71 \text{ mm}$ )

Additionally, the prediction quality was evaluated by calculating the regressions of the FE stresses and displacements (predicted vs. calculated). The Pearson regression coefficient of the stress tensors and displacement vector averaged between 0.68 and 0.89.

Detailed results for the individual components are presented for the SFM (Table 7.5 and figure 4.21) and the VSD subject 2 (Table 7.1 and figure 4.22). The complete evaluation for all five cases are presented in the appendix 7.

**Table 4.4:** Average accuracy of the patient-specific von Mises Stress prediction

Subject	VSD 2	VSD 3	VSD 8	VSD 14	SFM	Average
<b>Avg. error [MPa]</b>	2.27	2.30	1.58	2.44	1.60	2.04
<b>SD [MPa]</b>	4.30	3.89	2.88	4.27	2.86	3.64
<b>Pearson coeff.</b>	0.83	0.63	0.79	0.78	0.94	0.80

**Table 4.5:** Average accuracy of the patient-specific displacement (magnitude) prediction

Subject	VSD 2	VSD 3	VSD 8	VSD 14	SFM	Average
<b>Avg. error [MPa]</b>	3.15	1.42	0.65	1.35	0.67	1.21
<b>SD [MPa]</b>	0.47	0.48	0.26	0.63	0.42	0.38
<b>Pearson coeff.</b>	0.95	0.91	0.97	0.78	0.84	0.80

**Table 4.6:** Patient specific stress tensor and displacement vector prediction average accuracy of the SFM

Component	S	S11	S22	S33	S12	S13	S13	U	U1	U2	U3
				MPa						mm	
<b>Avg. error</b>	1.60	0.34	0.23	1.51	0.17	0.64	0.51	0.67	0.59	0.39	0.15
<b>SD</b>	2.86	0.88	1.09	2.74	0.52	1.05	0.93	0.42	0.39	0.34	0.10
<b>Pearson coeff.</b>	0.94	0.91	0.90	0.94	0.83	0.88	0.89	0.97	0.98	0.55	0.99

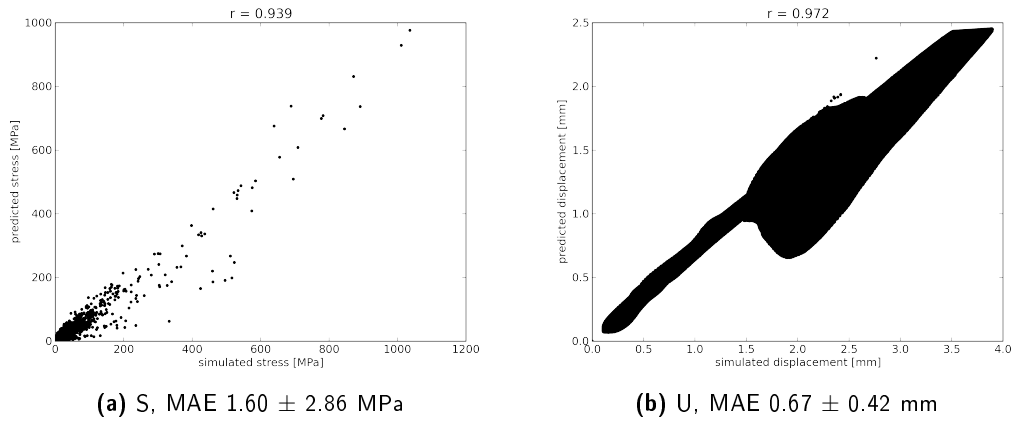


Figure 4.21: Displacement and Von Mises Stress prediction error of the SFM

Table 4.7: Patient specific stress tensor and displacement vector prediction average accuracy of the VSD subject 2

Component	S	S11	S22	S33	S12	S13	S13	U	U1	U2	U3
				MPa						mm	
Avg. error	2.27	0.30	0.22	2.13	0.15	0.48	0.32	3.15	0.95	0.38	3.04
SD	4.30	1.13	0.95	4.18	0.42	1.01	0.85	0.47	0.83	0.29	0.39
Pearson coeff.	0.83	0.83	0.88	0.84	0.85	0.84	0.90	0.95	0.97	0.29	0.99

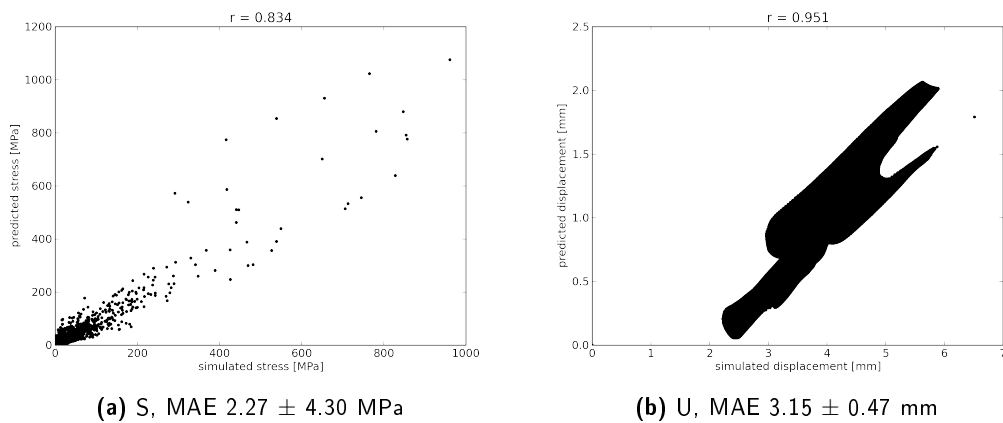


Figure 4.22: Displacement and Von Mises Stress prediction error of the VSD subject 2

### 4.5.3 Discussion

The SFM showed the best accuracy with Pearson coefficients between 0.83 and 0.99, only  $U_2$  direction showing 0.55. Another trend is documented by the average MAE. The  $S_{33}$  direction has the largest error and SD values. Interestingly, the prediction works best on the SFM, despite the fact that the SFM is a standard femur, but not an average of the human race while the selected VSD cases fitted the training population of the SAM. Having the mechanical properties of the SAM incorporated could be an explanation. Indeed, results of VSD subject 2 where the *patient-specific* mechanical properties were replaced by the average of the SAM showed slightly better results overall and significantly better results for  $U_2$ . While feasible for the SFM, using the average mechanical properties would remove some *patient-specific* for the VSD subjects.

The methods seems to fail to predict the  $U_2$  displacement accurately. The scatter plots support this finding with their unexpected patterns. However, the average MAE is in the same range as the other components, indicating unreliable results only in some regions. No obvious reasons for this behavior could be identified. A possible source of inaccuracy could be the anteversion angel of the femur (Figure 3.6). The introduced coordinate system in the femur model does not account for this angle, leading to behavior not represented in the prediction model. The highest stresses occur in the  $S_{33}$  direction. Therefore, a higher average MAE is perfectly acceptable since the relative error is still small enough.

The prediction itself remains almost instantaneous. However, with the presented method, segmentation and correspondence finding through the mesh morphing is required for the parameter finding. This step extends the overall processing effort to an unacceptable long time for clinical use. However, several options can be explored. For example a 2D-3D registration method, automatic segmentation or alternative parameter fitting are possible. Although no direct application is presented, the method shows its potential to be applied in different areas.

The prediction method is able to predict primary mechanical response parameter for *patient-specific* FE model. However, depending on the anatomical location, each component has to be carefully evaluated, since local inaccuracies can occur. This problem is primarily a problem of the FE model and not of the prediction itself. Although the prediction pipeline is generic, the prediction method cannot be applied to every anatomical structure but many options are available to find a suitable combination between SM, FE, and regression methods.



## Chapter 5

# Discussion, Conclusion and Outlook

### 5.1 Discussion

Functional requirements like searching, uploading, sharing, and managing of the database framework have been presented. These values were outlined with three projects in the database chapter (Chapter 3). The VSD features a unique ontology search which can find anatomical structures within datasets based on a comprehensive FMA ontology. The concept of this search functionality is not limited to the FMA but can be adapted to any other ontology available. For example, the RadLex (<http://www.radlex.org/>) ontology could provide the clinical terminology to annotate datasets.

The VSDUploader is able to handle different file types without the need of client side pre-processing. This generic approach allows the integration of heterogeneous technologies. The system can handle files added from a simple HTML-upload, a Flash or Java upload and even from a WebDAV client without restrictions. Thanks to the concepts of generic objects and the VSDuploader, the implementation of a new file type is a standardized process. A framework to read file type and metadata definitions is required, but there is no need to change the logic of the VSDuploader. As a disadvantage of the generic approach, the complete dataset has to be transmitted to the server before the system can detect the validity of the file. This limitation could be eliminated using the REST API. The client would be able to generate a response from the server without sending the dataset to the server. This feature is not yet included in the deployed REST API version, it has however been included in the latest specifications of the REST API (Appendix 6.3).

The VSD does not facilitate an identifiability of patients in an exam image (e.g. special plate, implant, rare malformation or head images). It was not the aim to provide the users of the VSD with a solution for this aspect. The VSD Web service focuses on providing a research community where the responsibility is given to the research unit. Users have to have the rights to upload such

data and protect the data privacy of the patients. To help protect the data and its sharing, the VSD features a separated folder-object permission concept. Together with the unique approach among research repositories, the object catalogue structure of the VSD makes it possible to control access to datasets without the knowledge of the subsequent usage thereof. To be more specific, with other repository software, it is only possible to share or hide the data. On the VSD, users can share a folder while protecting the dataset individually. It is even possible to collect datasets of other users and publish collections of datasets with heterogeneous permissions.

The Web technology used for the VSD provides the users with a responsive Web service including a consistent and informative interface for fast access to datasets and additional file information. Besides the provided preview images the VSD misses a full featured web based data viewer. However, this is not a priority because the online view of image data in the context of SSM is not crucial. Besides, with the WebDAV interface and a client image viewer it is possible to have similar functionality. On the other hand, a view for SM could give valuable information about its quality. The integration of such a service is being developed by the inventors of Statismo. A scala based Statismo integration framework and a related Web service allows to interactively explore a SM. Since the VSD hosts Statmismo SM files, this framework can provide such a functionality in near future on the VSD.

NoSQL databases are popular in the modern WWW because of their scalability potential, they are flexible and therefore perfect for polymorphic data and their data model is aligned with object oriented programming. One could argue that the use of a NoSQL database would be beneficial for the VSD because of the expected amount and heterogeneity of data .However, the VSD decided to rely on Microsoft SQL for several reasons. At the beginning of the development, NoSQL was a relatively new standard and the technical knowhow was simply not available. The Microsoft SQL is a proven, robust, secure, well-developed package and integrates perfectly into the development environment of .NET and C#.

A unique collection of 107 post mortem full body datasets is available with an almost complete set of metadata (only seven dataset are missing). For privacy reasons, the soft tissue of the head was removed from the scans. Privacy aspects were discussed in section 3.2.2 and the VSD was adapted according to the legal and ethical requirements. In addition to the full body datasets, the available in-house dataset were identified. However, this collection is not fully available to the users on the VSD yet. In addition, although the datasets are shared on the VSD, a dedicated option to publish such a collection with a full description is missing. The number of data in the VSD repository is not as big as others. For example, the cancer imaging archive (CIA) host over 2'600

mostly public datasets. Besides the traditional image acquisition, the VSD has the possibility to attract contributions through other channels. The BRATS as an example source was presented, a second could come from the fact that peer-reviewed journals nowadays often require the authors to provide the underlying research data with a publication. Even more, it would be possible to connect the VSD to a code hosting service like CodaLab ([www.codalab.org](http://www.codalab.org)). In this way, the VSD would serve as data storage and data provider in the open access trend. To improve the quality of research papers, the complete package (paper, data, code= should be available for reuse, reproduction, and review.

In chapter 4, a method to predict *patient-specific* FE results to bring FE closer to clinical application was presented. This was achieved by using a combination of SM and a pre-calculated database of FE simulation to predict *patient-specific* mechanical responses. However, to ensure accurate results a SMM which includes bone shape, material properties, and boundary conditions are required. The presented method does not reduce the amount of work to obtain mechanical results, but shifts the calculation time to a pre-processing step. A mostly automated process runs a large numbers of FE simulations. Based on these pre-calculations, it is possible to obtain instantaneous FE results offline, which paves the way for FE applications to enter the daily clinical routine. The methods could be integrated into a computer assisted planning routine. Or it could extend the spacial information provided with the corresponding mechanical response, in example for hip an impingement surgery. Although presented on a femur model, the method is not limited to the femur. The prediction pipeline itself is generic, but the model and prediction methods have to be evaluated for each specific case. Therefore, no general recommendation can be given. Several aspects need to be considered if a femur model actually should be developed for clinical usage.

The presented femur model is based only on published data which was evaluated by mechanical experiments or in-vivo data. However, no mechanical testing of the femur model was done since the acquisition of *patient-specific* experimental test data is either extremely difficulty or is even impossible. The SFM could offer an option to evaluate the model. But this experimental testing would be outside the scope of this thesis. For accurate mechanical properties, the CT data has to be accompanied by calibration data. And it is the general understanding that micro-structure of the bone could further increase a model's accuracy. However, high resolution CT images are required, but often not available because they are not routinely acquired. Again, a SM of the trabecular structure could be used to fill this missing information. The muscle insertion have to be distributed on an area instead of a single node to improve the FE model. A model ready for clinical

application should be validated against both the literature and a mechanical test. The model should include accurate mechanical property information from calibrated CT images and ideally include some information about the bone anisotropy.

The building of a SM has been presented in chapter 2 and 4. The assessment of a mesh based or image based SAM was part of the thesis of Bonaretti [Bonaretti, 2012] and therefore not repeated in this work. Nevertheless, these aspects are important and have to be completed to validate the SM. They are therefore briefly discussed here.

The quality of the surface registration can be verified by looking at the distance between the registered and template femur. The quality of the registered mesh is examined by using the normalized shape ratio (NSR) and a regularity measure of the tetrahedron as described in [Field, 2000]. Similarly, the volume morphing assessment can be done by comparing the NSR of the initial mesh with the NSR of the morphed mesh. Additionally, the quality of the FE strain fields of both, an manually meshed and a morphed mesh, can be analyzed.

The quality of the PCA can be quantified by its *compactness*. Each Eigenmode can be characterized drawing isolated instances with shape parameters from -3 to 3. The reconstruction error between a mesh build with a limited number of modes and the full (original) mesh can be calculated for the geometrical and the material properties. This can either be done for the representation or for the *generalization* of the model using the *leave-one-out* test. Similarly to the volume morphing accuracy assessment, the model's ability to predict strain distributions can be compared between a reduced model and the original model with percentage volume versus strain plots [Bryan et al., 2010]. Finally, the instance generation has to be validated. New instances should be realistic new bones. Although PCA implies that new instances are again an structure of the training data, the most extreme shapes probably do look like a femur but have unrealistic proportions. For the shape, this can be tested by looking at geometrical measurements (e.g. femoral shaft diameter) and comparing them to a population, for example to data available from the US National Health and Nutrition Examination Survey.

In this thesis, the PLS regression was used to relate input and output parameters. Although failing in some areas, the method is able to accurately predict mechanical responses. During the development, the PLS was compared against ANN. The PLS performed as good as the ANN and remained the method of choice. Given the fact that the femur model includes no anisotropy in the static analysis, the results remain linear and therefore PLS was expected to perform well. In other situations with different models, the PLS might fail and alternative methods like ANN, random forest or swarm optimization should be tested.

For the identification of the *patient-specific* model parameter, the surface mesh was morphed to the SAM and retrieved with an inverse instance generation formula 2.2. This procedure requires segmentation, landmark definition, and volume morphing which is time consuming. Available 2D-3D registration has the potential to overcome this limitation. Alternatively, in some situations it could be sufficient to identify principle geometrical parameters. Some inaccuracies could be eliminated if unsuitable data for the prediction could be identified in advance. In general as well as in this presented study, the training data is defined through demographic parameter like age, ethnicity, and gender. The tested VSD subjects matched the training population. However, other geometrical (image shape) or mechanical (image intensity) measures can probably be identified which allow to distinguish between data that can be predicted and unsuited data.

## 5.2 Conclusion

The database framework called VSD which integrates all aspects related to data handling and managing of SSM is presented in this thesis. The VSD offers a Web service where image data, segmentations and SSM can be stored, organized and distributed. As compared to existing repository software, the VSD features a flexible, object based design which enables easy extensibility to other data types and flexible file management. A sophisticated upload routine has been implemented for heterogeneous types of data: single files, combined files and multi file structure. This routine assists the user with data privacy and data protection, metadata extraction, and versioning, and is working independently of the technology used for the file upload.

As a result of legal and ethical aspects, the VSD is designed as an open access repository for research institutions and their members. The VSD offers data privacy protection mechanism but leaves the responsibility for their uploaded data with the user. The VSD offers the SSM community a Web service to organize, share, compare, and promote their data. Seeded with an initial collection of full body datasets, the aim of VSD is to generate a community which actively contributes content on the VSD. Due to the generic approach with focus on data sets leaving its purpose generic, the VSD platform can for instance serve as a:

- General research repository for statistical models.
- Platform for the distribution of medial image data in a controlled environment between medical personnel and researchers.
- Resource for general reference images and data collections.
- Data-hub for multi-centric research projects.

Having a data repository available allows different research areas to produce scientific output and to perform population based analysis. The medical image analysis community usually creates SM for their applications. In the field of biomechanics and FE simulations, such a database allows researcher to build *patient-specific* models. The goal of this thesis was to find and demonstrate a method which brings *patient-specific* FE models closer to clinical application. The presented concept involved statistical methods to generate a population model and to generate a mechanical model. It includes a FE femur model and a regression method to predict mechanical response of a patient.

First, a relevant femur model, based on the literature was proposed and used to develop a prediction method. An initial simple model was encouraging to investigate a more advanced approach based on PCA and a prediction model. For maximal stress and displacement detection, shape and mechanical information were not enough. The loading parameters had to be included in the prediction. We could show that Von Mises stress and displacement magnitude of in-silico femur instances could be accurately predicted. Even primary variables, stress tensor and displacement vector components, can be predicated reliably within negligible time. The *patient-specific* predictions were not as accurate as the in-silico data. In general, the prediction is still quite accurate. However, inaccuracies, which are masked by in the overall assessment can occur. Those seem to be model specific, and therefore need to be tackled for each model individually.

The prediction method was demonstrated using a femur model in a walking situation. However, the presented generic prediction pipeline can be applied to other applications. The limitations of the FE model, the prediction method, and SM have been identified and several optimization options have been discussed.

This thesis covered aspects to bring *patient-specific* FE closer to clinics by using statistical approaches. First, a database framework which fills the need for data and data management was presented. The VSD provides management option to track and store all data needed to build SM. Furthermore, the data can be organized and shared including essential metadata. Secondly, the prediction method presented, reduces the time to get a FE result.

### 5.3 Outlook

The VSD serves as a focal point for researchers in the biomedical field with focus on image processing and SSM. The Web repository can be used to distribute, manage, and obtaining relevant data. This simplifies research with medical image data in the *cloud era*. To keep this service alive, several tasks in various fields have to be tackled. First, to drive development and to enlarge the

visibility and user community of the repository, the VSD will be part of different research projects. For example, the EU-Chic project requires a repository to store patient questionnaire results and image data. As a consequence, the VSD will include a new file type, include a single sign on service, and extend the REST interface. A possible collaboration with Microsoft Research to provide a Code and Experiments platform (CodaLab) would improve the segmentation challenge service. To serve as a central and persistent source for reference datasets, the VSD feature set has to be enhanced with a dedicate option to present and publish such reference collections.

Secondly, the functionality to closely connect the VSD to the SSM workflow will be extended. Both previously mentioned REST and collection feature include useful methods for this aspect. It will be possible to select a collection on the VSD, to retrieve this data, and to build a SSM from a dedicated application. The final SSM can be pushed back to the VSD.

The VSD has to grow into a recognized source of medical image data in the field of biomedical engineering. To reach this goal, the VSD will actively look for new image sources. This generates a steady amount of newly pushed data to the VSD. In a long run, the percentage of data contribution from the VSD itself should decrease, and an active user community should take over large portion of the contributions. This is an ambitious goal, however, it should be possible to build an active community using a combination of excellent support, instructions, reliable service, medial and conference presence, and high quality scientific output related to the VSD.

To be able to provide the repository service of the VSD for a broader user base, the hardware setup will have to move from the actual research environment to an industrial level. This enhances the security and scalability level. Not only the hardware but also the database and data storage strategy may have to be adapted. For example, the transition into a NoSQL database or and hybrid SQL - NoSQL solution has to be evaluated.

As previously discussed, several aspect have to be optimized in order to bring the prediction method into clinical application. Some projects already work on these aspects. For example, work is in progress toward a SAM of the lower limb generated from calibrated VSD CT. Additionally, the efforts have been made to include the anisotropic information of the trabecular bone structure of the femur from  $\mu$ CT in this model. Both improve the accuracy of the model.

The femur model has to be validated against a mechanical test or existing literature data for a standard model like the SFM. A mechanical testing unit is available and will most probably be used to evaluate the leg model under development.

2D to 3D registration of the hip is already quite advanced [Zheng et al., 2009]. This approach can certainly help to generate *patient-specific* shape information from clinically available image

data. The FE prediction can then be based on these shape informations.

And lastly, the improvement of the prediction methods is another option to look at. Other popular methods can be adapted to predict the FE results. For example, the random forest or swarm optimization are being evaluated within another project. The approach is tested for the calculation of a pre-stressed cornea to speed up the cornea model used for surgery planning.



## Chapter 6

## Appendix A - VSD

### 6.1 User interface of the VSD

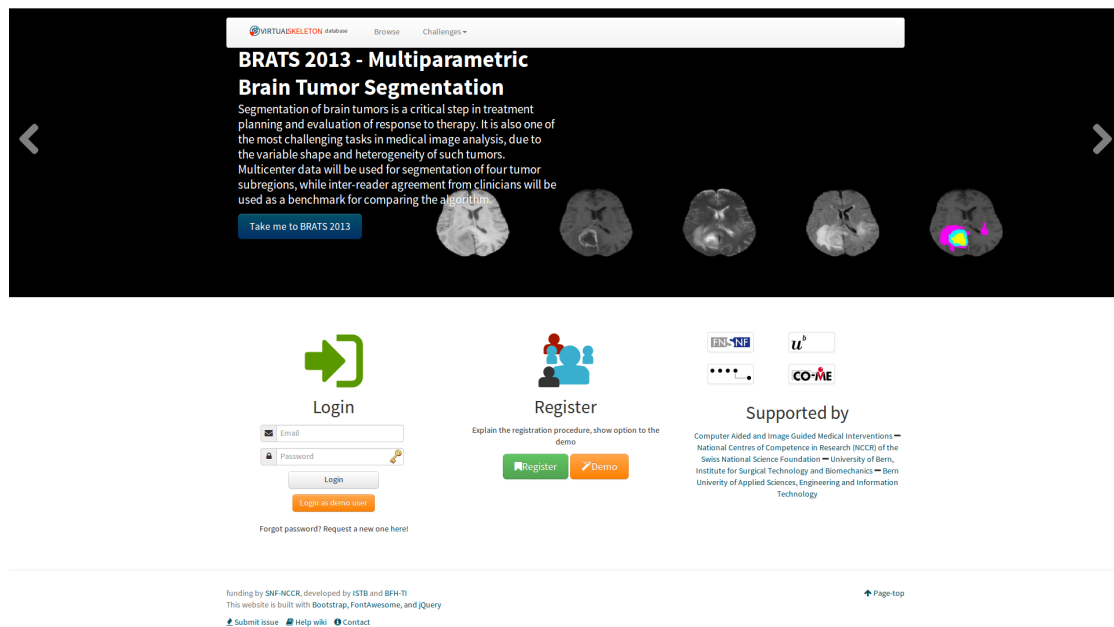









Figure 6.1: VSD landing page

VIRTUAI SKELETON database

Browse Upload MyVSD Forum Challenges Search

Places » MyProjects » VSDFullBody » 001

+ New folder Rename folder Delete folder Actions Manage selected Display selected

<input type="checkbox"/>		VSD.Body.089Y.M.CT.5909.000.nii 001 - Registered Full Body (Bem)		★★★★★ RAW .nii	30.10.2012 14:27:36 buchp1				
<input type="checkbox"/>		VSD.Lower_limb.088Y.M.CT.8.000.dcm Unt. Extr. ganz 1.25 B70s		☆☆☆☆☆ RAW .dcm	06.05.2011 18:08:15 kistm1				
<input type="checkbox"/>		VSD.Thorax.088Y.M.CT.7.000.dcm Th-Abd 1.25 eFoV 30		☆☆☆☆☆ RAW .dcm	06.05.2011 17:18:27 kistm1				
<input type="checkbox"/>		VSD.Head.XX.O.CT.6.000.dcm vsd1 head alt		☆☆☆☆☆ RAW .dcm	06.05.2011 16:55:10 kistm1				
<input type="checkbox"/>		VSD.Head.XX.O.CT.4.000.dcm vsd1 head		☆☆☆☆☆ RAW .dcm	06.05.2011 15:36:22 kistm1				
<input type="checkbox"/>		VSD.Thorax.088Y.M.CT.3.000.dcm Th-Abd 1.25 eFoV 70		☆☆☆☆☆ RAW .dcm	06.05.2011 15:00:06 kistm1				
<input type="checkbox"/>		VSD.Lower_limb.088Y.M.CT.2.000.dcm Unt. Extr. ganz 1.25 B30s		☆☆☆☆☆ RAW .dcm	06.05.2011 13:55:58 kistm1				

Shared Folders

Page Navigation

↑ Page-Top

↓ Page-Bottom

funding by SNF-NCCR, developed by ISTB and BFH-TI  
This website is built with Bootstrap, FontAwesome, and jQuery

Submit issue Help wiki Contact

↑ Page-top

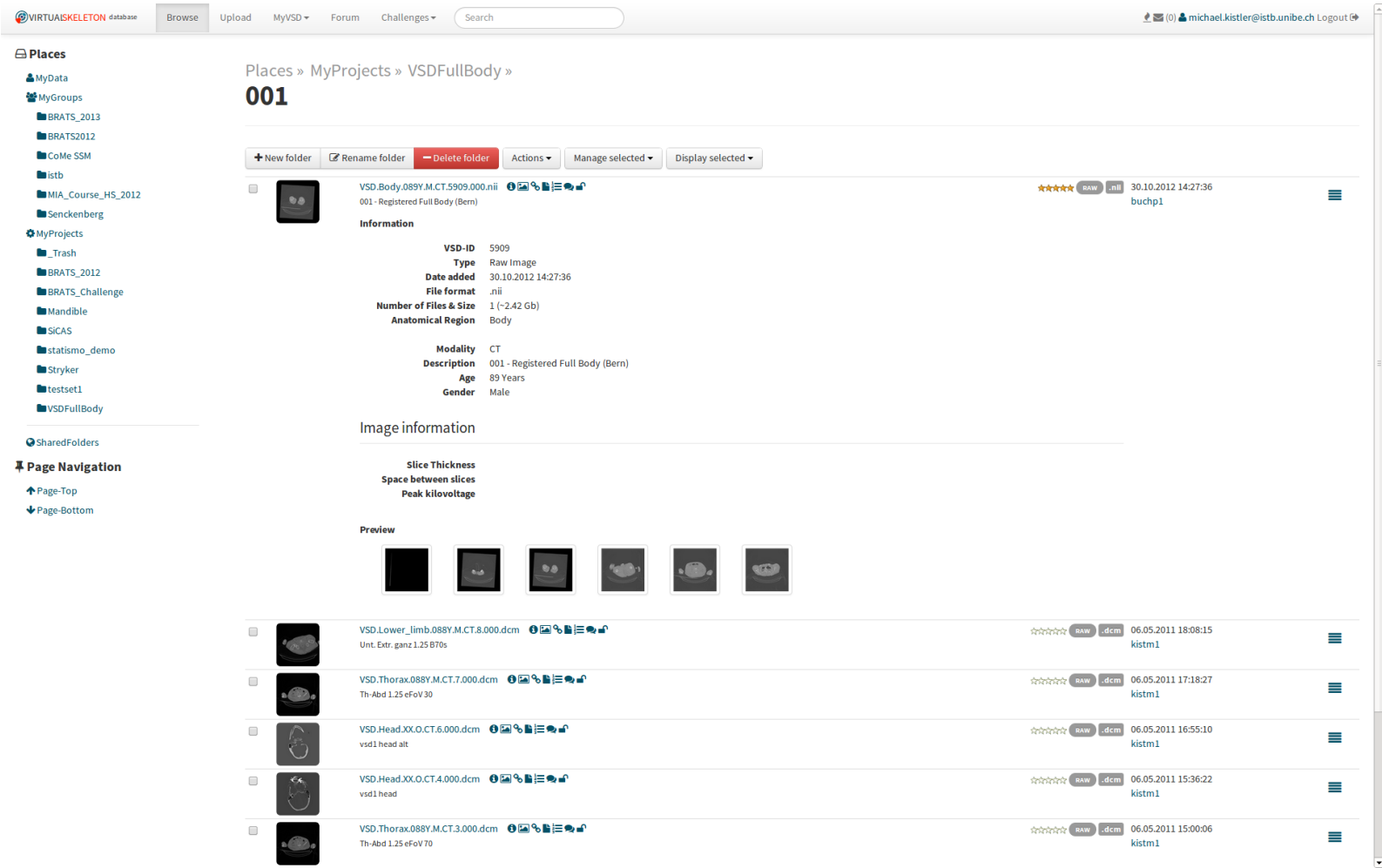
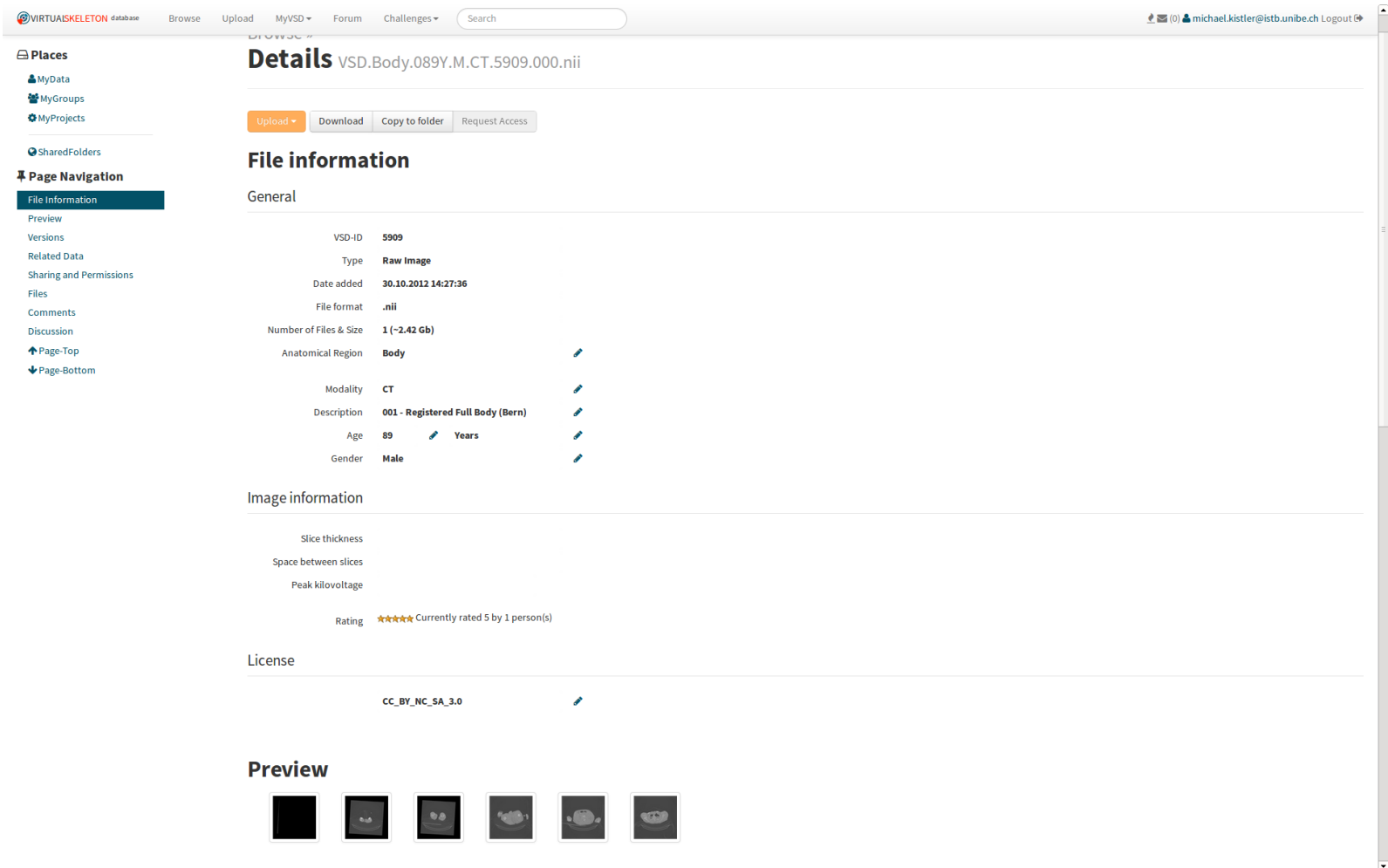


Figure 6.3: Expanded list view



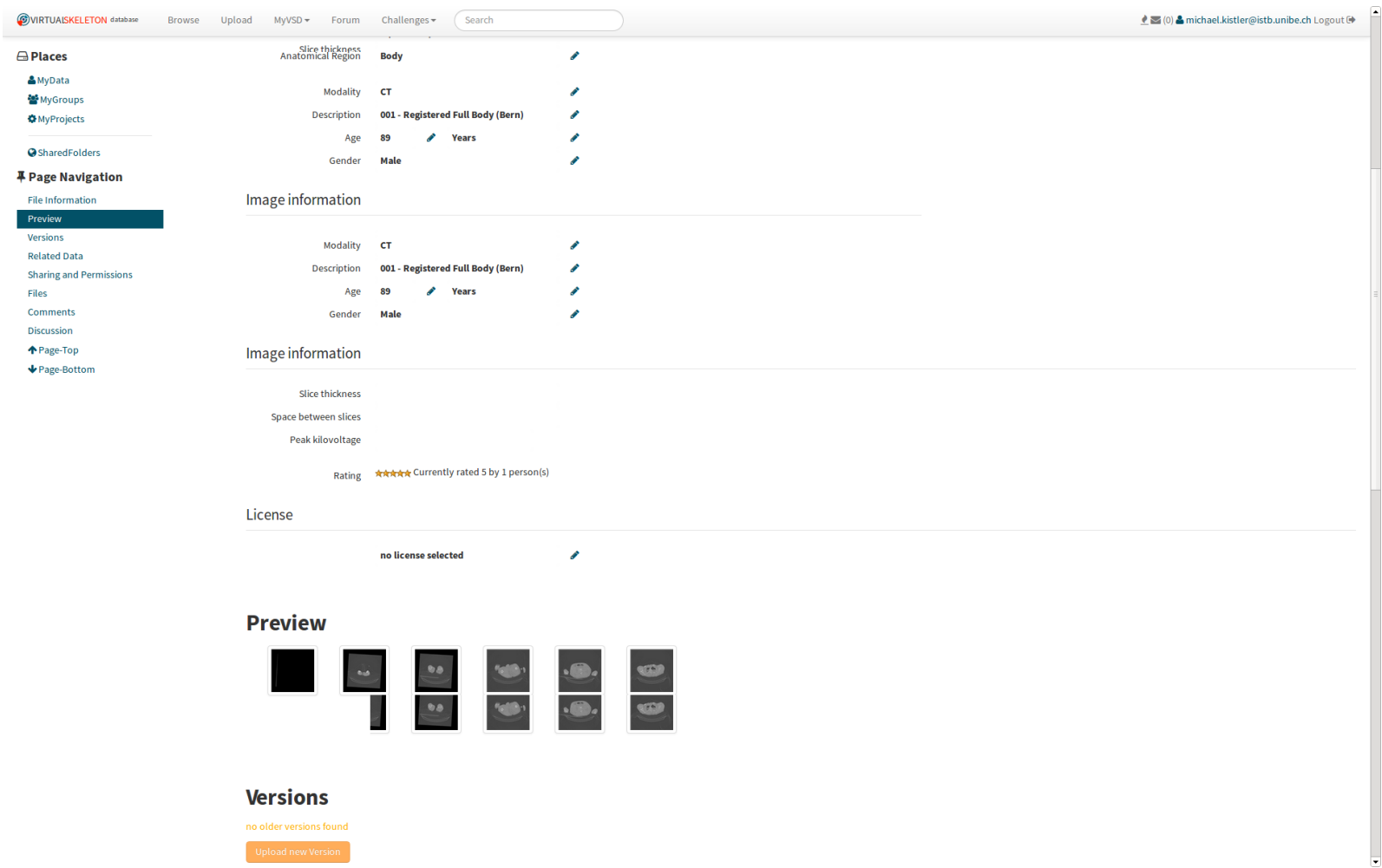


Figure 6.5: Object details page cont.

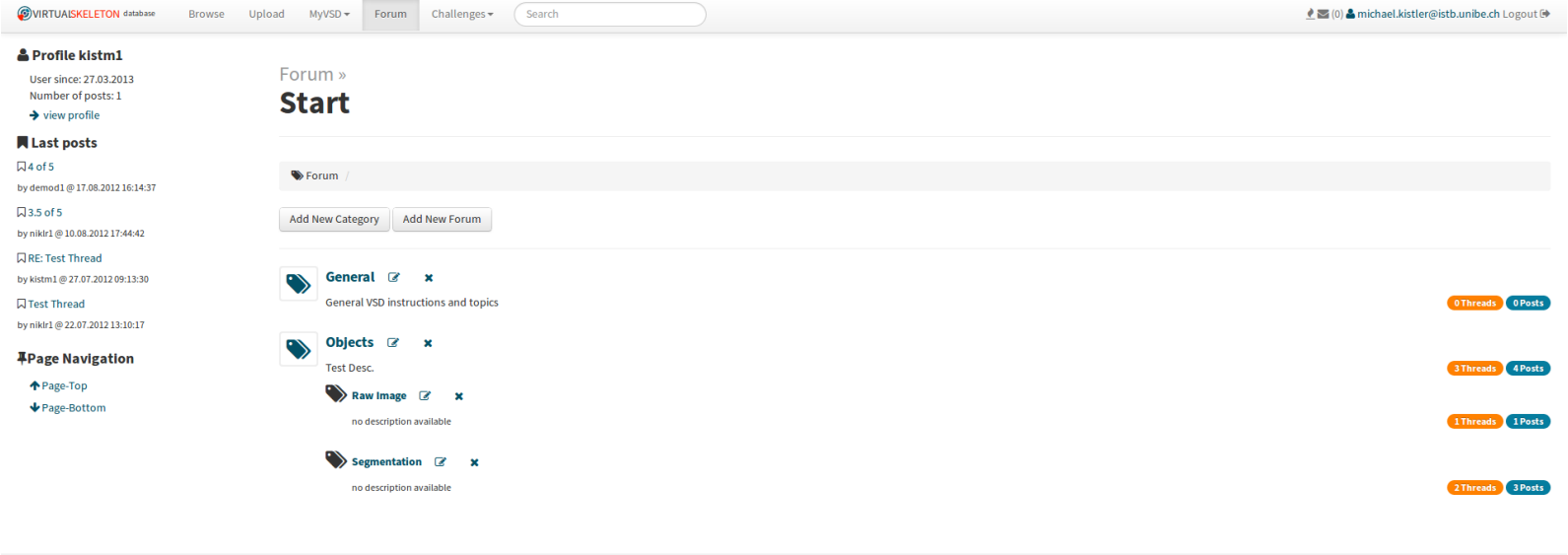


Figure 6.6: VSD Forum

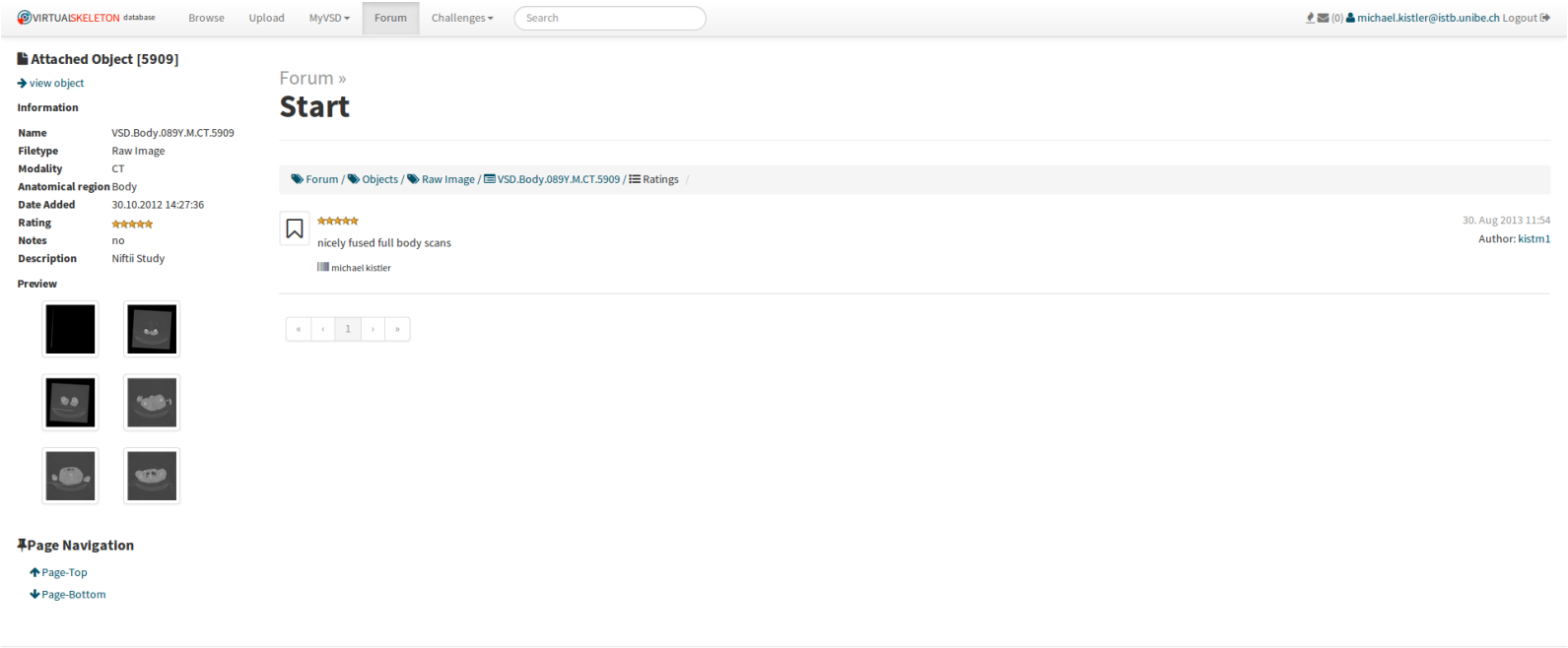


Figure 6.7: Object thread in the forum

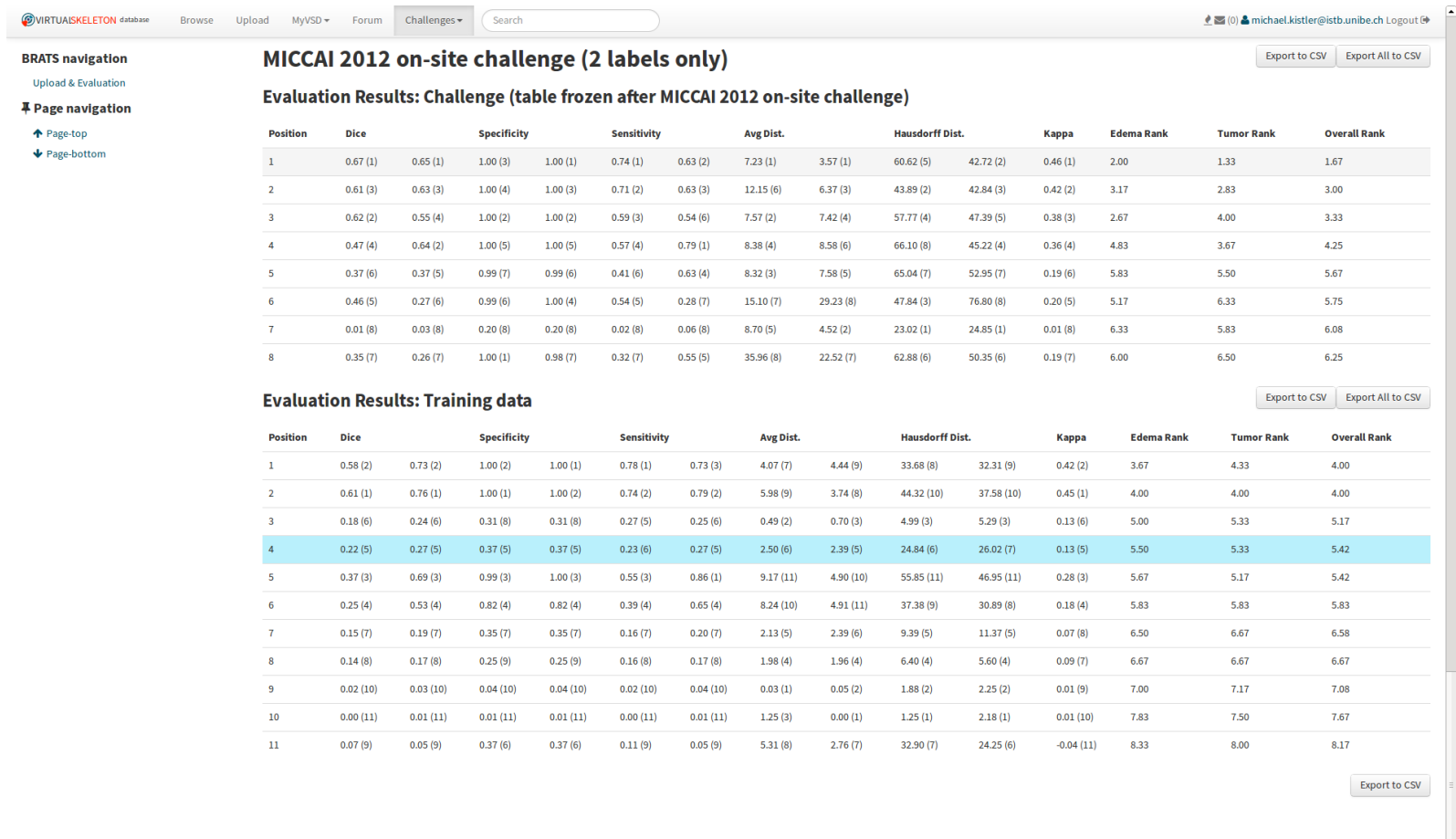


Figure 6.8: BRATS challenge results



## 6.2 FMA conversion

**Listing 6.1:** inference of the RDF graph to explicitly model the part\_of relation

```

WITH <http://virtualskeleton.ch/data/fma/inference>
INSERT
{
  ?subject <http://virtualskeleton.ch/vocab/part_of> ?fromWas
}

USING <http://virtualskeleton.ch/data/fma>
WHERE {
  {
    ?subject <http://www.w3.org/2000/01/rdf-schema#subClassOf> ?o .
    ?o      <http://www.w3.org/1999/02/22-rdf-syntax-ns#type>
            <http://www.w3.org/2002/07/owl#Restriction> ;
            <http://www.w3.org/2002/07/owl#onProperty>
            <http://bio2rdf.org/FMA:85927> ;
            <http://www.w3.org/2002/07/owl#someValuesFrom> ?fromWas .
    ?fromWas <http://www.w3.org/2000/01/rdf-schema#label> ?label .
  }

  UNION
  {
    ?subject <http://www.w3.org/2000/01/rdf-schema#subClassOf> ?o .
    ?o      <http://www.w3.org/1999/02/22-rdf-syntax-ns#type>
            <http://www.w3.org/2002/07/owl#Restriction> ;
            <http://www.w3.org/2002/07/owl#onProperty>
            <http://bio2rdf.org/FMA:85997> ;
            <http://www.w3.org/2002/07/owl#someValuesFrom> ?fromWas .
    ?fromWas <http://www.w3.org/2000/01/rdf-schema#label> ?label .
  }

  UNION
  {
    ?subject <http://www.w3.org/2000/01/rdf-schema#subClassOf> ?o .
    ?o      <http://www.w3.org/1999/02/22-rdf-syntax-ns#type>
            <http://www.w3.org/2002/07/owl#Restriction> ;

```

```

        <http://www.w3.org/2002/07/owl#onProperty>
        <http://bio2rdf.org/FMA:85928> ;
        <http://www.w3.org/2002/07/owl#someValuesFrom> ?fromWas .
?fromWas <http://www.w3.org/2000/01/rdf-schema#label> ?label .
}

UNION
{
?subject <http://www.w3.org/2000/01/rdf-schema#subClassOf> ?o .
?o      <http://www.w3.org/1999/02/22-rdf-syntax-ns#type>
        <http://www.w3.org/2002/07/owl#Restriction> ;
        <http://www.w3.org/2002/07/owl#onProperty>
        <http://bio2rdf.org/FMA:85868> ;
        <http://www.w3.org/2002/07/owl#someValuesFrom> ?fromWas .
?fromWas <http://www.w3.org/2000/01/rdf-schema#label> ?label .
}

}

```

## 6.3 REST API

## Security, Authentication, and Authorization

Productive releases of the VSD REST interface are only available using HTTPS protocol.

## Requests, Responses, and Errors

A successful completion of a request returns one of two possible states:

### **200 OK**

The default state. On GET requests, the response contains all the requested objects. On PUT and POST requests, the requested updates have been done correctly on the persistence layer.

### **201 Created**

Returned on successful PUT requests when one or more new objects have been created. The response contains information on the newly created objects, e.g. identification values.

Unsuccessful completion of a request returns one of:

### **400 Bad Request**

The format of the URL and/or of values in the parameter list is not valid. Or the URL indicates a non-existing action.

### **401 Unauthorized**

Either the request does not contain required authentication information or the authenticated user is not authorized to get a requested object or to do the request updated operation.

#### **404 Not Found**

The URL is correct, but the requested object does not (or no longer) exist.

#### **405 Method not Allowed**

Different action methods may be restricted to one or more of the HTTP methods (GET, PUT, or POST). The received request uses one that is not allowed with the action method specified in the URL. In this case, other parts of the URL are not validated.

#### **500 Internal Error**

When a method causes an exception that has no adequate handling in the method itself. Developers of client systems are kindly requested to report these response states to the developing team of the VSD and to transmit information about the respective request and the response objects.

#### **501 Not Implemented**

May occur during development. The requested action has been specified and documented, but not yet implemented.

### **HTTP method definitions**

GET	Getting a resource. (idempotent)
POST	Creating a resource. (not idempotent)
PUT	Updating a resource. (idempotent)
DELETE	Deleting a resource. (idempotent)

An idempotent HTTP method can be called many times without different outcomes.

## General definitions

The REST API supports Open Data protocol (OData). Offered query options by the ASP.NET Web API framework used to implement the REST API are listed in the following table. All URLs ending with \* can be called with those query options (GET method only).

Option	Description
\$expand	Expands related entities inline.  Example: GET http://localhost/products/1?\$expand=Category,Supplier
\$filter	Filters the results, based on a Boolean condition.
\$inlinecount	Tells the server to include the total count of matching entities in the response. (Useful for server-side paging.)
\$orderby	Sorts the result.
<del>\$select</del>	<del>Selects which properties to include in the response.</del>
\$skip	Skips the first n results.
\$top	Returns only the first n the results.

## Pagination

Besides OData query options, all URLs ending with \* can be called with the following parameters too.

Option	Value type	Default value	Description
rpp	int	50	Defines the amount of results included per page.  Allowed values = 0, 10, 25, 50, 100, 250, 500  Value 0 = all results are included at once.

## URL definitions

Remark: All REST request URLs start with the prefix **/rest/**.

In the descriptions below, URL parts embraced with **{ }** represent variables explained in the succeeding text. Some URLs support additional parameters to be defined in the query part of the URL. These parameters are not shown in the URL but listed and explained in the text.

All many-to-many relations are represented in the form foreignkey-to-foreignkey. For example object-to-fmaregions.

### **/rest/objects\***

Methods	GET
Response object	<b>PageResult</b> URLs <b>/rest/objects/{id}</b>

### **/rest/objects/{id}**

Methods	GET, PUT, DELETE
<i>id</i>	A number identifying the requested object.
Response object	<b>ObjectVersion</b>  Contains information about the contained files, especially their identification, which may be used to fetch the files using a loop with subsequent requests to  <u>Many-to-many relations:</u> <b>/rest/object-to-files/{id}</b> <b>/rest/object-to-objects/{id}</b> <b>/rest/object-to-fmaregions/{id}</b>

/rest/object-user-rights/{id}

/rest/object-group-rights/{id}

Many-to-one relations:

/rest/object-comments/{id}

/rest/objects/{objectId}/previews/{previewId}

One-to-many relations:

/rest/licenses/{id}

/rest/modalities/{id}

/rest/genders/{id}

/rest/segmentation-methods/{id}

### **/rest/objects/{id}/validate**

Methods PUT

Response object **ObjectVersion**

### **/rest/object-to-files\***

Methods GET

Response object **PageResult** with Array of URLs

/rest/object-to-files/{id}

### **/rest/object-to-files/{id}\***

Methods GET

*id* A number identifying the requested relation.

Response object **ObjectToFile**

### **/rest/object-to-objects\***

Methods	GET, POST
Request object	POST: <b>ObjectToObject</b> without <b>Id</b> value
Response object	GET: <b>PageResult</b> with Array of URLs <b>/rest/object-to-objects/{id}</b> POST: <b>ObjectToObject</b> with <b>Id</b> value

### **/rest/object-to-objects/{id}**

Methods	GET, PUT, DELETE
<i>id</i>	A number identifying the requested relation.
Request object	PUT: <b>ObjectToObject</b>
Response object	<b>ObjectToObject</b>

### **/rest/object-to-fmaregions\***

Methods	GET, POST
Request object	POST: <b>ObjectToFMARegion</b> without <b>Id</b> value
Response object	GET: <b>PageResult</b> with Array of URLs <b>/rest/object-to-fmaregions/{id}</b> POST: <b>ObjectToFMARegion</b> with <b>Id</b> value

### **/rest/object-to-fmaregions/{id}**

Methods	GET, PUT; DELETE
<i>id</i>	A number identifying the requested relation.
Request object	PUT: <b>ObjectToFMARegion</b>



Response object      **ObjectToFMARegion**

### **/rest/folder-to-objects\***

Methods              GET, POST

Request object      **FolderToObject** without **Id**

Response object     GET: **PageResult** with Array of URLs  
                         **/rest/folder-to-objects/{id}**  
                         POST: **FolderToObject** with **Id**

### **/rest/folder-to-objects/{id}**

Methods              GET, PUT, DELETE

*id*                      A number identifying the requested relation.

Request object      PUT: **FolderToObject**

Response object     **FolderToObject**

### **/rest/folder-to-folders\***

Methods              GET, POST

Request object      **FolderToFolder** without **Id**

Response object     GET: **PageResult** with Array of URLs  
                         **/rest/folder-to-folders/{id}**  
                         POST: **FolderToFolder** with **Id**

### **/rest/object-rights\***

Methods              GET

Response object     **PageResult** with Array of URLs

`/rest/object-rights/{id}`

**`/rest/object-rights/{id}`**

Methods	GET
<i>id</i>	A number identifying the requested right.
Response object	<b>ObjectRight</b>

**`/rest/object-user-rights*`**

Methods	GET, POST
Request object	<b>ObjectUserRight</b> without Id
Response object	GET: <b>PageResult</b> with Array of URLs <code>/rest/object-user-rights/{id}</code> POST: <b>ObjectUserRight</b> with Id

**`/rest/object-user-rights/{id}`**

Methods	GET, PUT, DELETE
<i>id</i>	A number identifying the requested right.
Request object	PUT: <b>ObjectUserRight</b>
Response object	<b>ObjectUserRight</b>

**`/rest/folder-user-rights*`**

Methods	GET, POST
Request object	<b>FolderUserRight</b> without Id
Response object	GET: <b>PageResult</b> with Array of URLs

`/rest/folder-user-rights/{id}`

POST: **FolderUserRight** with **Id**

### **`/rest/folder-user-rights/{id}`**

Methods	GET, PUT, DELETE
<i>id</i>	A number identifying the requested right.
Request object	PUT: <b>FolderUserRight</b>
Response object	<b>FolderUserRight</b>

### **`/rest/object-group-rights*`**

Methods	GET, POST
Request object	<b>ObjectGroupRight</b> without <b>Id</b>
Response object	GET: <b>PageResult</b> with Array of URLs <code>/rest/object-group-rights/{id}</code> POST: <b>ObjectGroupRight</b> with <b>Id</b>

### **`/rest/object-group-rights/{id}`**

Methods	GET, PUT, DELETE
<i>id</i>	A number identifying the requested right.
Request object	PUT: <b>ObjectGroupRight</b>
Response object	<b>ObjectGroupRight</b>

### **`/rest/folder-group-rights*`**

Methods	GET, POST
---------	-----------

Request object      **FolderGroupRight** without Id

Response object     GET: **PageResult** with Array of URLs  
                          /rest/folder-group-rights/{id}  
                          POST: **FolderGroupRight** with Id

#### **/rest/object-group-rights/{id}**

Methods             GET, PUT, DELETE

*id*                    A number identifying the requested right.

Request object      PUT: **FolderGroupRight**

Response object     **FolderGroupRight**

#### **/rest/object-right-sets\***

Methods             GET

Response object     **PageResult** with Array of URLs  
                          /rest/object-right-sets/{id}

#### **/rest/object-right-sets/{id}**

Methods             GET

*id*                    A number identifying the requested set.

Response object     **ObjectRightSet**

#### **/rest/folder-right-sets\***

Methods             GET

Response object     **PageResult** with Array of URLs

`/rest/folder-right-sets/{id}`

**`/rest/folder-right-sets/{id}`**

Methods	GET
<i>id</i>	A number identifying the requested set.
Response object	<b>FolderRightSet</b>

**`/rest/object-comments*`**

Methods	GET, POST
Request object	POST: <b>ObjectComment</b> without <b>Id</b> value
Response object	GET: <b>PageResult</b> with Array of URLs <code>/rest/object-comments/{id}</code> POST: <b>ObjectComment</b> with <b>Id</b> value

**`/rest/object-comments/{id}`**

Methods	GET, PUT; DELETE
<i>id</i>	A number identifying the requested comment.
Request object	PUT: <b>ObjectComment</b>
Response object	<b>ObjectComment</b>

**`/rest/objects/{objectId}/previews*`**

Methods	GET
<i>objectId</i>	A number identifying the requested object.
Response object	<b>PageResult</b> with Array of URLs

/rest/objects/{objectId}/previews/{previewId}

**/rest/objects/{objectId}/previews/{previewId}?  
isValidated={true/false}&isThumbnail={true/false}**

Methods	GET
<i>objectId</i>	A number identifying the requested object.
<i>previewId</i>	A number identifying the requested preview.
<i>isValidated</i>	Boolean to determine whether the object is validated.
<i>isThumbnail</i>	Boolean to determine whether the server should return a thumbnail.
Response object	Response with mime type set to <b>image/jpeg</b> .

**/rest/files\***

Methods	GET
Response object	<b>PageResult</b> URLs /rest/files/{id}

**/rest/files/upload**

Used to upload one single file.

Methods	POST
Request object	“Content-Type: multipart/form-data”
Response object	/rest/files/{id}

**/rest/files/{id}**

Allows to download one single file.

Methods	GET
<i>id</i>	A number identifying the requested file.
Response object	<b>File</b>

#### **/rest/files/{id}/download**

Methods	GET
<i>id</i>	A number identifying the requested file.
Response object	“Content-Type: binary”

#### **/rest/fma-regions\***

Methods	GET
Response object	<b>PageResult</b> with Array of URLs <b>/rest/fma-regions/{id}</b>

#### **/rest/fma-regions/{id}**

Methods	GET
<i>id</i>	A number identifying the requested fma region.
Response object	<b>FMARegion</b>

#### **/rest/licenses\***

Methods	GET
Response object	<b>PageResult</b> with Array of URLs <b>/rest/licenses/{id}</b>

### **/rest/licenses/{id}**

Methods GET

*id* A number identifying the requested license.

Response object **License**

### **/rest/modalities\***

Methods GET

Response object **PageResult** with Array of URLs

**/rest/modalities/{id}**

### **/rest/modalities/{id}**

Methods GET

*id* A number identifying the requested modality.

Response object **Modality**

### **/rest/folders\***

Methods GET

Response object **PageResult** with Array of URLs

**/rest/folders/{id}**

### **/rest/folders/{id}**

Methods GET

*id* A number identifying the requested folder.

Response object **Folder**



### **/rest/groups\***

Methods	GET
Response object	<b>PageResult</b> with Array of URLs <code>/rest/groups/{id}</code>

### **/rest/groups/{id}**

Methods	GET
<i>id</i>	A number identifying the requested folder.
Response object	<b>Group</b>

### **/rest/genders\***

Methods	GET
Response object	<b>PageResult</b> with Array of URLs <code>/rest/genders/{id}</code>

### **/rest/genders/{id}**

Methods	GET
<i>id</i>	A number identifying the requested gender.
Response object	<b>Gender</b>

### **/rest/segmentation-methods\***

Methods	GET
Response object	<b>PageResult</b> with Array of URLs <code>/rest/segmentation-methods/{id}</code>

### **/rest/segmentation-methods/{id}**

Methods	GET
<i>id</i>	A number identifying the requested segmentation method.
Response object	<b>SegmentationMethod</b>

### **/rest/objects/{id}/download**

Methods	GET
<i>id</i>	A number identifying the requested compressed object.
Response object	A zip file containing all the files of the compressed object.

### **/rest/folders/{id}/download**

Methods	GET
<i>id</i>	A number identifying the requested compressed folder.
Response object	A zip file containing all the files of the compressed folder.

### **/rest/compress-objects**

Allows to fetch one or multiple objects with one single request.

Methods	GET, POST
Request object	<b>CompressObjects</b>
Response object	A zip file containing all the files of the compressed objects.

### **/rest/compress-folders**

Methods	GET, POST
Request object	<b>CompressFolders</b>
Response object	A zip file containing all the files of the compressed folders.

### **/rest/users\***

Methods	GET, POST
Response object	<b>PageResult</b> with Array of URLs <b>/rest/users/{id}</b>

### **/rest/users/{id}**

Methods	GET, PUT, DELETE
<i>id</i>	A number identifying the requested user.
Response object	<b>User</b>

### **/rest/files/checksum**

Methods	GET, POST
Response object	<b>FileChecksum</b>

## **Possible extensions:**

### **/rest/objects/upload**

Uploading complete zipped objects instead of single raw files.

Methods	POST
Response object	<b>ObjectVersion</b>

## Object Specifications

### ObjectVersion

<i>Id</i>	An integer value identifying the object.
<i>FileRelationUrls</i>	An array of URLs <code>/rest/object-to-files/{id}</code>
<i>Files</i>	An array of <b>File</b> if <code>\$expand=Files</code>
<i>ObjectRelationUrls</i>	An array of URLs <code>/rest/object-to-objects/{id}</code>
<i>Objects</i>	An array of <b>ObjectVersion</b> if <code>\$expand=Objects</code>
<i>FMARegionRelationUrls</i>	An array of URLs <code>/rest/object-to-fmaregions/{id}</code>
<i>FMARegions</i>	An array of <b>FMARegion</b> if <code>\$expand=FMARegions</code>
<i>UserRightUrls</i>	An array of URLs <code>/rest/object-user-rights/{id}</code>
<i>UserRights</i>	An array of <b>ObjectUserRight</b> if <code>\$expand=UserRights</code>
<i>GroupRightUrl</i>	An array of URLs <code>/rest/object-group-rights/{id}</code>
<i>GroupRights</i>	An array of <b>ObjectGroupRight</b> if <code>\$expand=GroupRight</code>

### File

<i>Id</i>	An integer value identifying the file within an object. This value has to be used in requests to <code>/rest/files/{id}</code> .
-----------	--

<i>DownloadUrl</i>	<code>/rest/files/{id}/download</code>
<i>ObjectToFilesUrl</i>	An array of <code>/rest/object-to-files/{id}</code>
<i>Size</i>	The size of the file in bytes.

### **ObjectToObject**

<i>Id</i>	An integer value identifying the link.
<i>ObjectVersionUrl1</i>	An Url to the linked <b>ObjectVersion</b> 1.
<i>ObjectVersionUrl2</i>	An Url to the linked <b>ObjectVersion</b> 2.

### **ObjectToFMARegion**

Represents the many-to-many relation between **ObjectVersion** and **AnatomicalRegion**

<i>Id</i>	An integer value identifying the relation.
<i>ObjectVersionUrl</i>	An Url of the <b>ObjectVersion</b> .
<i>FMARegionUrl</i>	An Url of the <b>FMARegion</b> .

### **ObjectToFile**

<i>Id</i>	An integer value identifying the relation.
<i>ObjectVersionUrl</i>	An Url of the <b>ObjectVersion</b> .
<i>FileUrl</i>	An Url of the <b>File</b> .

### **FolderToObject**

<i>Id</i>	An integer value identifying the relation.
<i>FolderUrl</i>	An Url to the <b>Folder</b> .

*ObjectVersionUrl*      An Url of the **ObjectVersion**.

### **FolderToFolder**

*Id*      An integer value identifying the relation.

*FolderUrl1*      An Url to the **Folder** 1.

*FolderUrl2*      An Url of the **Folder** 2.

### **FMARegion**

*Id*      An integer value identifying the fma region.

*Name*      A name of the fma region.

### **License**

*Id*      An integer value identifying the license.

*Name*      A name of the license.

*Description*      A description of the license.

*ExternalUrl*      An external Url pointing to the license.

### **CompressObjects**

*List<Url>*      A list of Urls pointing to objects to be compressed.

### **CompressFolders**

*List<Url>*      A list of Urls pointing to folders to be compressed.

### **ObjectRight**

*Id*      An integer value identifying the right.

<i>Name</i>	The name of the right.
<i>Value</i>	The bit value of the right.

### **ObjectUserRight**

<i>Id</i>	An integer value identifying the right.
<i>ObjectVersionUrl</i>	An Url to the specified object.
<i>UserUrl</i>	An Url to the specific user.
<i>List&lt;Url&gt;</i>	A list of Urls pointing to object rights.

### **ObjectGroupRight**

<i>Id</i>	An integer value identifying the right.
<i>ObjectVersionUrl</i>	An Url to the specified object.
<i>GroupUrl</i>	An Url to the specific group.
<i>List&lt;Url&gt;</i>	A list of Urls pointing to object rights.

### **FolderUserRight**

<i>Id</i>	An integer value identifying the right.
<i>FolderUrl</i>	An Url to the specified folder.
<i>UserUrl</i>	An Url to the specific user.
<i>List&lt;Url&gt;</i>	A list of Urls pointing to folder rights.

### **FolderGroupRight**

<i>Id</i>	An integer value identifying the right.
<i>FolderUrl</i>	An Url to the specified folder.

<i>GroupUrl</i>	An Url to the specific group.
<i>List&lt;Url&gt;</i>	A list of Urls pointing to folder rights.

### **ObjectRightSet**

<i>Id</i>	An integer value identifying the set.
<i>Name</i>	The name of the set.

### **FolderRightSet**

<i>Id</i>	An integer value identifying the set.
<i>Name</i>	The name of the set.

### **ObjectToPermission**

<i>Id</i>	An integer value identifying the relation.
-----------	--

### **Folder**

<i>Id</i>	An integer value identifying the folder.
<i>ParentUrl</i>	An Url to the parent folder.
<i>GroupUrl</i>	An Url to the group (if it's a group folder)
<i>Name</i>	The name of the folder.
<i>FolderUrls</i>	An array of URLs <code>/rest/folders/{id}</code>
<i>ObjectUrls</i>	An array of URLs <code>/rest/objects/{id}</code>



## Group

<i>Id</i>	An integer value identifying the group.
<i>ParentUrl</i>	An Url to the parent group.
<i>Name</i>	The name of the group.
<i>Description</i>	The description of the group.
<i>IsVirtualGroup</i>	A boolean defining whether it is a virtual group.
<i>IsSystem</i>	A boolean defining whether it is a system group.

## Gender

<i>Id</i>	An integer value identifying the gender.
<i>Abbreviation</i>	The abbreviation of the gender.
<i>Description</i>	The description of the gender

## FileChecksum

<i>HashFunction</i>	A string identifying the Hash-function
<i>FileUrl</i>	The Url to the Object <code>/rest/file/{id}</code>
<i>Checksum</i>	A string of the checksum value

### 6.3.1 Example use case

This is a typical use case in for SSM. The user has organized the required segmentations into a folder on the VSD. Now he wants to process the data on his machine. He stores the final SSM on the VSD. The process can be divided into four step:

- Download segmentation files from a folder on the VSD to create a SM offline
- Upload the SM back to the VSD
- Validate the SM
- Move it to the original folder

Prerequisites:

- all files in the folder are segmentations,
- user has an account on the VSD.

Assumptions

- Folder *Basel*, id=1
- ObjectsId = [1,2,3,4,5]

#### Instructions

#### Download the segmentations

##### Step 0

Authentication

```
POST /login
-> Token %has to be sent with each request
```

##### Step 1

Look for the *Basel* folder

```
GET /rest/folders?$filter="Basel"
-> list of /rest/folder/{ids}
%select the folder URL for folder 1
rest/folders/1
```

**Step 2**

Retrieve the folder object containing the files and folders locate in the folder.

```
GET /rest/folders/1
-> Folder:
    URLs /rest/folders/{ids}
    URLs /rest/objects/{ids}
```

**Step 3**

Select the object to download: /rest/objects/1 (repeat 3-6 for all segmentation objects) and retrieve the object.

```
GET /rest/objects/1
-> Object:
    description
    vsd template name
    URL to gender
    URL to age
    URLs to /rest/object-to-files/{ids}
```

to get the gender, age, directly, do an \$expand=gender, age

**Step 4**

Download the file: get the download URLs of each file in the object (4-6). Loop to get every file of the object

```
GET /rest/object-to-files/1
-> Object-to-file:
    URL /rest/files/1
    URL /rest/object/1
```

**Step 5**

Get the file download URL

```
GET /rest/files/1
-> File:
    URL /rest/files/1/download
    size
    format
```

**Step 6**

Download the file

```
GET /rest/files/1/download
-> binary
```

repeat for all objects, then do the SM

**Upload the SM to the VSD****Step 0**

Authenticate

```
POST /login
-> Token
```

**Step 1**

Upload the file

```
POST /rest/files/upload
-> URL /rest/files/1
```

**Step 2**

find the ID of the generated object through the object-file relation

```
GET /rest/files/1
-> ObjectToFile:
URLs /rest/object-to-files/{id}
```

```
GET /rest/object-to-files/{id}?$expand=Object
-> Object:
isValidated
CreatedDate
RegionsCount
list of URLs /rest/object-to-fmaregions/0
URL /rest/objects/1
```

select the correct object (CreatedDate = latest, isValidated = false). Save this URL /rest/objects/1

**Step 3****Validation of the dataset**

set the anatomical region: here Femur, repeat this step for the number of `/rest/object-to-fmaregions/0` URLs (Retrieved in step 2)

```
GET /rest/fma-regions*?$filter="femur"
-> List of FMARegion URL:
URL /rest/fma-regions/{ids}
```

search all fma regions for the desired region by iteration:

```
GET /rest/fma-regions/id
-> FMARegion:
Preferred Name
Alternative Name
FMAID
```

retrieve empty ObjectToFMARegion

```
GET /rest/object-to-fmaregions/0
ObjectToFMARegion:
    empty URL /rest/fma-regions
    empty URL /rest/objects
```

write the URL `/rest/fma-regions/1` and the `/rest/objects/1` to the local ObjectToFMARegion

write the ObjectToFMARegion to the VSD

```
POST /rest/object-to-fmaregions
-> URL /rest/object-to-fmaregions/1
```

to set other attributes

```
GET /rest/licenses* or GET /rest/licenses*?$filter="CC-BY"
-> List of Licenses:
URL /rest/license/{1,2,3} %(1=CC-BY-AT)
```

search all licenses for the desired license by iteration:

```
GET /rest/license/1
-> License:
Name
ShortName
```

or directly filter for the desired license

```
GET /rest/licenses*?$filter="CC-BY"
-> List of Licenses:
URL /rest/license/{1,2,3} %(1=CC-BY-AT)
```

insert this URL `/rest/license/1` in the local object. Set the other information (permissions, links, comments etc.) in the same way

### Write the informations to the VSD

Save the updated object to the VSD:

```
PUT /rest/objects/1
```

### Validate the object

to validate execute

```
GET /rest/objects/1/validate
-> status '200' return (ok)
or status 'error' and missing:
-> URL /rest/object/1
with missing regions:
URL /rest/object-to-fmaregions/0
```

## Move SM into a folder

### Step 0

Authenticate

```
POST /login
-> Token
```

### Step 1

Look for the *Basel* folder

```
GET /rest/folders?$filter="Basel"
-> list of /rest/folder/{ids}
```

### Step 2

Generate an `ObjectToFolder` object (holds an object and an folder ID)

```
GET /rest/object-to-folders/0 %0 generates an empty structure
-> FolderToObject:
empty /rest/objects/{id}
empty /rest/folders/{id}
```

Add the /rest/folders/1 and /rest/objects/1 to the FolderToObject object

### Step 3

```
PUT /rest/object-to-folders
-> URL /rest/object-to-folders/1
```





## Chapter 7

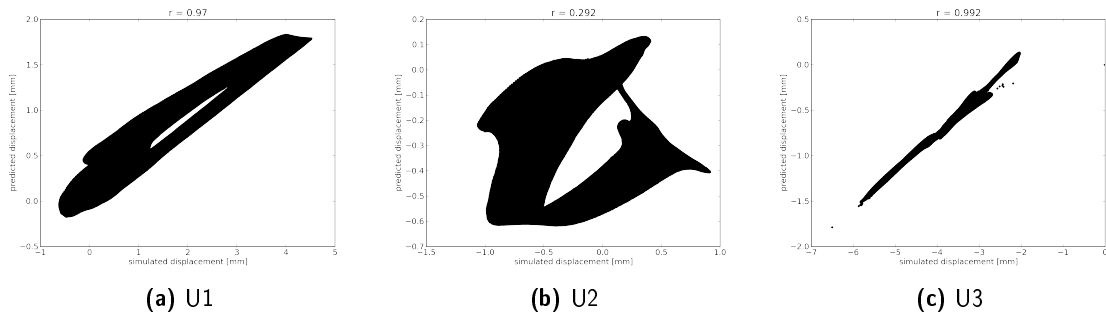
## Appendix B - Prediction model

### 7.1 Patient-specific results

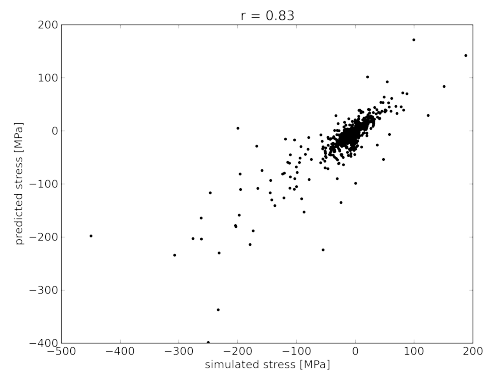
#### 7.1.1 VSD subject 2

**Table 7.1:** Patient specific stress tensor and displacement vector prediction average accuracy of the VSD subject 2

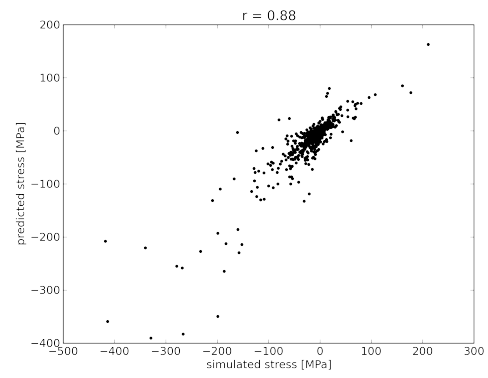
Component	S	S11	S22	S33	S12	S13	S13	U	U1	U2	U3
				MPa						mm	
<b>Avg. error</b>	2.27	0.30	0.22	2.13	0.15	0.48	0.32	3.15	0.95	0.38	3.04
<b>SD</b>	4.30	1.13	0.95	4.18	0.42	1.01	0.85	0.47	0.83	0.29	0.39
<b>Pearson coeff.</b>	0.83	0.83	0.88	0.84	0.85	0.84	0.90	0.95	0.97	0.29	0.99



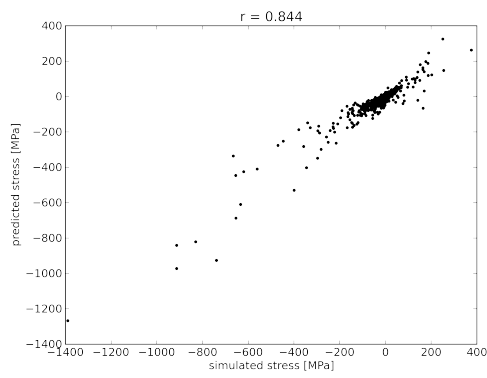
**Figure 7.1:** Displacement prediction error of the VSD subject 2



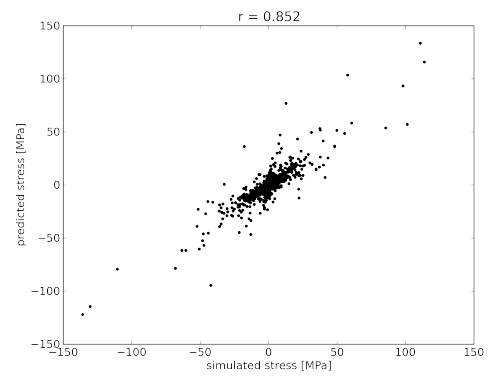
(a) S11



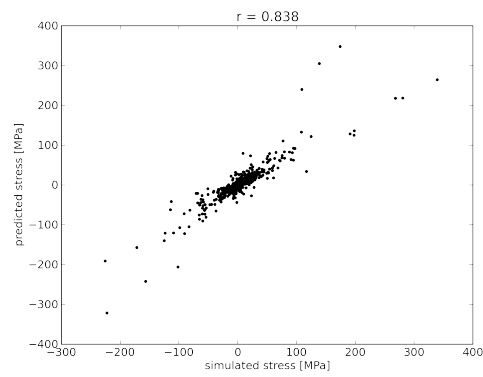
(b) S22



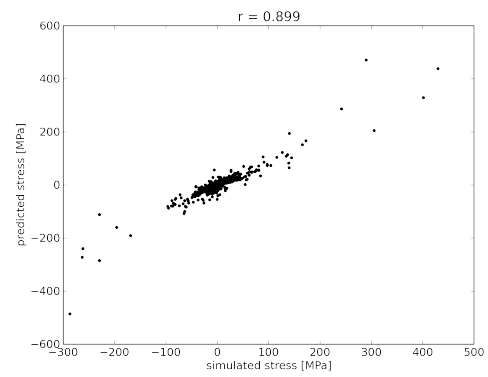
(c) S33



(d) S12



(e) S13



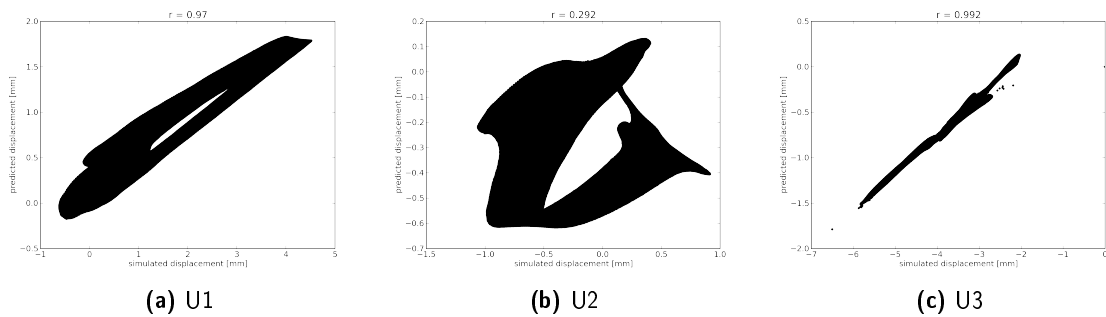
(f) S23

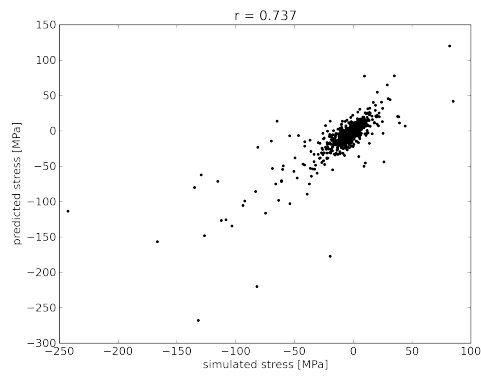
Figure 7.2: Stress prediction error of the VSD subject 2

**Table 7.2:** Patient specific stress tensor and displacement vector prediction average accuracy of the VSD subject 3

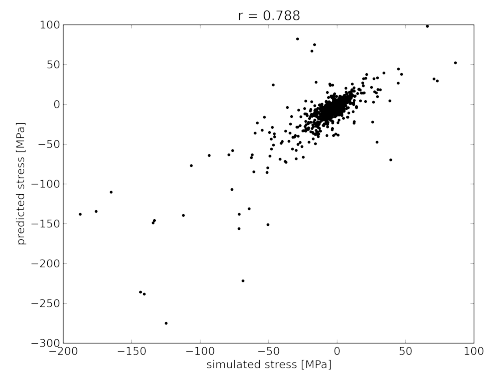
Component	S	S11	S22	S33	S12	S13	S13	U	U1	U2	U3
				MPa						mm	
<b>Avg. error</b>	2.30	0.29	0.20	2.71	0.16	0.62	0.41	1.42	0.78	0.50	1.16
<b>SD</b>	3.98	0.77	0.74	4.88	0.37	0.97	0.71	0.48	0.71	0.38	0.39
<b>Pearson coeff.</b>	0.63	0.74	0.79	0.48	0.67	0.55	0.78	0.91	0.87	0.24	0.87

### 7.1.2 VSD subject 3

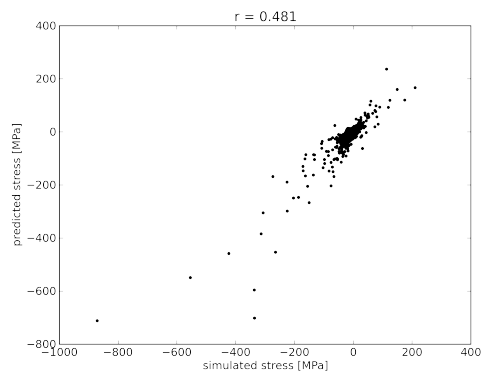
**Figure 7.3:** Displacement prediction error of the VSD subject 3



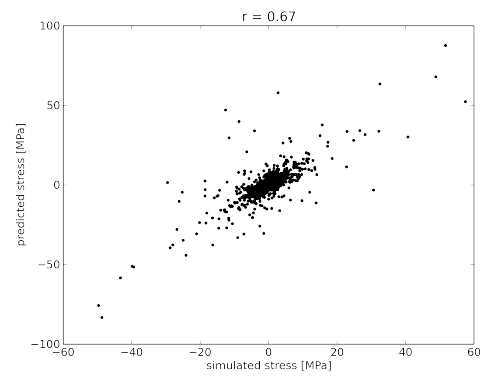
(a) S11



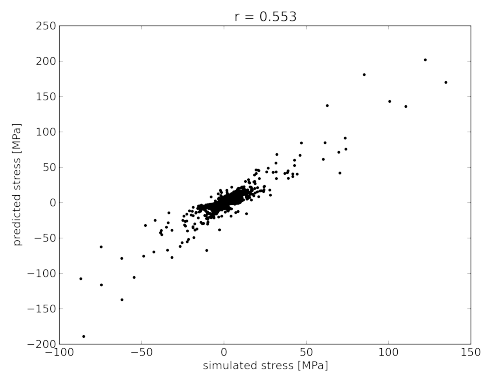
(b) S22



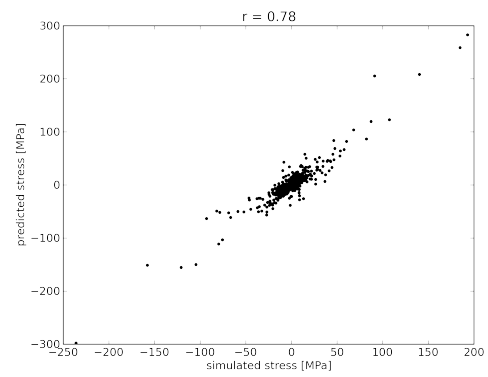
(c) S33



(d) S12



(e) S13



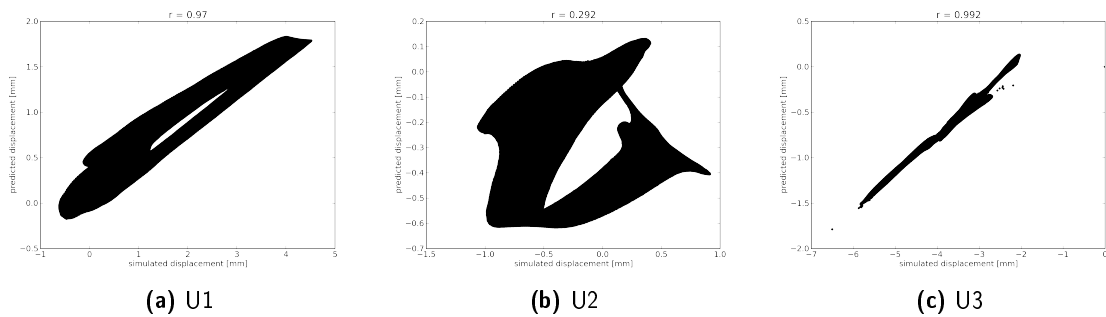
(f) S23

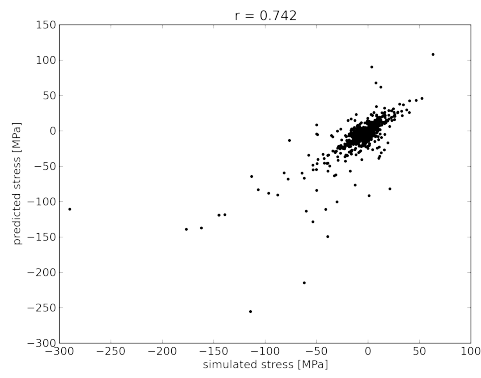
Figure 7.4: Stress prediction error of the VSD subject 3

**Table 7.3:** Patient specific stress tensor and displacement vector prediction average accuracy of the VSD subject 8

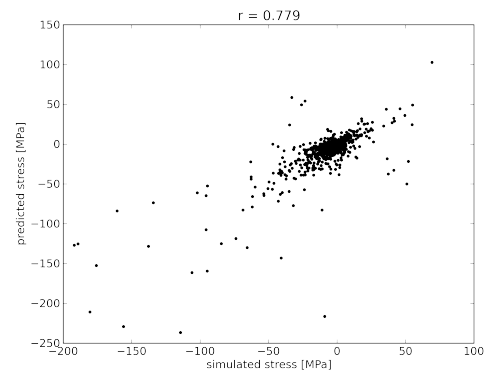
Component	S	S11	S22	S33	S12	S13	S13	U	U1	U2	U3
				MPa						mm	
<b>Avg. error</b>	1.58	0.23	0.18	1.59	0.14	0.43	0.36	0.65	0.39	0.44	0.47
<b>SD</b>	2.88	0.76	0.74	3.00	0.31	0.80	0.68	0.26	0.35	0.36	0.21
<b>Pearson coeff.</b>	0.79	0.74	0.78	0.78	0.75	0.71	0.80	0.97	0.95	0.12	0.97

### 7.1.3 VSD subject 8

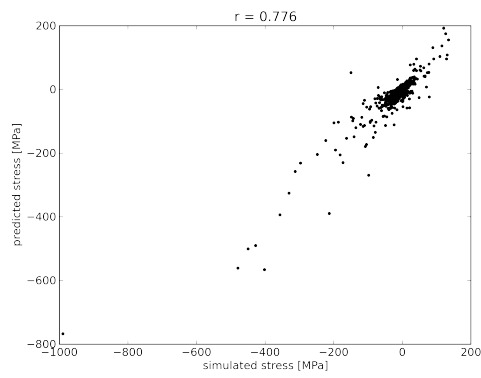
**Figure 7.5:** Displacement prediction error of the VSD subject 8



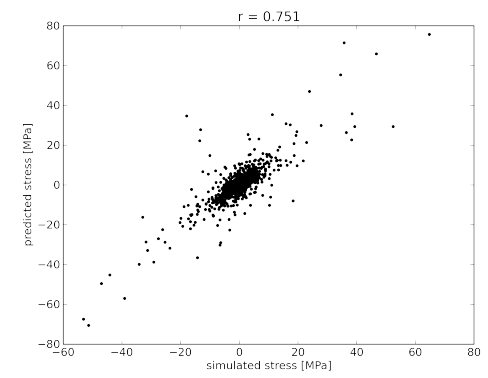
(a) S11



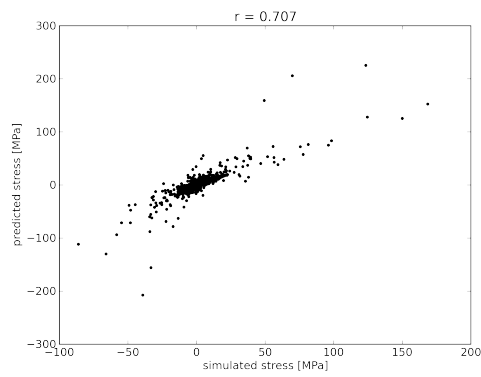
(b) S22



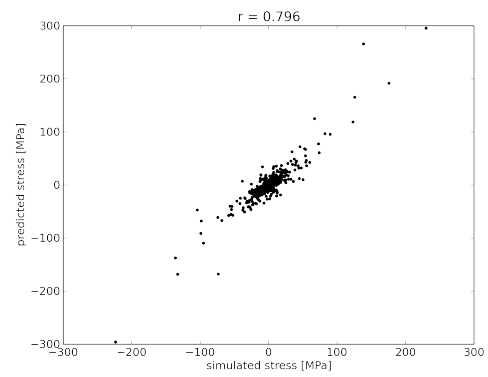
(c) S33



(d) S12



(e) S13



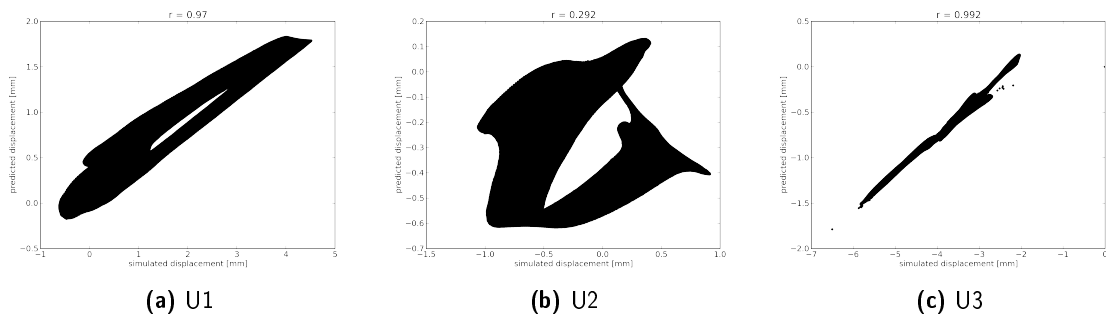
(f) S23

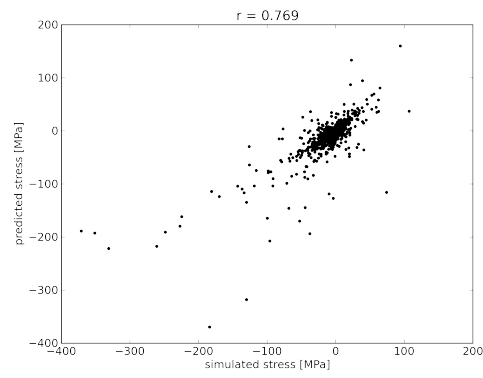
Figure 7.6: Stress prediction error of the VSD subject 8

**Table 7.4:** Patient specific stress tensor and displacement vector prediction average accuracy of the VSD subject 14

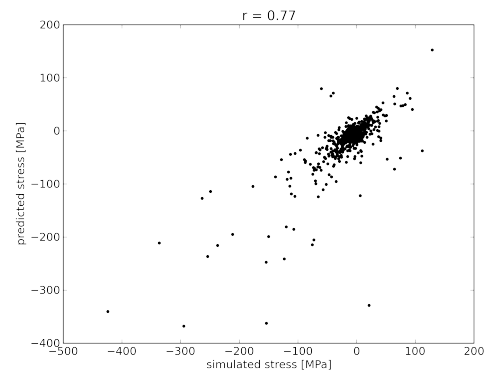
Component	S	S11	S22	S33	S12	S13	S13	U	U1	U2	U3
				MPa						mm	
<b>Avg. error</b>	2.44	0.34	0.29	2.27	0.21	0.64	0.61	1.35	0.87	0.72	0.76
<b>SD</b>	4.27	1.14	1.20	4.13	0.50	1.17	1.09	0.63	0.80	0.64	0.36
<b>Pearson coeff.</b>	0.83	0.77	0.77	0.84	0.75	0.75	0.80	0.99	0.87	0.12	0.99

#### 7.1.4 VSD subject 14

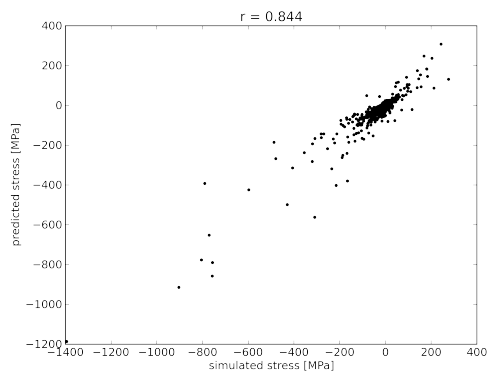
**Figure 7.7:** Displacement prediction error of the VSD subject 14



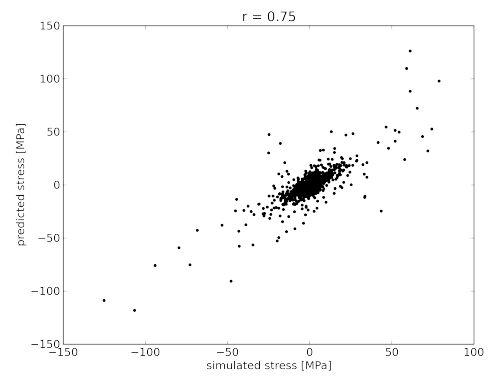
(a) S11



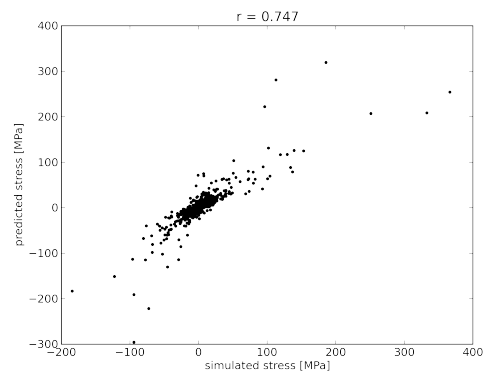
(b) S22



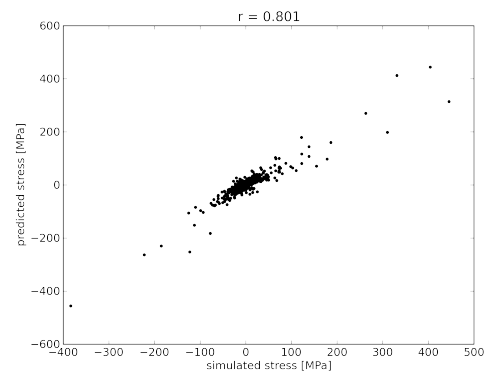
(c) S33



(d) S12



(e) S13



(f) S23

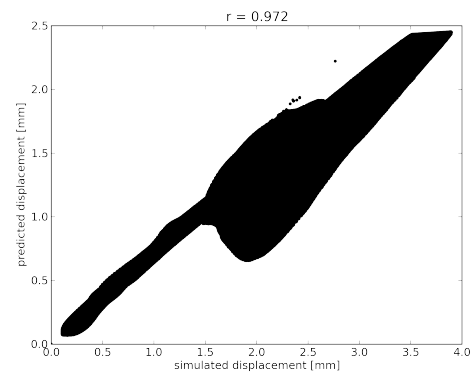
Figure 7.8: Stress prediction error of the VSD subject 14



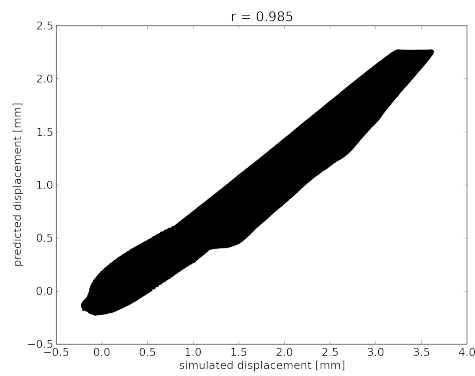
## 7.1.5 Standard Femur Model

**Table 7.5:** Patient specific stress tensor and displacement vector prediction average accuracy of the SFM

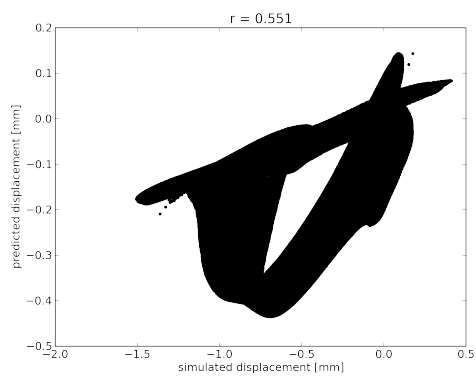
Component	S	S11	S22	S33	S12	S13	S13	U	U1	U2	U3
				MPa						mm	
<b>Avg. error</b>	1.60	0.34	0.23	1.51	0.17	0.64	0.51	0.67	0.59	0.39	0.15
<b>SD</b>	2.86	0.88	1.09	2.74	0.52	1.05	0.93	0.42	0.39	0.34	0.10
<b>Pearson coeff.</b>	0.94	0.91	0.90	0.94	0.83	0.88	0.89	0.97	0.98	0.55	0.99



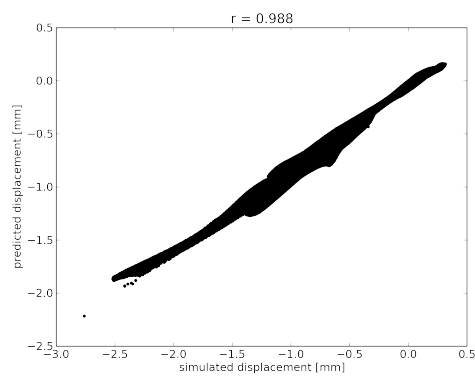
(a) U3



(b) U1



(c) U2



(d) U3

**Figure 7.9:** Displacement prediction error of the SFM

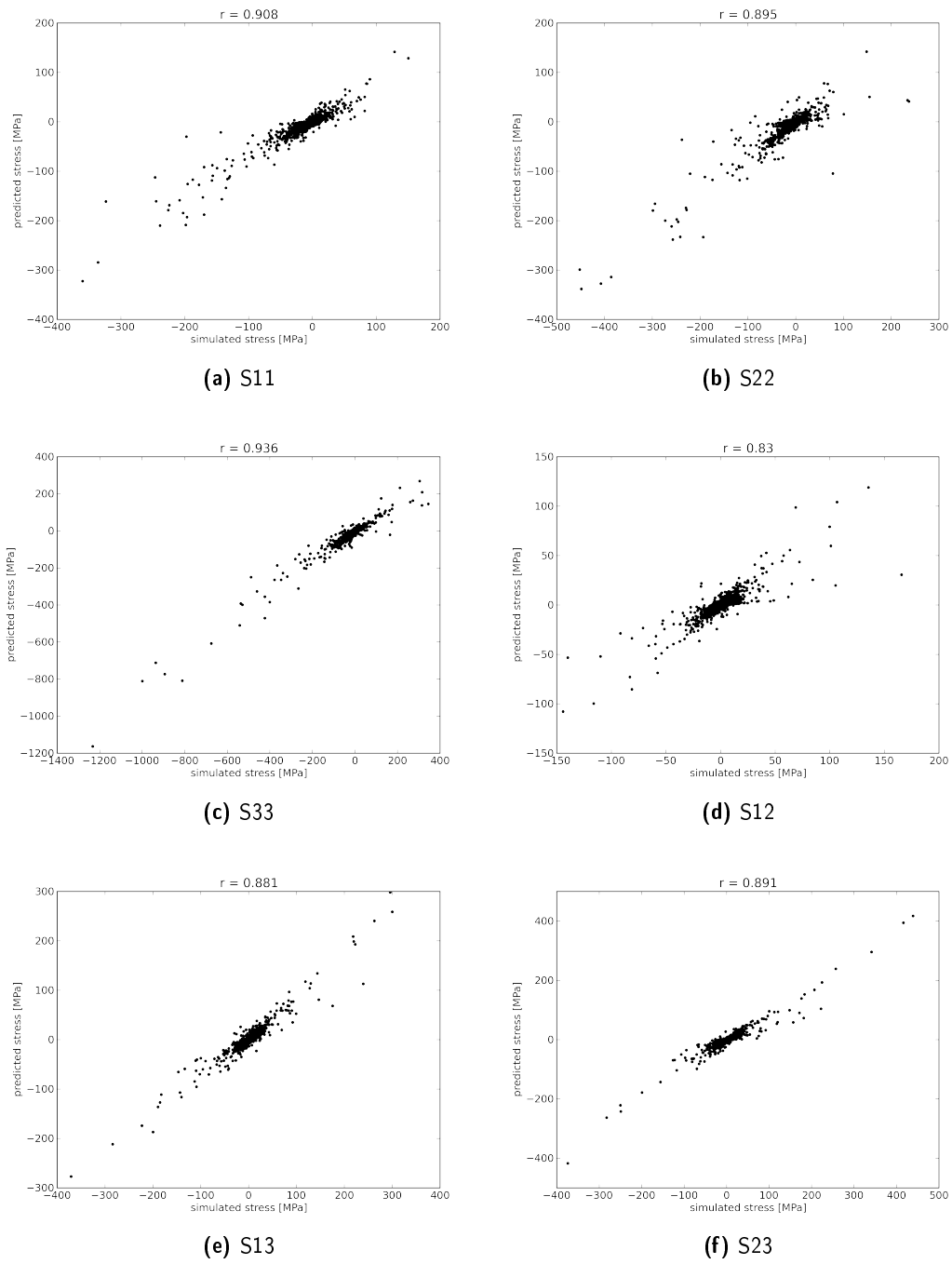


Figure 7.10: Stress prediction of the SFM

# Bibliography

Internet brain segmentation repository. URL <http://www.webcitation.org/6IE3j8NkQ><http://www.nitrc.org/projects/ibsr>.

Living human project. URL <http://www.webcitation.org/6IE3fXdz7><http://www.livinghuman.org/>.

*Terminologia Anatomica: International Anatomical Terminology*. Thieme Medical Publishers., New York, 1998.

Ddsm: Digital database for screening mammography, 2009. URL <http://marathon.csee.usf.edu/Mammography/Database.html>.

The cancer imaging archive, 2009. URL <https://cabig.nci.nih.gov/tools/NCIA>.

Uthscsa library: Medical image databases on the internet, 2009. URL <http://www.library.uthscsa.edu/find/databases.cfm>.

Standard femur model version 4, 2010. URL <http://www.biomedtown.org/>. 101

Thomas Albrecht, Marcel Luthi, and Thomas Vetter. A statistical deformation prior for non-rigid image and shape registration. In *2008 IEEE Conference on Computer Vision and Pattern Recognition*, pages 1–8, Anchorage, jun, 2008. IEEE. ISBN 978-1-4244-2242-5. doi: 10.1109/CVPR.2008.4587394.

Mark a Baldwin, Joseph E Langenderfer, Paul J Rullkoetter, and Peter J Laz. Development of subject-specific and statistical shape models of the knee using an efficient segmentation and mesh-morphing approach. *Computer methods and programs in biomedicine*, 97(3):232–40, mar, 2010. ISSN 1872-7565. doi: 10.1016/j.cmpb.2009.07.005. 89

Stefan Bauer, Roland Wiest, Lutz-P Nolte, and Mauricio Reyes. A survey of mri-based medical image analysis for brain tumor studies. *Physics in medicine and biology*, 58(13):R97–129, jul, 2013. ISSN 1361-6560. doi: 10.1088/0031-9155/58/13/R97.

URL <http://stacks.iop.org/0031-9155/58/i=13/a=R97?key=crossref.f5d87890e52190a8b3681035112ecdfehttp://www.ncbi.nlm.nih.gov/pubmed/23743802>.

Said Benameur, Max Mignotte, Stefan Parent, Hubert Labelle, Wafa Skalli, and Jacques de Guise. 3d/2d registration and segmentation of scoliotic vertebrae using statistical models. *Computerized medical imaging and graphics : the official journal of the Computerized Medical Imaging Society*, 27(5):321–37, 2003. ISSN 0895-6111. URL <http://www.ncbi.nlm.nih.gov/pubmed/12821026>. 89

G Bergmann, J Siraky, A Rohlmann, and R Koelbel. A comparison of hip joint forces in sheep, dog and man. *Journal of biomechanics*, 17(12):907–21, jan, 1984. ISSN 0021-9290. URL <http://www.ncbi.nlm.nih.gov/pubmed/6520139>. 70

G Bergmann, F Graichen, and a Rohlmann. Hip joint loading during walking and running, measured in two patients. *Journal of biomechanics*, 26(8):969–90, aug, 1993. ISSN 0021-9290. URL <http://www.ncbi.nlm.nih.gov/pubmed/8349721>. 67, 74, 76

G. Bergmann, G. Deuretzbacher, M. Heller, F. Graichen, A. Rohlmann, J. Strauss, and GN Duda. Hip contact forces and gait patterns from routine activities. *Journal of Biomechanics*, 34(7):859–871, 2001. URL <http://linkinghub.elsevier.com/retrieve/pii/S0021929001000409>.

G Bergmann, F Graichen, A Rohlmann, P Westerhoff, B Heinlein, A Bender, and R Ehrig. Design and calibration of load sensing orthopaedic implants. *Journal of biomechanical engineering*, 130(2):021009, apr, 2008. ISSN 0148-0731. doi: 10.1115/1.2898831. URL <http://www.ncbi.nlm.nih.gov/pubmed/18412496>.

Der Grosse Rat des Kantons Bern. Kantonales datenschutzgesetz, 1986. URL [http://www.sta.be.ch/belex/d/1/152\\_04.html](http://www.sta.be.ch/belex/d/1/152_04.html).

Der Regierungsrat des Kantons Bern. Forschungsverordnung, 1998. URL [http://www.sta.be.ch/belex/d/8/811\\_05.html](http://www.sta.be.ch/belex/d/8/811_05.html).

V. Blanz, A. Mehl, T. Vetter, and H. P. Seidel. A statistical method for robust 3d surface reconstruction from sparse data. In *Int. Symp. on 3D Data Processing, Visualization and Transmission*, Thessaloniki, Greece, 2004. 1, 82, 89

Volker Blanz, Albert Mehl, Thomas Vetter, Hans-peter Seidel, Restorative Dentistry, and Department Informatik. A statistical method for robust 3d surface reconstruction from sparse data 2. *Journal of Dentistry*, pages 1–8.

Serena Bonaretti. *Statistical Models of Shape and Density for Population-based Analysis of Bone Mechanics with Applications to Fracture Risk Assessment and Implant*. Phd thesis, Bern, 2012. URL <http://scholar.google.com/scholar?hl=en&btnG=Search&q=intitle:Statistical+models+of+shape+and+density+for+population-based+analysis+of+bone+mechanics+with+applications+to+fracture+risk+assessment+and+implant+design#0>.

Serena Bonaretti, Nils Reimers, Mauricio Reyes, Andrei Nikitsin, Anders Joensuu, Lutz-peter Nolte, and Philippe Büchler. Assessment of peri-articular implant fitting based on statistical finite element modeling. *Bone*, pages 1–10, 2008. vii, 2, 81

Bootstrap. Sleek, intuitive, and powerful front-end framework for faster and easier web development, 2013. URL <http://www.webcitation.org/6II1URr0Whttp://getbootstrap.com/2.3.2/>.

Habib Bou-Sleiman, Lucas E Ritacco, Lutz-Peter Nolte, and Mauricio Reyes. Minimization of intra-operative shaping of orthopaedic fixation plates: a population-based design. *Medical image computing and computer-assisted intervention : MICCAI ... International Conference on Medical Image Computing and Computer-Assisted Intervention*, 14(Pt 2):409–16, jan, 2011. URL <http://www.ncbi.nlm.nih.gov/pubmed/21995055>.

WA Brekelmans, HW Poort, and TJ Slooff. A new method to analyse the mechanical behaviour of skeletal parts. *Acta orthopaedica Scandinavica*, 43(5):301–317, 1972.

F Brinkley and C Rosse. Imaging informatics and the human brain project: the role of structure. *Image (Rochester, N.Y.)*, 2002.

Rebecca Bryan, Prasanth B Nair, and Mark Taylor. Use of a statistical model of the whole femur in a large scale, multi-model study of femoral neck fracture risk. *Journal of biomechanics*, 42(13):2171–6, sep, 2009. ISSN 1873-2380. doi: 10.1016/j.jbiomech.2009.05.038. URL <http://www.ncbi.nlm.nih.gov/pubmed/19646700>. vii, 2, 30, 34, 81, 82, 83, 89, 92

Rebecca Bryan, P Surya Mohan, Andrew Hopkins, Francis Galloway, Mark Taylor, and Prasanth B Nair. Statistical modelling of the whole human femur incorporating geometric and material

- properties. *Medical engineering & physics*, 32(1):57–65, jan, 2010. ISSN 1873-4030. doi: 10.1016/j.medengphy.2009.10.008. URL <http://www.ncbi.nlm.nih.gov/pubmed/19932044>.
- Rebecca Bryan, Prasanth B Nair, and Mark Taylor. Influence of femur size and morphology on load transfer in the resurfaced femoral head: A large scale, multi-subject finite element study. *Journal of biomechanics*, 45(11):1952–8, jul, 2012. ISSN 1873-2380. doi: 10.1016/j.jbiomech.2012.05.015. URL <http://www.ncbi.nlm.nih.gov/pubmed/22704609>. vii, 29, 30, 34, 89
- D R Carter and W C Hayes. The compressive behavior of bone as a two-phase porous structure. *The Journal of bone and joint surgery. American volume*, 59:954–962, 1977. ISSN 0021-9355.
- E F Codd. A relational model of data for large shared data banks. 1970. *M.D. computing : computers in medical practice*, 15(3):162–6, 1970. ISSN 0724-6811. URL <http://www.ncbi.nlm.nih.gov/pubmed/9617087>.
- Dianna D Cody, Gary J Gross, Fu J Hou, Horace J Spencer, Steven A Goldstein, and David P Fyhrie. Femoral strength is better predicted by finite element models than qct and dxa. *Journal of biomechanics*, 32(10):1013–20, oct, 1999. ISSN 0021-9290. 75
- T. F. Cootes, D. H. Cooper, C. J. Taylor, and J. Graham. A trainable method of parametric shape description. In *Proceedings of the British Machine Vision Conference 1991*, pages 8.1–8.8. Springer-Verlag London Limited, 1991. ISBN 3-540-19715-X. doi: 10.5244/C.5.8. URL <http://www.bmva.org/bmvc/1991/bmvc-91-008.html>.
- T.F. Cootes, C.J. Taylor, D. H. Cooper, and J. Graham. Training models of shape from sets of examples. In *In Proc. British Machine Vision Conference*, pages 9–18. Springer-Verlag, 1992. doi: 10.1.1.18.1478. 76
- Tf Cootes, A Hill, Cj Taylor, and J Haslam. Use of active shape models for locating structures in medical images. *Image and Vision Computing*, 12(6):355–365, jul, 1994. ISSN 02628856. doi: 10.1016/0262-8856(94)90060-4. URL <http://linkinghub.elsevier.com/retrieve/pii/0262885694900604>.
- T.F. Cootes, C.J. Taylor, D.H. Cooper, and J Graham. Active shape models-their training and application. *Computer Vision and Image Understanding*, 61(1):38–59, jan, 1995. ISSN 10773142. doi: 10.1006/cviu.1995.1004. URL <http://linkinghub.elsevier.com/retrieve/pii/S1077314285710041>. 27, 89, 90

- T.F. Tim F. Cootes and Chris J C.J. Taylor. Statistical models of appearance for medical image analysis and computer vision. *SPIE proceedings series*, pages 236–248, 2001. ISSN 0277786X. doi: 10.1117/12.431093. URL <http://link.aip.org/link/?PSI/4322/236/1&Agg=doi>. vii, 1, 82
- Ronald Cornet and Nicolette de Keizer. Forty years of snomed: a literature review. *BMC medical informatics and decision making*, 8 Suppl 1:S2, jan, 2008. ISSN 1472-6947. doi: 10.1186/1472-6947-8-S1-S2. URL <http://www.pubmedcentral.nih.gov/articlerender.fcgi?artid=2582789&tool=pmcentrez&rendertype=abstract>.
- W R Crum. Non-rigid image registration: theory and practice. *British Journal of Radiology*, 77 (suppl\_2):S140–S153, dec, 2004. ISSN 0007-1285. doi: 10.1259/bjr/25329214. URL <http://bjr.birjournals.org/cgi/doi/10.1259/bjr/25329214>.
- Daniel Dalet. D-maps, 2013. URL <http://www.webcitation.org/6IIldkzvT>[http://d-maps.com/carte.php?num\\_car=30074&lang=en](http://d-maps.com/carte.php?num_car=30074&lang=en).
- Db-engines. Db-engines ranking - popularity ranking of database management systems. URL <http://db-engines.com/en/ranking>.
- Fani Deligianni, Adrian J Chung, and Guang-Zhong Yang. Nonrigid 2-d/3-d registration for patient specific bronchoscopy simulation with statistical shape modeling: phantom validation. *IEEE transactions on medical imaging*, 25(11):1462–71, nov, 2006. ISSN 0278-0062. doi: 10.1109/TMI.2006.883452. URL <http://www.ncbi.nlm.nih.gov/pubmed/17117775>. 89
- DSpace. Dspace, an open-source solution for accessing, managing and preserving scholarly works. URL <http://www.webcitation.org/6IUdfqB0p><http://www.dspace.org/>.
- G N Duda, M Heller, J Albinger, O Schulz, E Schneider, and L Claes. Influence of muscle forces on femoral strain distribution. *Journal of biomechanics*, 31(9):841–6, sep, 1998. ISSN 0021-9290. URL <http://www.ncbi.nlm.nih.gov/pubmed/9802785>. 68
- EPrints. The original institutional repository solution. URL <http://www.webcitation.org/6IE9pVcpm><http://www.eprints.org/>.
- Alain Farron, Alexandre Terrier, and Philippe Büchler. Risks of loosening of a prosthetic glenoid implanted in retroversion. *Journal of shoulder and elbow surgery / American Shoulder and Elbow Surgeons ... [et al.]*, 15(4):521–6, 2006. ISSN 1058-2746. doi: 10.1016/j.jse.2005.10.003. URL <http://www.ncbi.nlm.nih.gov/pubmed/16831661>. 75

David A Field. Qualitative measures for initial meshes. 906(May 1998):887–906, 2000.

Roy T. Fielding and Richard N. Taylor. Principled design of the modern web architecture. *ACM Transactions on Internet Technology*, 2(2):115–150, may, 2002. ISSN 15335399. doi: 10.1145/514183.514185. URL <http://portal.acm.org/citation.cfm?doid=514183.514185>.

RT Fielding. Architectural styles and the design of network-based software architectures. page 180, 2000. URL <http://jpkc.fudan.edu.cn/picture/article/216/35/4b/22598d594e3d93239700ce79bce1/7ed3ec2a-03c2-49cb-8bf8-5a90ea42f523.pdf>.

Clare K Fitzpatrick, Mark A Baldwin, Paul J Rullkoetter, and Peter J Laz. Combined probabilistic and principal component analysis approach for multivariate sensitivity evaluation and application to implanted patellofemoral mechanics. *Journal of biomechanics*, 44(1):13–21, sep, 2010. ISSN 1873-2380. doi: 10.1016/j.jbiomech.2010.08.016. URL <http://www.ncbi.nlm.nih.gov/pubmed/20825941>. 30, 89

J Michael Fitzpatrick, Derek L G Hill, and Calvin R Maurer. Image registration. chapter 8, pages 447–514. 2008. URL <http://tango.andrew.cmu.edu/~gustavor/42431-intro-bioimaging/readings/ch8.pdf>.

Karl D. Fritscher, Agnes Grünerbl, and Rainer Schubert. 3d image segmentation using combined shape-intensity prior models. *International Journal of Computer Assisted Radiology and Surgery*, 1(6):341–350, feb, 2007. ISSN 1861-6410. doi: 10.1007/s11548-007-0070-z. URL <http://www.springerlink.com/index/10.1007/s11548-007-0070-z>. 89

Fuseki. Fuseki: serving rdf data over http, 2013. URL [https://jena.apache.org/documentation/serving\\_data/](https://jena.apache.org/documentation/serving_data/).

U Glitsch and W Baumann. The three-dimensional determination of internal loads in the lower extremity. *Journal of biomechanics*, 30(11-12):1123–31, 1997. ISSN 0021-9290. URL <http://www.ncbi.nlm.nih.gov/pubmed/9456380>.

Ballester Gonzalez.

Henry Gray. *Gray’s Anatomy*. Chancellor Press, masterclas edition, 1985. ISBN 0907486827.

Thomas R Gruber. A translation approach to portable ontology specifications by a translation approach to portable ontology specifications. 5(April):199–220, 1993.



- Thomas R. Gruber. Toward principles for the design of ontologies used for knowledge sharing? *International Journal of Human-Computer Studies*, 43(5-6):907–928, nov, 1995. ISSN 10715819. doi: 10.1006/ijhc.1995.1081. URL <http://linkinghub.elsevier.com/retrieve/pii/S1071581985710816>.
- Stig Hansson. A conical implant-abutment interface at the level of the marginal bone improves the distribution of stresses in the supporting bone. an axisymmetric finite element analysis. *Clinical oral implants research*, 14(3):286–93, jun, 2003. ISSN 0905-7161. URL <http://www.ncbi.nlm.nih.gov/pubmed/12830797>. 88
- D J Hawkes, D Barratt, J M Blackall, C Chan, P J Edwards, K Rhode, G P Penney, J McClelland, and D L G Hill. Tissue deformation and shape models in image-guided interventions: a discussion paper. *Medical image analysis*, 9(2):163–75, apr, 2005. ISSN 1361-8415. doi: 10.1016/j.media.2004.11.007. URL <http://www.ncbi.nlm.nih.gov/pubmed/15721231>.
- Tobias Heimann and Hans-Peter Meinzer. Statistical shape models for 3d medical image segmentation: a review. *Medical image analysis*, 13(4):543–63, aug, 2009. ISSN 1361-8423. doi: 10.1016/j.media.2009.05.004. URL <http://www.ncbi.nlm.nih.gov/pubmed/19525140>.
- Benedikt Helgason, Egon Perilli, Enrico Schileo, Fulvia Taddei, Sigurdur Brynjólfsson, and Marco Viceconti. Mathematical relationships between bone density and mechanical properties: a literature review. *Clinical biomechanics (Bristol, Avon)*, 23(2):135–46, 2008a. ISSN 0268-0033. doi: 10.1016/j.clinbiomech.2007.08.024. URL <http://www.ncbi.nlm.nih.gov/pubmed/17931759>.
- Benedikt Helgason, Fulvia Taddei, Halldór Pálsson, Enrico Schileo, Luca Cristofolini, Marco Viceconti, and Sigurthur Brynjólfsson. A modified method for assigning material properties to fe models of bones. *Medical engineering & physics*, 30(4):444–53, may, 2008b. ISSN 1350-4533. doi: 10.1016/j.medengphy.2007.05.006. URL <http://www.ncbi.nlm.nih.gov/pubmed/17627862>.
- M O Heller, G Bergmann, G Deuretzbacher, L Dürselen, M Pohl, L Claes, N P Haas, and G N Duda. Musculo-skeletal loading conditions at the hip during walking and stair climbing. *Journal of biomechanics*, 34(7):883–93, jul, 2001. ISSN 0021-9290. URL <http://www.ncbi.nlm.nih.gov/pubmed/11410172>. 26, 42, 67
- M O Heller, G Bergmann, J-P Kassi, L Claes, N P Haas, and G N Duda. Determination of muscle loading at the hip joint for use in pre-clinical testing. *Journal of biomechanics*, 38(5):

- 1155–63, may, 2005. ISSN 0021-9290. doi: 10.1016/j.jbiomech.2004.05.022. URL <http://www.ncbi.nlm.nih.gov/pubmed/15797596>. vii, 67, 68, 69, 71, 74, 76, 92
- C J Hernandez and T M Keaveny. A biomechanical perspective on bone quality. *Bone*, 39(6):1173–81, dec, 2006. ISSN 8756-3282. doi: 10.1016/j.bone.2006.06.001. URL <http://www.pubmedcentral.nih.gov/articlerender.fcgi?artid=1876764&tool=pmcentrez&rendertype=abstract>. 75
- Maureen N Hood and Hugh Scott. Introduction to picture archive and communication systems. *Journal of Radiology Nursing*, 25(3):69–74, sep, 2006. ISSN 15460843. doi: 10.1016/j.radnu.2006.06.003. URL <http://linkinghub.elsevier.com/retrieve/pii/S1546084306000733>.
- W Hoogland and H. Weber. Statement concerning cern w3 software release into public domain, 1993.
- Ian Horrocks, Bijan Parsia, Peter Patel-schneider, and James Hendler. Semantic web architecture : Stack or two towers ? 2005. URL <http://www.cs.ox.ac.uk/ian.horrocks/Publications/download/2005/HPPH05.pdf>.
- Najah Hraiech. *Mesh morphing and shape indexing in human femur modeling applications*. Phd thesis, Université de Rennes, 2010. 76, 82, 90
- R Huiskes and S J Hollister. From structure to process, from organ to cell: recent developments of fe-analysis in orthopaedic biomechanics. *Journal of biomechanical engineering*, 115(4B):520–7, nov, 1993. ISSN 0148-0731. URL <http://www.ncbi.nlm.nih.gov/pubmed/8302035>.
- Julien Jomier, Stephen R. Aylward, Charles Marion, Joowhi Lee, and Martin Styner. A digital archiving system and distributed server-side processing of large datasets. pages 726413–726413–8, feb, 2009. doi: 10.1117/12.812227. URL <http://proceedings.spiedigitallibrary.org/proceeding.aspx?doi=10.1117/12.812227><http://proceedings.spiedigitallibrary.org/proceeding.aspx?articleid=816239>.
- JQuery. The write less, do more, javascript library, 2013. URL <http://www.webcitation.org/6IUeDur35><http://jquery.com/>.
- W A. Kalender, D Felsenberg, H K Genant, M Fischer, J Dequeker, and J Reeve. The european spine phantom—a tool for standardization and quality control in spinal bone mineral measure-

- ments by dxa and qct. *European journal of radiology*, 20(2):83–92, jul, 1995. ISSN 0720-048X. URL <http://www.ncbi.nlm.nih.gov/pubmed/7588873>.
- J.H. Keyak, J.M. Meagher, H.B. Skinner, and C.D. Mote. Automated three-dimensional finite element modelling of bone: a new method. *Journal of Biomedical Engineering*, 12(5):389–397, sep, 1990. ISSN 01415425. doi: 10.1016/0141-5425(90)90022-F. URL <http://linkinghub.elsevier.com/retrieve/pii/014154259090022F> \delimeter"026E30F\$npapers2://publication/doi/10.1016/0141-5425(90)90022-Fhttp://linkinghub.elsevier.com/retrieve/pii/014154259090022F.
- Iman Khalaji, Kamran Rahemifar, and Abbas Samani. Accelerated statistical shape model-based technique for tissue deformation estimation. *Proc. of SPIE*, 7261(1):1–9, 2009. doi: 10.1117/12.813859. vii, 2, 30, 82, 89
- Michael Kistler, Serena Bonaretti, Marcelo Elias de Oliveira, Christelle Boichon, Michel Rochette, and Philippe Büchler. Statistical model of appearance to accelerate finite element calculations in biomechanics. In *Journal of Biomechanics*, volume 45, page S257. Elsevier Ltd, jul, 2012. doi: 10.1016/S0021-9290(12)70258-0. URL <http://linkinghub.elsevier.com/retrieve/pii/S0021929012702580>. 98
- Ralf U Kleemann, Markus O Heller, Ulrich Stoeckle, William R Taylor, and Georg N Duda. Tha loading arising from increased femoral anteversion and offset may lead to critical cement stresses. *Journal of orthopaedic research : official publication of the Orthopaedic Research Society*, 21(5):767–74, sep, 2003. ISSN 0736-0266. doi: 10.1016/S0736-0266(03)00040-8. URL <http://www.ncbi.nlm.nih.gov/pubmed/12919861>. 68
- Nina Kozic, Stefan Weber, Philippe Büchler, Christian Lutz, Nils Reimers, Miguel A González Ballester, and Mauricio Reyes. Optimisation of orthopaedic implant design using statistical shape space analysis based on level sets. *Medical image analysis*, 14(3):265–75, jun, 2010. ISSN 1361-8423. doi: 10.1016/j.media.2010.02.008. URL <http://www.ncbi.nlm.nih.gov/pubmed/20359938>.
- Hans Lamecker, Martin Seeba, Hans-christian Hege, Peter Deu, and Visual Concepts Gmbh. A 3d statistical shape model of the pelvic bone for segmentation. *Training*, (section 4).
- Hans Lamecker, Thomas Lange, and Martin Seebass. A statistical shape model for the liver 2 building a statistical shape model. *Medical Image Computing and Computer-Assisted Intervention*, pages 421–427, 2002. 1, 89

- Peter J Laz, Joshua Q Stowe, Mark A Baldwin, Anthony J Petrella, and Paul J Rullkoetter. Incorporating uncertainty in mechanical properties for finite element-based evaluation of bone mechanics. *Journal of Biomechanics*, 40(13):2831–2836, jan, 2007. ISSN 0021-9290. doi: 10.1016/j.jbiomech.2007.03.013. vii, 2, 82
- Hector J. Levesque. Foundations of a functional approach to knowledge representation. *Artificial Intelligence*, 23(2):155–212, jul, 1984. ISSN 00043702. doi: 10.1016/0004-3702(84)90009-2. URL <http://linkinghub.elsevier.com/retrieve/pii/0004370284900092>.
- J Paige Little and Clayton Adam. Patient-specific computational biomechanics for simulating adolescent scoliosis surgery: Predicted vs clinical correction for a preliminary series of six patients. *International Journal for Numerical Methods in Biomedical Engineering*, 27(3):347–356, mar, 2011. ISSN 20407939. doi: 10.1002/cnm.1422. URL <http://doi.wiley.com/10.1002/cnm.1422>. 88
- Brent J Liu, H K Huang, Fei Cao, Michael Z Zhou, Jianguo Zhang, and Greg Mogel. Informatics in radiology (inforad): A complete continuous-availability pacs archive server. *Radiographics : a review publication of the Radiological Society of North America, Inc*, 24(4):1203–9, 2004. ISSN 1527-1323. doi: 10.1148/rg.244035051. URL <http://www.ncbi.nlm.nih.gov/pubmed/15256640>.
- J Lötjönen, S Kivistö, J Koikkalainen, D Smutek, and K Lauerma. Statistical shape model of atria, ventricles and epicardium from short- and long-axis mr images. *Medical image analysis*, 8(3):371–86, sep, 2004. ISSN 1361-8415. doi: 10.1016/j.media.2004.06.013. URL <http://www.ncbi.nlm.nih.gov/pubmed/15450230>. 89
- Marcel Lüthi, Thomas Albrecht, Tobias Gass, OrcunK Goksel, Michael Kistler, Habib Bousleiman, Mauricio Reyes, Buechler Philippe, Philippe C Cattin, and Thomas Vetter. Statismo - a framework for pca based statistical models . *The Insight Journal*, pages 1–18, 2012. URL <http://hdl.handle.net/10380/3371>. 41
- J B Antoine Maintz and Max A Viergever. A survey of medical image registration methods. 2(1): 1–36, 1998.
- S Majumdar, M Kothari, P Augat, D C Newitt, T M Link, J C Lin, T Lang, Y Lu, and H K Genant. High-resolution magnetic resonance imaging: three-dimensional trabecular bone architecture and biomechanical properties. *Bone*, 22(5):445–54, may, 1998. ISSN 8756-3282. URL <http://www.ncbi.nlm.nih.gov/pubmed/9600777>.

- Kenneth A Mann and Leatha A Damron. Predicting the failure response of cement-bone constructs using a non-linear fracture mechanics approach. *Journal of biomechanical engineering*, 124(4):462–70, aug, 2002. ISSN 0148-0731. URL <http://www.ncbi.nlm.nih.gov/pubmed/12188213>. 75
- Daniel S Marcus, Timothy R Olsen, Mohana Ramaratnam, and Randy L Buckner. The extensible neuroimaging archive toolkit: an informatics platform for managing, exploring, and sharing neuroimaging data. *Neuroinformatics*, 5(1):11–34, jan, 2007. ISSN 1539-2791. URL <http://www.ncbi.nlm.nih.gov/pubmed/17426351>.
- D.S. Marcus, T. Olsen, M. Ramaratnam, and R.L Buckner. Xnat: a software framework for managing neuroimaging laboratory data. In *Proceedings of the 12th Annual Meeting of the Organization for Human Brain Mapping Held in Florence*, pages 11–15, Florence, 2006. URL <http://scholar.google.com/scholar?hl=en&btnG=Search&q=intitle:Xnat:+a+software+framework+for+managing+neuroimaging+laboratory+data#0>.
- B. Menze, A. Jakab, S Bauer, M. Reyes, M. Prastawa, and K. van Leemput. Brats 2012 - miccai 2012 challenge on multimodal brain tumor segmentation. In *Preceedings of MICCAI-BRATS 2012*, Nice, 2012. URL <http://www.imm.dtu.dk/projects/BRATS2012>.
- Microsoft. Microsoft security bulletin, 2013. URL <http://technet.microsoft.com/en-US/security/dn481339>.
- MongoDB. Nosql databases explained. URL <http://www.mongodb.com/learn/nosql#nosql>.
- Elise F Morgan, Harun H Bayraktar, and Tony M Keaveny. Trabecular bone modulus-density relationships depend on anatomic site. *Journal of biomechanics*, 36(7):897–904, jul, 2003. ISSN 0021-9290. doi: 10.1016/S0021-9290(03)00071-X. URL <http://linkinghub.elsevier.com/retrieve/pii/S002192900300071X><http://www.ncbi.nlm.nih.gov/pubmed/12757797>. 24, 30, 42, 83, 92
- Seyed Reza Mousavi, Iman Khalaji, Ali Sadeghi Naini, Kaamran Raahemifar, and Abbas Samani. Statistical finite element method for real-time tissue mechanics analysis. *Computer methods in biomechanics and biomedical engineering*, 15(6):595–608, jun, 2012. ISSN 1476-8259. doi: 10.1080/10255842.2010.550889. 31, 89

- NIC. Cip survey of biomedical imaging archives. URL <https://wiki.nci.nih.gov/display/CIP/CIP+Survey+of+Biomedical+Imaging+Archives>.
- Lawrence Page, Sergey Brin, Rajeev Motwani, and Terry Winograd. The pagerank citation ranking: Bringing order to the web. Technical report, Stanford Digital Library Technologies Project, 1998. URL <http://citeseerx.ist.psu.edu/viewdoc/summary?doi=10.1.1.31.1768>.
- Douglas R Pedersen, Richard A Brand, and Dwight T Davy. Pelvic muscle and acetabular contact forces during gait. *Journal of Biomechanics*, 30(9):959–965, sep, 1997. ISSN 00219290. doi: 10.1016/S0021-9290(97)00041-9. URL <http://linkinghub.elsevier.com/retrieve/pii/S0021929097000419>.
- Josien P W Pluim, J B Antoine Maintz, and Max a Viergever. Mutual-information-based registration of medical images: a survey. *IEEE transactions on medical imaging*, 22(8):986–1004, aug, 2003. ISSN 0278-0062. doi: 10.1109/TMI.2003.815867. URL <http://www.ncbi.nlm.nih.gov/pubmed/12906253>.
- Sander Poelert, Edward Valstar, Harrie Weinans, and Amir a Zadpoor. Patient-specific finite element modeling of bones. *Proceedings of the Institution of Mechanical Engineers. Part H, Journal of engineering in medicine*, 227(4):464–78, apr, 2013. ISSN 0954-4119. doi: 10.1177/0954411912467884. URL <http://www.ncbi.nlm.nih.gov/pubmed/23637222>.
- K. Polgar, H. S. Gill, M. Viceconti, D. W. Murray, and J. J. O'Connor. Development and numerical validation of a finite element model of the muscle standardized femur. *Proceedings of the Institution of Mechanical Engineers, Part H: Journal of Engineering in Medicine*, 217(3):165–172, mar, 2003. ISSN 0954-4119. doi: 10.1243/095441103765212668. URL <http://pih.sagepub.com/lookup/doi/10.1243/095441103765212668>. 68, 70
- K Polgár, H S Gill, M Viceconti, D W Murray, and J J O'Connor. Strain distribution within the human femur due to physiological and simplified loading: finite element analysis using the muscle standardized femur model. *Proceedings of the Institution of Mechanical Engineers. Part H, Journal of engineering in medicine*, 217(3):173–89, jan, 2003. ISSN 0954-4119. URL <http://www.ncbi.nlm.nih.gov/pubmed/12807158>. 70
- PJ Prendergast. Finite element models in tissue mechanics and orthopaedic implant design. *Clinical Biomechanics*, 12(6):343–366, sep, 1997. ISSN 02680033. doi: 10.1016/S0268-0033(97)00018-1. URL <http://linkinghub.elsevier.com/retrieve/pii/S0268003397000181>.

Belenguer Querol. vii, 2, 29, 81, 89

Kumar T Rajamani, Martin a Styner, Haydar Talib, Guoyan Zheng, Lutz P Nolte, and Miguel a González Ballester. Statistical deformable bone models for robust 3d surface extrapolation from sparse data. *Medical image analysis*, 11(2):99–109, 2007. ISSN 1361-8415. doi: 10.1016/j.media.2006.05.001. URL <http://www.ncbi.nlm.nih.gov/pubmed/17349939>. vii, 1, 82

B Reggiani, L Cristofolini, E Varini, and M Viceconti. Predicting the subject-specific primary stability of cementless implants during pre-operative planning: preliminary validation of subject-specific finite-element models. *Journal of biomechanics*, 40(11):2552–8, jan, 2007. ISSN 0021-9290. doi: 10.1016/j.jbiomech.2006.10.042. URL <http://www.ncbi.nlm.nih.gov/pubmed/17229427>. 88

Cornelius Rosse and José L V Mejino. A reference ontology for biomedical informatics: the foundational model of anatomy. *Journal of biomedical informatics*, 36(6):478–500, dec, 2003. ISSN 1532-0464. doi: 10.1016/j.jbi.2003.11.007. URL <http://www.ncbi.nlm.nih.gov/pubmed/14759820>.

Abhijit Sinha Roy and William J Dupps. Patient-specific modeling of corneal refractive surgery outcomes and inverse estimation of elastic property changes. *Journal of biomechanical engineering*, 133(1):011002, jan, 2011. ISSN 1528-8951. doi: 10.1115/1.4002934. URL <http://www.ncbi.nlm.nih.gov/pubmed/21186892>. 88

Enrico Schileo, Fulvia Taddei, Andrea Malandrino, Luca Cristofolini, and Marco Viceconti. Subject-specific finite element models can accurately predict strain levels in long bones. *Journal of biomechanics*, 40(13):2982–9, jan, 2007. ISSN 0021-9290. doi: 10.1016/j.jbiomech.2007.02.010. URL <http://www.ncbi.nlm.nih.gov/pubmed/17434172>.

Enrico Schileo, Enrico Dall’ara, Fulvia Taddei, Andrea Malandrino, Tom Schotkamp, Massimiliano Baleani, and Marco Viceconti. An accurate estimation of bone density improves the accuracy of subject-specific finite element models. *Journal of Biomechanics*, 41(11):2483–91, aug, 2008a. ISSN 0021-9290. doi: 10.1016/j.jbiomech.2008.05.017. URL <http://www.ncbi.nlm.nih.gov/pubmed/18606417>. 83, 92

Enrico Schileo, Fulvia Taddei, Luca Cristofolini, and Marco Viceconti. Subject-specific finite element models implementing a maximum principal strain criterion are able to estimate failure risk and fracture location on human femurs tested in vitro. *Journal of biomechanics*, 41(2):356–67, jan, 2008b. ISSN 0021-9290. doi: 10.1016/j.jbiomech.2007.09.009. 75

- J  rome Schmid and Nadia Magn  nat-Thalmann. Mri bone segmentation using deformable models and shape priors. *Medical image computing and computer-assisted intervention : MICCAI ... International Conference on Medical Image Computing and Computer-Assisted Intervention*, 11(Pt 1):119–26, jan, 2008. doi: 10.1109/ICCPHOT.2012.6215223. URL <http://www.ncbi.nlm.nih.gov/pubmed/18979739>. 89
- Benedikt Schuler, Karl D Fritscher, Volker Kuhn, Felix Eckstein, Thomas M Link, and Rainer Schubert. Assessment of the individual fracture risk of the proximal femur by using statistical appearance models. *Medical physics*, 37(6):2560–71, jun, 2010. ISSN 0094-2405. URL <http://www.ncbi.nlm.nih.gov/pubmed/20632568>.
- Steffen Schumann, Li Liu, Moritz Tannast, Mathias Bergmann, Lutz-P Nolte, and Guoyan Zheng. An integrated system for 3d hip joint reconstruction from 2d x-rays: A preliminary validation study. *Annals of biomedical engineering*, may, 2013. ISSN 1573-9686. doi: 10.1007/s10439-013-0822-6. URL <http://www.ncbi.nlm.nih.gov/pubmed/23670657>.
- Christof Seiler, Xavier Pennec, Lucas Ritacco, and Mauricio Reyes. Femur specific polyaffine model to regularize the log-domain demons registration. In Benoit M. Dawant and David R. Haynor, editors, *Proceedings of SPIE*, pages 79620G–79620G–6, mar, 2011. doi: 10.1117/12.878316. URL <http://proceedings.spiedigitallibrary.org/proceeding.aspx?articleid=724526>.
- Vickie B Shim, Rocco P Pitto, Robert M Streicher, Peter J Hunter, and Iain a Anderson. The use of sparse ct datasets for auto-generating accurate fe models of the femur and pelvis. *Journal of biomechanics*, 40(1):26–35, jan, 2007. ISSN 0021-9290. doi: 10.1016/j.jbiomech.2005.11.018. URL <http://www.ncbi.nlm.nih.gov/pubmed/16427645>.
- Vickie B Shim, Rocco P Pitto, Robert M Streicher, Peter J Hunter, and Iain A Anderson. Development and validation of patient-specific finite element models of the hemipelvis generated from a sparse ct data set. *Journal of biomechanical engineering*, 130(5):051010, oct, 2008. ISSN 0148-0731. doi: 10.1115/1.2960368. URL <http://www.ncbi.nlm.nih.gov/pubmed/19045517>.
- Aristeidis Sotiras, Christos Davatzikos, and Nikos Paragios. Deformable medical image registration: a survey. *IEEE transactions on medical imaging*, 32(7):1153–90, jul, 2013. ISSN 1558-254X. doi: 10.1109/TMI.2013.2265603. URL <http://www.ncbi.nlm.nih.gov/pubmed/23739795>.



- Andrew D Speirs, Markus O Heller, Georg N Duda, and William R Taylor. Physiologically based boundary conditions in finite element modelling. *Journal of biomechanics*, 40(10):2318–23, jan, 2007. ISSN 0021-9290. doi: 10.1016/j.jbiomech.2006.10.038. URL <http://www.ncbi.nlm.nih.gov/pubmed/17166504>. vii, 42, 68, 69, 74, 76, 77, 92
- V M Spitzer and D G Whitlock. The visible human dataset: the anatomical platform for human simulation. *The Anatomical record*, 253(2):49–57, apr, 1998. ISSN 0003-276X. URL <http://www.ncbi.nlm.nih.gov/pubmed/9605360>.
- Joes Staal, Michael D Abràmoff, Meindert Niemeijer, Max A Viergever, and Bram van Ginneken. Ridge-based vessel segmentation in color images of the retina. *IEEE transactions on medical imaging*, 23(4):501–9, apr, 2004. ISSN 0278-0062. doi: 10.1109/TMI.2004.825627. URL <http://www.ncbi.nlm.nih.gov/pubmed/15084075>.
- Thornton Staples, Ross Wayland, and Sandra Payette. The fedora project. *D-Lib Magazine*, 9(4), apr, 2003. ISSN 1082-9873. doi: 10.1045/april2003-staples. URL <http://www.dlib.org/dlib/april03/staples/04staples.html>.
- F. Taddei, S. Martelli, B. Reggiani, L. Cristofolini, and M. Viceconti. Finite-element modeling of bones from ct data: sensitivity to geometry and material uncertainties. *IEEE Transactions on Biomedical Engineering*, 53(11):2194–2200, 2006a. URL [http://ieeexplore.ieee.org/xpls/abs\\_all.jsp?arnumber=1710160](http://ieeexplore.ieee.org/xpls/abs_all.jsp?arnumber=1710160).
- Fulvia Taddei, Alberto Pancanti, and Marco Viceconti. An improved method for the automatic mapping of computed tomography numbers onto finite element models. *Medical engineering & physics*, 26(1):61–9, jan, 2004. ISSN 1350-4533. URL <http://www.ncbi.nlm.nih.gov/pubmed/14644599>. 24, 75
- Fulvia Taddei, Luca Cristofolini, Saulo Martelli, H S Gill, and Marco Viceconti. Subject-specific finite element models of long bones: An in vitro evaluation of the overall accuracy. *Journal of biomechanics*, 39(13):2457–67, 2006b. ISSN 0021-9290. doi: 10.1016/j.jbiomech.2005.07.018. URL <http://www.ncbi.nlm.nih.gov/pubmed/16213507>.
- Fulvia Taddei, Saulo Martelli, Barbara Reggiani, Luca Cristofolini, and Marco Viceconti. Finite-element modeling of bones from ct data: sensitivity to geometry and material uncertainties. *IEEE transactions on bio-medical engineering*, 53(11):2194–200, nov, 2006c. ISSN 0018-9294. doi: 10.1109/TBME.2006.879473. URL <http://www.ncbi.nlm.nih.gov/pubmed/17073324>. 2, 82

- M E Taylor, K E Tanner, M a Freeman, and a L Yettram. Stress and strain distribution within the intact femur: compression or bending? *Medical engineering & physics*, 18(2):122–31, mar, 1996. ISSN 1350-4533. URL <http://www.ncbi.nlm.nih.gov/pubmed/8673318>. 68
- Tdbloader. Tdb command-line utilities, 2013. URL <https://jena.apache.org/documentation/tdb/commands.html>.
- A Terrier, P Büchler, and A Farron. Bone-cement interface of the glenoid component: stress analysis for varying cement thickness. *Clinical biomechanics (Bristol, Avon)*, 20(7):710–717, aug, 2005. URL [http://linkinghub.elsevier.com/retrieve/pii/S0268-0033\(05\)00078-1](http://linkinghub.elsevier.com/retrieve/pii/S0268-0033(05)00078-1)file:///localhost/Users/pbuech/Documents/Papers/2005/Terrier/Clinicalbiomechanics(BristolAvon)2005Terrier.pdfpapers://c4ffa5ac-087d-4003-9406-0d2219626a78/Paper/p79. 88
- Sami P Väänänen, Jukka S Jurvelin, and Hanna Isaksson. Estimation of 3d shape, internal density and mechanics of proximal femur by combining bone mineral density images with shape and density templates. *Biomechanics and modeling in mechanobiology*, 11(6):791–800, jul, 2012. ISSN 1617-7940. doi: 10.1007/s10237-011-0352-9. URL <http://www.ncbi.nlm.nih.gov/pubmed/21986796>. 89
- E Verhulp, B van Rietbergen, and R Huiskes. Comparison of micro-level and continuum-level voxel models of the proximal femur. *Journal of biomechanics*, 39(16):2951–7, jan, 2006. ISSN 0021-9290. doi: 10.1016/j.jbiomech.2005.10.027. URL <http://www.ncbi.nlm.nih.gov/pubmed/16359680>.
- Marco Viceconti, Giovanni Brusi, Alberto Pancanti, and Luca Cristofolini. Primary stability of an anatomical cementless hip stem: a statistical analysis. *Journal of biomechanics*, 39(7):1169–79, jan, 2006. ISSN 0021-9290. doi: 10.1016/j.jbiomech.2005.03.024. URL <http://www.ncbi.nlm.nih.gov/pubmed/15927191>.
- Mario Viceconti, Massimiliano Casali, B Massari, Luca Cristofolini, Sanzio Bassini, and Aldo Toni. The 'standardized femur program' proposal for a reference geometry to be used for the creation of finite element models of the femur. *Journal of biomechanics*, 29(9):1241, sep, 1996. ISSN 0021-9290. doi: 10.1016/0021-9290(95)00164-6. URL <http://www.ncbi.nlm.nih.gov/pubmed/8872285>. 69
- Wikipedia. Web typography, 2013. URL [https://en.wikipedia.org/wiki/Web\\_typography](https://en.wikipedia.org/wiki/Web_typography).

- Adam Wittek, Karol Miller, Ron Kikinis, and Simon K Warfield. Patient-specific model of brain deformation: application to medical image registration. *Journal of biomechanics*, 40(4):919–29, jan, 2007. ISSN 0021-9290. doi: 10.1016/j.jbiomech.2006.02.021. URL <http://www.ncbi.nlm.nih.gov/pubmed/16678834>. 88
- Zohar Yosibash, Royi Padan, Leo Joskowicz, and Charles Milgrom. A ct-based high-order finite element analysis of the human proximal femur compared to in-vitro experiments. *Journal of biomechanical engineering*, 129:297–309, 2007. ISSN 01480731. doi: 10.1115/1.2720906.
- C Zannoni, R Mantovani, and M Viceconti. Material properties assignment to finite element models of bone structures: a new method. *Medical engineering & physics*, 20(10):735–40, dec, 1998. ISSN 1350-4533. doi: S1350453398000812[pii]. URL <http://www.ncbi.nlm.nih.gov/pubmed/10223642>.
- Guoyan Zheng, Sebastian Gollmer, Steffen Schumann, Xiao Dong, Thomas Feilkas, and Miguel A González Ballester. A 2d/3d correspondence building method for reconstruction of a patient-specific 3d bone surface model using point distribution models and calibrated x-ray images. *Medical image analysis*, 13(6):883–99, dec, 2009. ISSN 1361-8423. doi: 10.1016/j.media.2008.12.003. URL <http://www.ncbi.nlm.nih.gov/pubmed/19162529>. 34, 89, 111
- Barbara Zitová and Jan Flusser. Image registration methods: a survey. *Image and Vision Computing*, 21(11):977–1000, oct, 2003. ISSN 02628856. doi: 10.1016/S0262-8856(03)00137-9. URL <http://linkinghub.elsevier.com/retrieve/pii/S0262885603001379>.



# Resume

## Personal data

Name	Michael Kistler
Date of birth	September 15, 1980
Place of birth	Nelspruit (Mpumalanga), South Africa
Nationality	Swiss

## Education

2009-2014	PhD Student in Biomedical Engineering, University of Bern, Institute for Surgical Technology and Biomechanics, Bern, Switzerland
2006-2009	Master of Science in Biomedical Engineering, University of Bern, Bern, Switzerland, Focus area: Musculoskeletal System
2001-2006	Bachelor's Level in Human Medicine, University of Basel, Basel, Switzerland
1992-2000	Matura Type C, Kantonsschule Alpenquai, Lucerne, Switzerland

## Work experience

2009	Bioengineer, Bern University Hospital, Cardiovascular Research Center, Bern, Switzerland
2008-2009	Research Assistant, University of Bern, Institute for Surgical Technology and Biomechanics, Bern, Switzerland
April 2005	Project Manager Assistant, nspm ag, Meggen, Switzerland
September 2004	Project Manager Assistant, nspm ag, Meggen, Switzerland

## Teaching experience

Spring 2010	Finite Element Course I, Master Course Biomedical Engineering, University of Bern
Spring 2011	Finite Element Course I, Master Course Biomedical Engineering, University of Bern

Spring 2012      Finite Element Course I, Master Course Biomedical Engineering, University of Bern

Fall 2012        Finite Element Course II, Master Course Biomedical Engineering, University of Bern

## **Publications**

Journal articles    Marion Berner, David Clément, Mathieu Stadelmann, Michael Kistler, Yves Boone, Thierry P Carrel, Hendrik T Tevaearai, and Sarah L Longnus. Development of an ultra mini-oxygenator for use in low-volume, buffer-perfused preparations. *The International journal of artificial organs*, 35(4):308–315, April 2012. ISSN 1724-6040. doi: 10.5301/ijao.5000075. URL <http://www.ncbi.nlm.nih.gov/pubmed/22505202>.

Michael Kistler, Serena Bonaretti, Marcel Pfahrer, Roman Niklaus, and Philippe Büchler. The Virtual Skeleton Database: An Open Access Repository for Biomedical Research and Collaboration. *Journal of Medical Internet Research*, 15(11):e245, November 2013. ISSN 14388871. doi: 10.2196/jmir.2930. URL <http://www.jmir.org/2013/11/e245/>.

Marcel Lüthi, Thomas Albrecht, Tobias Gass, OrcunK Goksel, Michael Kistler, Habib Bousleiman, Mauricio Reyes, Buechler Philippe, Philippe C Cattin, and Thomas Vetter. Statismo - A framework for PCA based statistical models . *The Insight Journal*, pages 1–18, 2012. URL <http://hdl.handle.net/10380/3371>. 41

Conference articles    Serena Bonaretti, Benedikt Helgason, Christof Seiler, Michael Kistler, Mauricio Reyes, and Philippe Büchler. A statistical shape model of bone anatomical variability for finite element assessment of bone mechanics. In *Congress of the European Society of Biomechanics. Vol. 39. Edinburgh, Scotland*, 2010a.

Serena Bonaretti, Michael Kistler, Christof Seiler, Mauricio Reyes, and Philippe Büchler. Combined statistical model of bone shape and mechanical properties for bone and implant modeling. In *9th International Symposium on Computer Methods in Biomechanics and Biomedical Engineering. Valencia*,

Spain, Valencia, 2010b.

Marcelo Elias de Oliveira, Michael Kistler, Rudolf de Almeida Prado Hellmuth, Nicolas Gerber, Steffen Schumann, Serena Bonaretti, and Philippe Büchler. a Consistent Method for Modelling Subject Specific Musculoskeletal Systems. In *Journal of Biomechanics*, volume 45, page S496. Elsevier Ltd, July 2012. doi: 10.1016/S0021-9290(12)70497-9. URL <http://linkinghub.elsevier.com/retrieve/pii/S0021929012704979>.

Michael Kistler, Nicolas Biedermann, Rajib Mitra, Marcel Pfahrer, and Philippe Büchler. The Virtuals Skeleton Database: A web repository for medical images and processed data. In *Swiss Society for Biomedical Engineering*, page 1, 2011a.

Michael Kistler, Christelle Boichon, Michel Rochette, and Philippe Büchler. Statistical Shape Models to Accelerate Finite Element Calculations in Biomechanics: A Preliminary Study on Femoral Bones. In *International Society of Biomechanics*, pages 1–2, 2011b.

Michael Kistler, Serena Bonaretti, Christelle Boichon, Michel Rochette, and Philippe Buechler. Methods to accelerate finite element calculation in biomechanics using a statistical database of pre-calculated simulations. In *The Proceedings of the 10th International Symposium on Computer Methods in Biomechanics and Biomedical Engineering*, pages 380–385, Berlin, 2012a.

Michael Kistler, Serena Bonaretti, Marcelo Elias de Oliveira, Christelle Boichon, Michel Rochette, and Philippe Büchler. Statistical Model of Appearance To Accelerate Finite Element Calculations in Biomechanics. In *Journal of Biomechanics*, volume 45, page S257. Elsevier Ltd, July 2012b. doi: 10.1016/S0021-9290(12)70258-0. URL <http://linkinghub.elsevier.com/retrieve/pii/S0021929012702580>. 98

Michael Kistler, Marcel Pfahrer, Roman Niklaus, Viktor Tomas, and Philippe Büchler. The Virtual Skeleton Database : An open access repository for biomedical research and collaboration. In *OpenRepository*, Charlottetown, PEI, Canada, 2013.

## **Declaration of Originality**

**Last name, first name:**

**Matriculation number:**

I hereby declare that this thesis represents my original work and that I have used no other sources except as noted by citations.

All data, tables, figures and text citations which have been reproduced from any other source, including the internet, have been explicitly acknowledged as such.

I am aware that in case of non-compliance, the Senate is entitled to withdraw the doctorate degree awarded to me on the basis of the present thesis, in accordance with the “Statut der Universität Bern (Universitätsstatut; UniSt)”, Art. 69, of 7 June 2011.

Place, date

Signature